Chapter 1

Diffuse interstellar HI clouds: Nature and Kinematics

1.I Introduction

1.1.1 Background

Interstellar gas was discovered by Hartmann in 1904 from the observation of the H and K ($\lambda\lambda$ 3933, 3968Å) absorption lines of singly ionised Ca, which differed from those seen in the spectra of high temperature stars in depth, form and radial velocities, indicating their interstellar origin. Moreover, the lines seen towards binary stars did not share the periodic shift in frequency seen for the stellar lines caused by the orbital motion of the stars. These "stationary" lines were added evidence of the interstellar nature of the gas. The existence of the D_1, D_2 lines of neutral Na ($\lambda\lambda$ 5889, 5895Å), the other commonly seen interstellar line, was postulated by V.M Slipher as early as 1909, but had to wait till 1919 for observational confirmation.

The notion of the intertellar medium (ISM) evolved gradually. Eddington (1926) in his Bakerian Lecture had proposed a truly interstellar origin for these lines, as separate from the atmospheres of stars. Accurate and systematic observations, especially by Plaskett and Pearce (1933) from the Dominion Astrophysical Observatory, and Merrill et *al.*(1937) from the Mount Wilson Observatory followed. The work of Plaskett and Pearce clearly established the influence of Galactic rotation on interstellar matter. The radial velocities of the CaII line towards —300 bright stars revealed that typically the radial velocities showed a Galactic rotation shift corresponding to half the distance to the star. This seemed to indicate a uniform distribution of the ISM. However, the line intensities and

1936), which should be the case if differential Galactic rotation was the main cause of the observed line widths. Wilson and Merrill (1937) analysed the Merrill et *al.* data and concluded that the observations could be accounted for by making the hypothesis that **"interstellar sodium occurs in discrete aggregations or clouds, which, while participating in general galactic rotation, have in addition considerable random motions"** (from Münch 1968). This led to the "discrete cloud" model of the ISM, originally proposed by Ambartsumian and Gordeladse (1938) and Ambartsumian (1940) in relation to the distribution of interstellar'dust, the basic tenet of which has remained unchanged till date.

In 1949 Adams studied the CaII H and K lines towards 300 bright O and B stars. This extensive study laid the basis for the early models of the ISM. These observations were extended to distant and high latitude stars by Munch (1957) and Münch and Zirrin (1961), and to the Na D lines by Hobbs (1969) with much better spectral resolution. All these observations reinforced the picture of the ISM being distributed in condensations or clouds. In a seminal study, Blaauw (1952) analysed the radial velocities of these absorption lines. A major conclusion of this study was that the distribution of velocities seemed to exhibit a high velocity tail. The distribution did not lend itself to being described by a single gaussian and was fit better by an exponential function. This aspect is of great relevance for the study described in this chapter and will be discussed in detail later on.

The cloud model already had originally been arrived at from studies of interstellar reddening towards nearby stars caused by intervening dust. Drawing mainly from observations of interstellar reddening, the condensations or clouds that one sees in optical absorption are categorised into at least two main classes (Spitzer 1968). **The "standard" cloud has a radius of $\sim$ 7 pc and causes an extinction of 0.2 magnitudes, with 8 to 12 clouds present per kiloparsec. The "large" clouds are denser, with an extinction of 1 magnitude, radius of 15 pc with less than 1 cloud seen per kiloparsec.** This simple classification assumes a spherical shape for the cloud.

Spitzer (1956) conjectured the existence of a hot intercloud medium when he first postulated a Galactic corona. Several observational and theoretical indications led him to this conclusion. Prominent among these was the existence of "clouds" seen in optical absorption at very high latitudes (Munch, 1957). These clouds were possibly confined by the pressure of the intercloud medium. Theoretical basis for this "two-phase" model came from the seminal work of Field (1965)

at $\sim 10^4$ K, maintained by cosmic ray heating. They showed that such a phase of the ISM would be thermally unstable, leading to the formation of condensations or "clouds" in pressure equilibrium with the hot medium.

Although a clear picture of the ISM had emerged from these and other related efforts, the current global models of the ISM are largely based on extensive observations of the 21 cm line of neutral hydrogen (HI). The Dutch astronomer van de Hulst predicted the detectability of this line in 1945, the discovery of which was announced simultaneously by Ewen and Purcell of Harvard, along with Muller and Oort at Leiden in 1951, and confirmed by Christiansen and Hindman from Australia in 1952. Our understanding of the structure and kinematics of the Galaxy has been based to a large extent on the information gleaned from this important line. The density of the gas in the ISM was derived from studies of HI in emission. A global picture of the ISM emerged from HI absorption studies (Clark 1965; Radhakrishnan *et al.*1972a). According to the now widely accepted "standard model", the ISM consists of relatively cool diffuse HI clouds at a spin temperature $T_s \sim 80$ K in pressure equilibrium with warm (T, $\leq$ 8000 K) "intercloud" gas . The basic data that differentiate between the two is shown in Fig 1.1 from Radhakrishnan *et al.*(1972b). This shows both emission and absorption spectra. The narrow emission components (which have absorption counterparts) arise in the Cold Neutral Medium. The broad emission components do not have absorption counterparts and arise in the Warm Neutral Medium. The opacity τ is inversely proportional to the spin temperature and so the Cold Neutral Medium shows up in absorption whereas the broad Warm Neutral Medium component seen in emission is absent in absorption. The width of the Warm Neutral Medium features found in emission are of the order of 5 to 17 km s^{-1}(Mebold 1972) whereas the mean width of the Cold Neutral Medium is $\sim$ 1.7 km s^{-1}in optical depth (absorption) profiles and $\sim$ 2.2 km s^{-1}in emission (Crovisier, 1981). The term diffuse "HI cloud" itself derives from the fact that the narrow absorption features are associated with separate clumps in analogy with "clouds" seen in optical absorption. We will explore the correlation between the two populations in detail in the following sections. But first a word of caution: detailed emission maps of the HI sky reveal structures which resemble sheets, shells and filaments; spherical clumps or clouds are rarely seen.

The attempts to better understand the kinematics and structure of the ISM through optical absorption studies have continued. High resolution spectra of

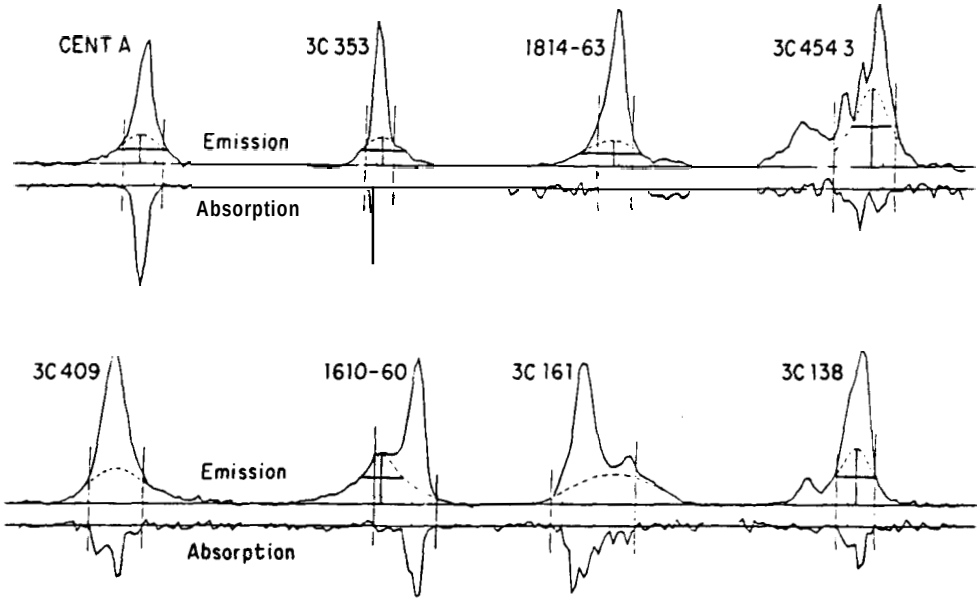

Figure 1.1: Comparison of eight emission and absorption spectra obtained at intermediate latitudes (Radhakrishnan et al., 1972b). The quantity plotted is equivalent to $\Delta T_{b(\nu)}$ from equation 1.4, i.e., the brightness temperature after removal of the background source contribution. The velocity limits of absorption are marked by vertical lines. A fit to an optically thin component is shown by dotted lines.

(eg; Welty, Hobbs and Kulkarni, 1994) have been obtained towards a number of stars. The velocities and line widths of these and UV absorption features of other atoms have been studied to explore their nature. The abundances of these elements and the physical conditions in the gas in which they are found have vielded inportant information about the ISM. Some of these studies, and the inferences drawn by them, will be discussed in the light of our results later in this chapter.

1.1.2 Motivation and Objective of our study

The main theme of the study described in this chapter pertains to the correspondence between the two families of interstellar clouds described in the previous section: The clouds seen in optical and ultraviolet absorption and the HI clouds seen both in absorption and emission. Although these two pictures of the ISM have coexisted for several decades now, the question remains as to how the different subsets of clouds seen in the optical and ultraviolet are to be related to their radio counterparts.

The typical HI cloud has a neutral hydrogen column density $N(HI) \sim 0.6 \times 10^{20}$ cm $^{-2}$, nearly four times smaller than the standard "optical" cloud. However this discrepancy seems to stem from selection effects arising from the sensitivity limitations of the optical techniques (Kulkarni and Heiles, 1987). Essentially, the sensitivity of optical extinction measurements limits one to sampling only the densest of diffuse HI clouds and so the typical column densities one derives from these measurements are severely biased. A more serious discrepancy persists with regard to two other parameters: **the number of clouds seen per kpc and the velocity distribution of the clouds.** The optical estimates for the number of clouds per kpc has always tended to be higher than the HI estimate. The velocity distribution shows a high velocity tail in the optical. Such a population of high velocity clouds is not seen in HI absorption surveys of the Galaxy. Indeed, as we will see they are missing in HI emission as well. It is conceivable that these two discrepancies could be traced to a common cause. This brings us to the basic motivation behind the present study.

Velocity Distributions

The CaII and NaI absorption studies of Adams (1949), Münch (1957), Münch and Zirrin (1961), Hobbs (1969) and others revealed two sets of absorption fea-

(< 10 km s^{-1}) and another at higher (> 10 km s^{-1}) velocities. The high velocity components were generally weaker than the low velocity features. Further evidence for two distinct populations of "clouds" came from the fact that the NaI to CaII ratio was sytematically lower for the high velocity features (Routly and Spitzer, 1952; Merrill and Wilson, 1947). In his important study of the velocities of features seen in Adams' spectra, Blaauw (1952) concluded that there was a distinct *high velocity tail* extending upto even 100 km s^{-1}. In order to account for effects of Galactic rotation, Blaauw removed the Galactic rotation component of the velocity *computed for half the distance of the star* for each feature. An exponential distribution with a velocity dispersion of 7 and 11 km s^{-1} for the close ($\sim$ 250 pc) and distant ($\sim$ 900 pc) stars respectively was fitted by Blaauw (Fig 1.2A). He estimated the number of clouds per kpc to be between 8 and 12. Although allowance was made for the blending of features in the spectra given the resolution ($\sim$ 9 km s^{-1}), Blaauw did not discuss the possibility of two distinct populations in his study.

Radio observations have also indicated the presence of a population of fast clouds, although this is still controversial. From an analysis of the HI absorption spectrum measured towards the Galactic center with the Parkes interferometer, Radhakrishnan and Sarma (1980) inferred the existence of a low optical depth broad feature ($a \sim 35$ km s^{-1}) (Fig1.2B). On the basis of this result, Radhakrishnan and Srinivasan (1980) proposed a two population picture of HI clouds. The broad component seen in the absorption spectrum was attributed to a "fast" population of clouds with velocity dispersion of 35 km s–'and a peak optical depth of 0.3. The spin temperature (T_s) estimate for these clouds was of the order of 300 K. The spectrum also showed a deep narrow absorption feature which was identified with the standard cool diffuse HI cloud associated with the Cold Neutral Medium described earlier. This "slow" population had a peak optical depth of 4.3 and a velocity dipersion of 5.0 km s^{-1} consistent with previous estimates for the cool component. Schwarz, Ekers and Goss (1982) attempted to verify these results using the Westerbork Synthesis Radio Telescope but concluded that there was no evidence for a wide distribution. They were of the opinion that any "fast" population could exist only at a level which was less than one third of that claimed by Radhakrishnan and Sarma.

More evidence for a possible population of fast clouds came from the work of Shaver et *al.*(1982) and Anantharamiah, Radhakrishnan and Shaver (1984).

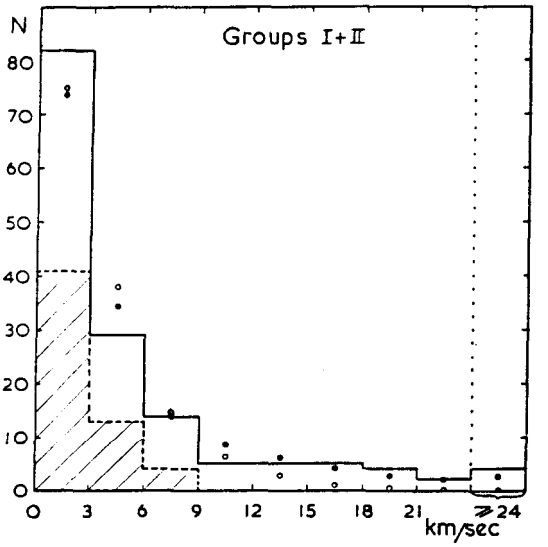

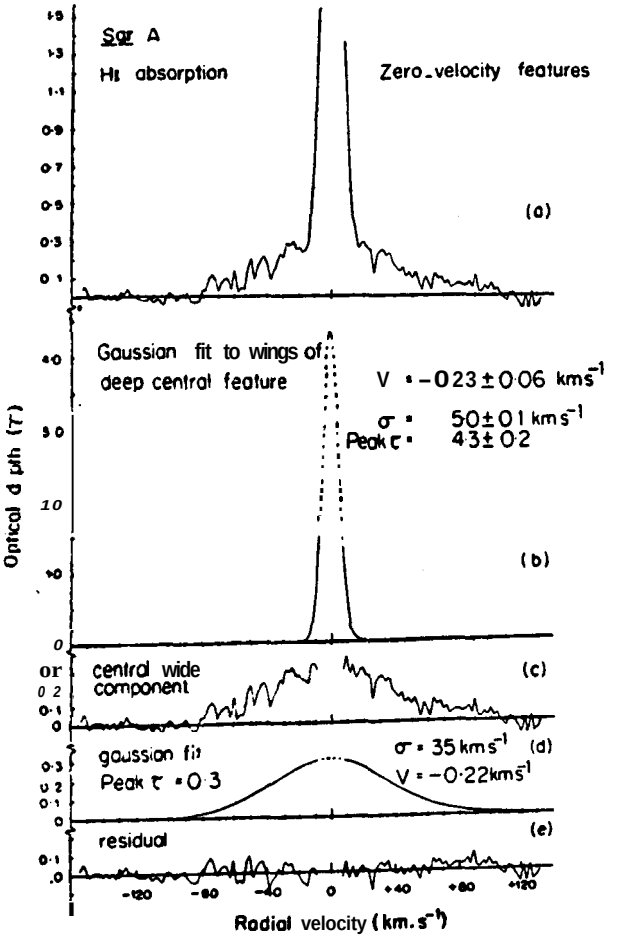

Figure 1.2: Left panel **(A):** Reproduced from Blaauw (1952). Groups I+II represent stars whose distances were < 500 pc. The solid line represents the observed number of velocities in intervals of **3** km s^{-1}in groups I+II. The dashed line represents the contributions due to the components with intensities > 6 in Adams' (1949) scale. The circles represent a gaussian fit to the distribution and the dots are from an exponential fit. Right panel (B): From Radhakrishnan and Sarma (1980). Resolution of the zero velocity features (a),in the HI absorption spectrum of sgr A towards the Galactic centre into two gaussians b and **d;** the residuals **c** and **e** after subtraction of these components.

gions with known distances (arrived at from recombination line velocities) they concluded that there was a definite case for a fast population, though perhaps lesser in number than the previous estimate by Radhakrishnan and Srinivasan. Although Kulkarni and Fich (1985) argued against the reliability of this method they nevertheless found evidence of HI emission at high velocities.

Radhakrishnan and Srinivasan had tentatively identified the fast population with the high velocity features found in optical absorption. They argued that these could be a population of relatively high temperature "shocked" clouds, with supernova explosions as the source of energy. The correlation of optical depth with spin temperature found by Dickey, Salpeter and Terzian (1978) for low optical depth features provided support for this conjecture. The low optical depth could also account for the discrepancy in the number of clouds per kiloparsec derived from various measurements. This number has been estimated to be 8 to 12 clouds per kpc by Blaauw in his study based on Adams' data. Hobbs (1974) estimated a smaller number of 4.5 clouds per kpc from KI absorption measurements. The estimates from radio observations were even lower at 2.5 clouds per kpc (Radhakrishnan and Goss 1972). This number depends on the sensitivity and velocity resolution of each of these techniques. Given these limitations, Radliakrishnan and Srinivasan argued that the actual number of clouds per kpc could be of the order of 15 to 20, a view endorsed by Anantharamiah, Radhakrishnan and Shaver.

To summarize, there seems to be evidence for two different kinds of interstellar clouds. There is firm evidence for this from optical absorption studies. In the radio the picture is less clear, with contradicting claims.

We next turn to attempts to relate the picture of the ISM as deduced from optical and radio observations. This was first attempted by several groups of investigators working in the late sixties and seventies. These investigations centered around HI emission measurements in the direction of stars which show both high and low velocity absorption features in their optical spectra (Takakubo, 1967; Habing, 1968, 1969; Goldstein and MacDonald, 1969, Goniadzki, 1972; Heiles, 1974 and others). Habing's study in particular targetted selected stars to attempt a direct face off. The results of these early studies threw up an intriguing fact. *The low velocity features appeared to be well correlated in HI emission and optical absorption, i.e., wherever the optical spectra showed a low velocity absorption feature ($V < 10\ km\ s^{-1}$), there was HI emission at the corresponding velocity.*

to low limits (< 1 *K). This seemed to be the case in all directions in the sky.*

As mentioned earlier, the fast clouds seen in the optical have a NaI to CaII ratio lesser than the value for the high velocity population. This could be attributed to the ionisation of NaI in these clouds. This fact, along with the absence of HI emission from these clouds, prompted the conjecture that these could be ionised gas (Habing, 1969; Heiles, 1974). Based on a seeming excess of *negative velocities* in the high velocity population, Schlüter, Schmidt and Stumpf (1953) proposed that these could well be circumstellar material accelerated in the environs of bright stars and seen in absorption. This possibility was considered by Habing as well. In an important study Siluk and Silk (1974) showed that the high velocity features could not be explained by Galactic rotation and conjectured that they arose in SNRs along the line of sight. Modelling of the physical conditions in these clouds given the observed N(NaI)/N(CaII) ratio was attempted by Pottasch (1972) and his study pointed to the possibility of high temperatures of a few thousand degrees. Pottasch had assumed that the lower NaI/CaII ratios in the fast clouds was due to the ionization of NaI. However, later investigations revealed that the NaI to CaII ratios of the fast clouds were much closer to the cosmic abundance values than those of the slow clouds. Thus it seemed that preferential depletion of CaII to the dust phase in the slow population was the reason for the difference in the ratios rather than ionisation of NaI in the fast clouds. The investigation of Hobbs (1974) also showed that CaII abundance tends to fluctuate for different samples. As for the circumstellar nature, it seems unlikely that clouds could be accelerated to such high velocities by nearby stars (Pottasch 1972). Another possibility advanced by Habing for the missing HI emission was that the fast population were small cold clumps of HI. The relatively large beam size ($\sim 0.5°$) used in emission measurements causes beam dilution to weaken the signal. Moreover a small dense clump could have depletion of HI into molecular hydrogen (H_2) compounding the difficulty.

All these controversies centered around HI emission measurements. An attempt to relate the two populations of clouds through an HI *absorption* experiment has not been made till date, and this is precisely the main objective of our study. The focus is on studying the nature of the fast clouds "missing" in emission. An absorption measurement will complement the existing emission data and overcome two of the limitations mentioned before. The resolution achievable in an interferometric measurement will be similar to that of the optical and thus will

emission measurements makes it difficult to attribute one-to-one correspondence between the various features seen in the HI and optical spectra. This effect is thought to be one of the reasons for the lack of similarity between HI emission and optical absorption features in some cases (Blades et *al.*1997). The high resolution achieved in the HI absorption observations will overcome this difficulty, as long as one samples a line of sight close to the star. The other advantage is the sensitivity to cold dense features, if indeed they are the fast population. If one fails to detect the fast clouds in absorption despite these advantages the case for high temperature, low optical depth component would be strengthened. As for the low velocity population, emission measurements already exist in many cases. The spin temperatures of these clouds can be determined if absorption measurements also existed. This would help to firmly identify their place in the hierarchy of the various components in the standard models of the ISM.

The importance of the fast population of clouds cannot be overstated. For example, Radhakrishnan and Srinivasan estimate the total mass of the weakly absorbing fast clouds could be twice that of the cool, low velocity clouds and therefore the total kinetic energy of the fast population could be two orders of magnitude higher than that of the cold clouds. This would make the high velocity clouds the major reservoir of energy in the ISM. Any model of the ISM must be able to account for their distribution of velocities and the difference in velocity clistribution from the cold clouds. In this context, the absorption experiment described here is a fresh attempt at reopening a long standing, important and controversial question.

At this point we would like to differentiate between the better known High Velocity Clouds (HVCs) seen at high latitudes and the "fast population" being discussed here. The HVCs show extreme (> 100 km s^{-1}) velocities, whereas the velocities of the "fast clouds" are moderate. The other essential difference is that the HVCs are not seen in absorption in the optical (or any other wavelength) down to very small optical depth limits (e.g, Danly et al., 1992). Only of late have high sensitivity measurements started to reveal absorption in optical and UV from the HVCs (e.g., Savage et al., 1993). This clearly puts them as a separate population from the disk gas we are concerned with. The Intermediate Velocity Gas (IVG) also has this feature. Another warm, tenuos and partly high velocity population is the warm halo gas. A detailed study of this gas in absorption towards distant halo stars has been undertaken by Spitzer and Fitzpatrick (1993) (one of the

and UV absorption towards the halo also have been extensively studied (e.g., Danly et al., 1992 and others). Part of the halo gas seems to be warm ($\sim$ 1000 K) and in the velocity range $\sim$ 20 km s^{-1}. The abundance of elements also follows the trend of less depletion for the high velocity components. These "halo clouds" have differing temperature ranges in various sight lines (Spitzer and Fitzpatrick, 1993). However they do appear in HI emission, and the relation with the fast disk population is unclear.

1.2 21 cm radiation: A brief overview

1.2.1 The "spin flip"

In the hydrogen atom, the magnetic moment of the proton interacts with the combined magnetic field of the orbiting electron and the magnetic moment of the electron. This results in "hyperfine" structure for the energy levels, splitting all energy levels into nearly equal sub-levels. The hyperfine splitting of the ground state is responsible for the 21 cm line radiation. The electron in the ground state can have its spin "up" or "down" and the same holds for the proton, leading to 4 possible spin states. The 4 stationary states of the atom can be described as

1. Electron "up", proton "up",
2. Electron "down", proton "down",
3. A combination of electron "down^{n}-proton "up" + proton "down"- electron "up",
4. A combination of electron "down^{v}-proton^{u}up" – proton "down^{v}- electron "up".

The first three states have identical energy levels, which are higher than that of the 4th state by $\sim 10^{-6}$ ev ($\sim$ .07 K, through $E = kT$). It is the transition from any of the degenerate states 1, 2 or 3 to state 4 which results in 21 cm radiation. These "spin-flip" transitions (so called since they result primarily from spin-spin interaction) are magnetic dipole transitions. The Einstein-A coefficient is only of the order 2.85 x 10^{-15} s^{-1} and an HI atom in the excited state typically spends 12 million years before decaying. The average ISM temperatures are much greater than .07 K, and a typical collision between atoms has enough energy to excite the HI atom. Given the densities and temperatures prevalent in most

much smaller than the spontaneous emission timescale. Therefore collisions can establish equilibrium population, i.e $\sim$ 3 atoms in the upper level to every one in the lower level. Since collisions dominate, the populations n_1 and n_2 in the upper and lower levels will be more or less the same as in thermal equilibrium, though 21 cm photon density is much lesser than equilibrium density. Hence the Boltzmann formula,

$$\frac{n_2}{n_1} = \frac{g_2}{g_1} e^{-h\nu/kT_s}$$

where $g_2/g_1 = 3$, holds. The "spin" temperature T, is therefore the same as the kinetic temperature of the atoms. While this is true for the cool diffuse component of HI ($T\sim$ 80 K), collisional equilibrium does not hold for the warm ($T>3000$ K) component. However excitation by Lyman α photons, rather fortuitously, still maintain $T_s = T_{kinetic}$ (see Kulkarni and Heiles, 1987).

1.2.2 21 cm: Radiative transfer

The general form of the radiative transfer equation is

$$\frac{dI_\nu}{ds} = j(\nu) - k(\nu)I_\nu \tag{1.1}$$

Here I, is the specific intensity at frequency ν, $j(\nu)$ and $k(\nu)$ are the volume emission and absorption coefficients. Physically, the equation implies that the change in I, over a pathlength "s" equals the increase by source contribution offset by the loss due to absorption. At low frequencies (certainly at cm wavelengths) where $h\nu \ll kT$, $I(\nu)$ is approximated by $2\nu^2 kT_B/c^2$ (the Rayleigh-Jeans limit). T_B, the brightness temperature (the temperature of a hypothetical black body which has the same specific intensity at a particular frequency as the source) is thus linearly related to I, and is commonly used in radio astronomy. The radiative transfer equation for the HI line can then be couched as

$$\frac{dT_B(\nu)}{d(\tau_\nu)} = T_s - T_B(\nu) \tag{1.2}$$

where $\tau_\nu = -\int k_\nu ds$ is the opacity along the line of sight. At large values of τ_ν, $T_s = T_B$, i.e the brightness temperature equals the physical temperature for a black body. For an single homogeneous HI cloud, equation 1.2 gives

$$T_B(\nu) = T_{bg}(\nu)e^{-\tau_\nu} + T_{src}(1 - e^{-\tau_\nu}) \tag{1.3}$$

where T_{bg} is the incident radiation on the far side of the cloud and T_{src} is the spin temperature of the cloud. On removing T_{bg} from the measured T_B we get

which are the profiles shown in Fig 1.1 The optical depth

$$\tau(\nu) = \frac{\mathrm{N}(\nu)}{\mathrm{C} \times \mathrm{T_s}} \tag{1.5}$$

Where N is the column density or number of particles seen projected per unit area and the constant $\mathrm{C} = 1.83 \times 10^{18} \mathrm{cm}^{-2} \mathrm{K}^{-1}$. It is clear that the cloud can be seen in absorption or emission depending on whether T_{src} is greater than T_{bg} or vice-versa. In a single dish measurement equation 1.4 gives the measured quantity and to extract the optical depth the contribution of the cloud has to be separately estimated (typically by looking at emission from the cloud in directions one beamwidth away from the compact background source) and removed. Any structure in the absorbing cloud on the scale of a beamwidth will result in error in the estimation of the cloud emission. An interferometer, on the other hand, acts as a spatial filter. Over a baseline B it responds only to structure in the sky with spatial frequency of $\sim \mathrm{B}/\lambda$, where A is the wavelength. Most of the HI structure seen in emission are of scales larger than 1 arcminute. Hence an interferometer with a fringe spacing smaller than an arcminute (but larger than the size of the background source) responds only to the background source, eliminating the need for a separate estimate of the cloud emission. Thus interferometers measure the absorption spectrum $1 - \mathrm{e}^{-\tau(\nu)}$ directly. To estimate the spin temperature, however, we need to estimate the cloud contribution, again running into the aforementioned limitations. The spin temperature then is given by

$$\mathrm{T_s(v)} = \mathrm{T_B}(\nu)/(1 - \mathrm{e}^{-\tau_\nu}) \tag{1.6}$$

It must be noted that the spin temperature estimated in this manner is a harmonic mean of spin temperatures of various components in the line of sight.

1.3 Galactic rotation

Our Galaxy rotates differentially, with the innermost part of the disk (< 3 kpc) in almost solid body rotation with a rotation velocity that rises outward. The outer parts show an almost constant rotation velocity, with a slow decline outwards. Given such a rotation pattern, one would expect stars towards Galactic longitude $1 = 0$" and 180" not to have a radial velocity component with respect to the Sun since they are moving entirely perpendicular to us. Likewise at 90° and 270°. the nearby stars share the same circular orbital velocity as the sun and

at 135° they are being overtaken, resulting in positive (receding) and negative (approaching) radial velocities, respectively. Thus, heuristically, one expects a periodic behaviour for the radial velocity component of Galactic rotation as one scans in Galactic longitude. The general formula for the radial velocity component of Galactic rotation is given by

$$V_r = (\omega - \omega_0)R \sin l \tag{1.7}$$

where w is the angular rotation velocity at a galactocentric distance R and ω_0 is the angular velocity of the Sun. For the solar neighbourhood

$$V_r = Ad \sin 2l \tag{1.8}$$

where A is the Oort's constant, and d the heliocentric distance.

The behaviour of the radial velocity component from l= 0° to 90° and 90" to 180° according to the above formulae is schematically sketched in Fig 1.3. This also shows the distance ambiguity in the inner quadrant. Extensive HI emission measurements have yielded rotation models for the Galaxy, giving *w* as a function of galactocentric radius. For a given distance and longitude, we plug in the *w* from such a model into the formula to give the expected radial velocity component. In the subsequent discussion we often refer to the maximum allowed Galactic rotation velocity for an absorption feature. Since the absorption arises at some point along the line of sight to the star (the distance to which is known), the range of allowed radial velocities because of Galactic rotation can be calculated, which allows us to put these limits. We have adopted the rotation model presented by Burton (1987).

1.4 Scope of the present observations

We have chosen 25 stars, all of which show both low and high velocity absorption features in their optical spectra from CaII or NaI atoms or both. Two of the stars HD 14134 and 14143 are close together and in the same field and hence we have measured absorption in a total of 24 fields. The positions of all the selected stars as projected on the plane of the Galaxy are shown in Fig 1.4. The Galactic spiral arms shown in this figure are from the model by Taylor and Cordes (1993). In 13 of these directions HI emission measurements had been carried out by Habing (1968,1969) in an attempt to correlate radio emission features with the optical

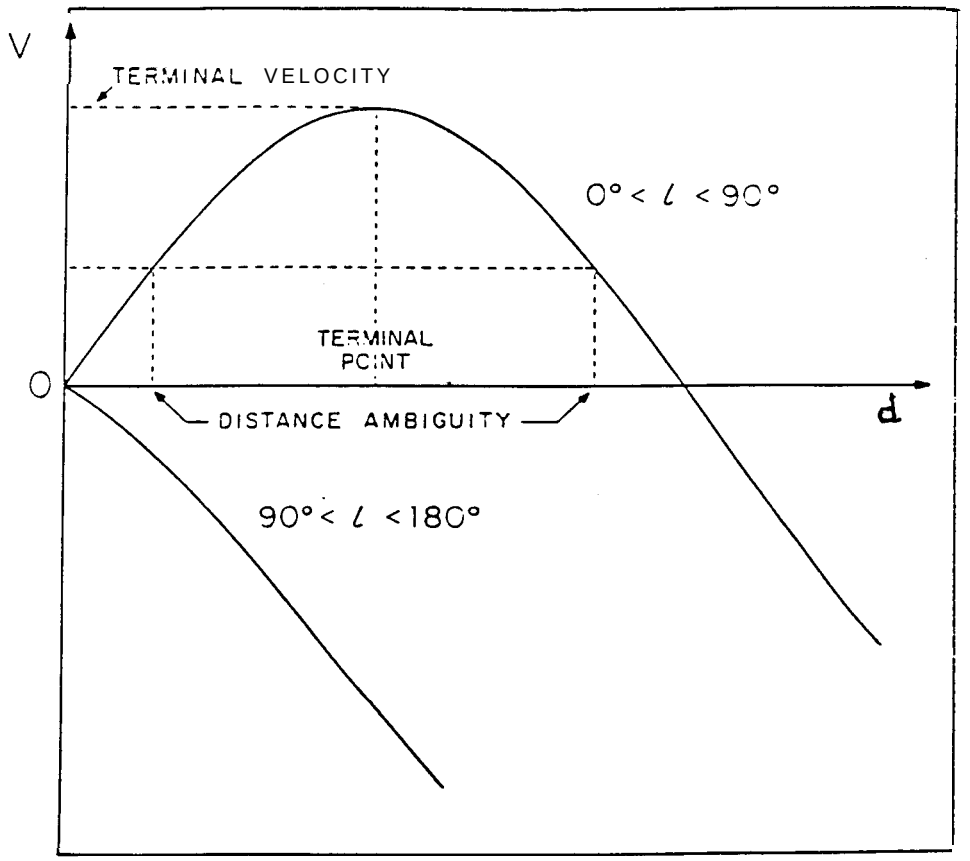

Figure 1.3: Velocities w.r.t local standard of rest are plotted as a function of heliocentric distance. The two curves are for the first ($0° < l < 90°$) and second ($90° < l < 180°$) quadrants. The distance ambiguity for the inner Galaxy is shown in the curve for the first quadrant.

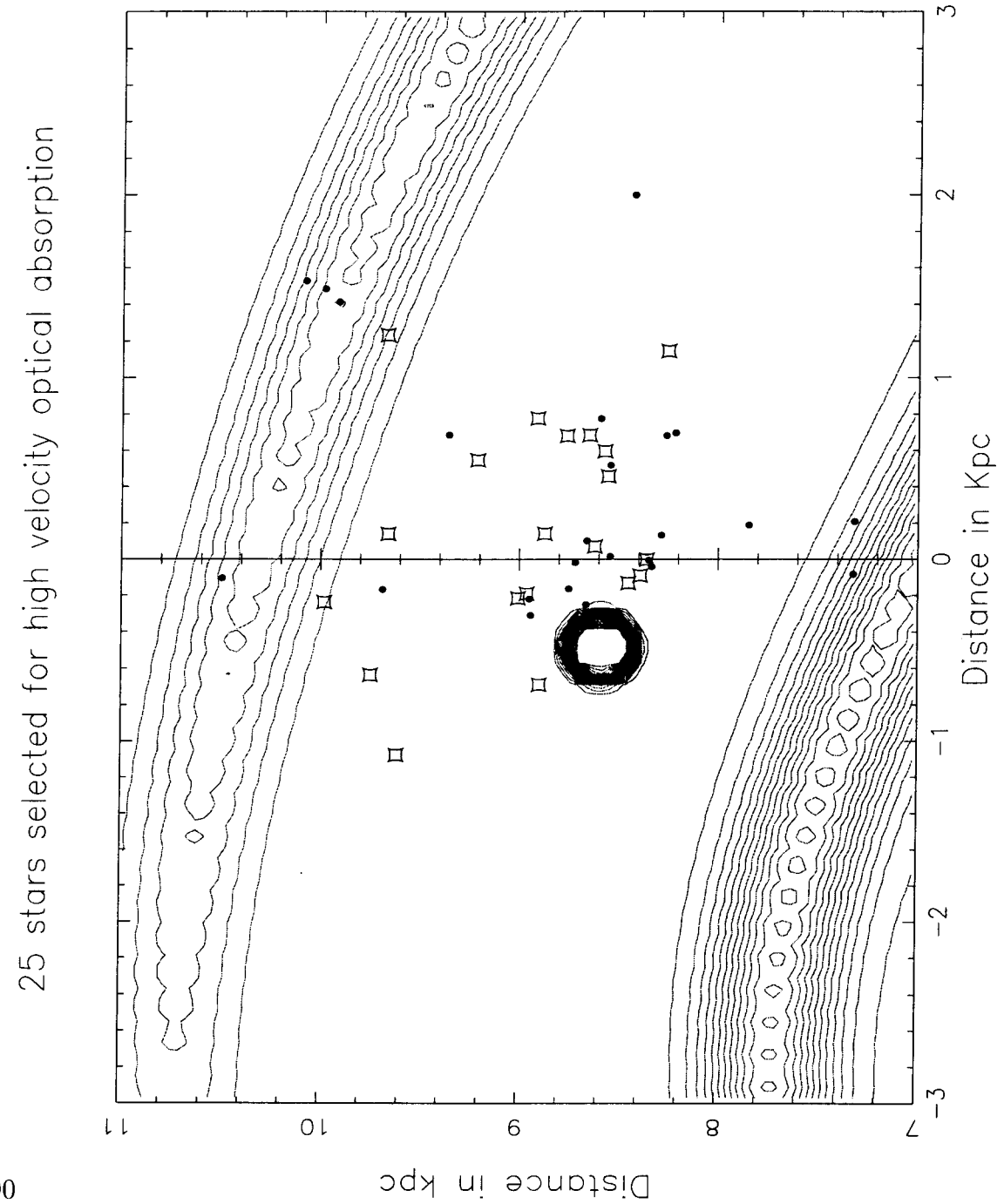

Figure 1.4: 24 of our sample of 25 stars (HD 119608 lies outside the region shown) are shown as dots on the contour plot of the Galactic spiral arms from Taylor and Cordes. The squares show the local OB associations from Blaauw (1985). The Sun is at 8.5 kpc. The location of the Gum Nebula is indicated. The outer arm shown is the Perseus arm, while the inner one is the Sagittarius arm. The three stars bunched together well inside the Perseus arm are HD 14134, 14143

HI emission arising in the plane. Four stars, however, are at $|b| < 10°$ and were selected since they show CaII velocities well outside the limits of Galactic rotation at the respective distances. Out of the remaining fields, 3 have been investigated by Goniadzki(1972) for HI emission and 1 by Takakubo (1967). The rest of the stars have not been investigated in the radio in any specific program. However, we have been able to get emission temperatures and column densities of HI in these directions from the Leiden-Green Bank survey of Burton (1985).

In the observations described below we have obtained HI absorption spectra towards a radio source whose line of sight is close to that of the star. In the previous section we described some of the advantages of such an absorption experiment. On the other hand, in order to sample any HI in the line of sight to the star one has to identify a radio source of reasonable strength near the star as seen in projection. We have been able to identify fairly strong radio sources (in most cases $\gtrsim 50$ mJy at 21 cm) within 30 to 40' of the star in each field. More than half are within 10' and several are within 5' of the star in question. If one places the cloud halfway to the star, this 5' separation is adequate to sample a minimum size of less than 1 pc for the farthest stars in the sample which are about 2 kpc away. This is well within the range of accepted sizes for standard clouds (Spitzer 1978). These separations therefore are adequate to sample the cloud even in the "small clump scenario", where the conjectured cloud size is $\sim$1 pc. In some fields we had to arrive at a compromise between the minimum cloud size we could sample (*i.e.*, the proximity of the background source to the star) and the optical depth sensitivity we could achieve. The latter constrains us to fairly strong radio sources for reasonable integration times. This flux density requirement limits the number of sources that one can find close to the star and hence the trade off. Most of the sources which we have selected are from the NRAO/VLA Sky Survey (Condon etal., 1996). We targetted an optical depth sensitivity of $\tau = 0.1$ and have done better than that in several cases. In all cases the detection limit on optical depth is less than 0.4. The limited sensitivity of absorption measurements to hot gas (since τ scales inversely as T,) imposes a limitation here. However, we hope to be able to set firm upper limits on the

1.5 Observations

We obtained the absorption spectra using the Very Large Array (VLA[1]) in the D and B configurations.The maximum baselines available are —1.3 and —36 km, giving a synthesized beam size of 44" and 4" respectively at 21 cm. The observations were carried out in the frequency switched mode with a total bandwidth of 1.56 MHz using both polarizations and 128 channels. We used 0134+329 as the primary calibrator to calibrate fluxes. For each source we observed a nearby secondary calibrator source for both phase and bandpass calibration. The calibrator was observed with the frequency band switched by 1.5 MHz, coresponding to a velocity shift of $\sim$ 200 km s^{-1}. This shift in velocity suffices to move the band away from any Galactic features which might affect the bandpass calibration. Typically, each of these calibrators were observed for $\sim$ 10 minutes. The typical strength of these calibrator sources being $>$ 1 Jy, 10 minutes of integration time was sufficient to achieve a signal-to-noise ratio greater ($\sim$ factor of 2) than that on the source itself. After on line Hanning smoothing over 2 channels, the frequency resolution obtained was $\sim$ 12 KHz which corresponds to a velocity resolution of $\sim$ 2.5 km s^{-1}. The integration time on each source was chosen to give an optical depth sensitivity of $\tau = 0.1$ and ranged from a few minutes to more than an hour. In all, a total of $\sim$ 30 hours were spent on the sources, split over several sessions of observing.

1.5.1 Analysis

The analysis was carried out using the AIPS software from NRAO. The first step was to make continuum images of each field and examine them for bright ($>$ 3 a) sources, including the targetted source. The spectra towards each of these sources were analysed later. At this stage some interference editing was also carried out. Our observations coincided with the ongoing NRAO/VLA Sky Survey (in the B and D configurations) and hence most of the observations were carried out during the daytime. Hence we had to contend with moderate to strong levels of interference over most of the band. For the first level of editing we flagged any time scans or baselines which showed excessive interference, in the continuum data set. This flagging was later transferred to *all channels* of the spectral line data. The calibrators and source spectral line data was then

[1]The VLA is operated by the National Radio Astronomy Observatory (NRAO). The NRAO is a facility of the National Science Foundation operated under cooperative agreement by As-

subjected to interference editing as well. In all fields, the editing was carried out primarily using the task CLIP, which enables flagging of all visibilities beyond a set level. The clipping level was determined by examining the visibility over most baselines and time scans using the task UVPLT. The next stage involved removing the continuum level from all channels. The task used for this was UVLIN. The continuum level to be removed is determined from a linear fit to the visibility levels in selected channels, which are chosen to be free of interference as well as any spectral features. Finally the image cubes were made. The imaging was typically done over an area of 512 by 512 pixels. In cases were necessary, several cubes were synthesised for different areas in the same field, to cover all sources of interest. The spectra towards each of the sources were analysed with tlie Groningen Image Processing System (GIPSY; van der Hulst et *al.*(1992)), which was used for fitting gaussian profiles to the absorption features.

1.6 Results

Table 1.1 lists the details of all the fields observed. In most of these fields we have detected several radio sources within the primary beam in addition to the source initially targetted. We have obtained spectra towards these sources as well if they turned out to be strong enough to detect reasonable optical depths (~ 0.1). Column 1 gives the HD number of the star. Column 2 and 3 show the distance to the star (as listed in the SKY 2000 catalogue of bright stars) and its galactic coordinates, respectively. Column 4 gives the angular separation of the star from the radio source(s) towards which absorption has been detected. Column 5 lists the HI absorption velocities (LSR). These velocities have been derived by fitting Gaussian profiles to the absorption features. Columns 6 shows the detection limit in τ (towards the strongest source in the field). Column 7 shows the radial component of the Galactic rotation velocity at the distance to the star. Table 1.2 lists the "matching" features *i.e.*, absorption features whose velocities "agree" with the velocity of the optical absorption feature. Column 2 lists the LSR velocities of all the optical absorption features seen in each line of sight (most of the listed velocities are from CaII observations). Velocities of the matching HI absorption features follow in column 3. Column 4 shows the radial component of the Galactic rotation velocity at the distance to the star to facilitate comparison with the optical absorption velocities. Column 5 has

Field	d	l^{II}, b^{II}	θ	V_{lsr}	τ	V_{Gal}
	pc		arcmin	km s^{-1}		km s^{-1}
21291	1100	141, 3	36.0	−31.2, −7.0, −4.9	0.07	-10
14143-14134	2000 2100	135, −4	10.0	−52.8, −50.3, −46.1, −11.2, −8.2	0.09	-25
14818	2200	136, −4	10.0	−55.8, −14.0, −3.7	0.05	-25
159176	1180	356, 0	5.3	−20.8, −74.0	0.28	0
166937	1200	10, − 2	5.0, 7.0	34.6, 47.2, 35.7	0.39	5
175754	680	16, −10	<10.0	6.8	0.09	10
25558	220	185, −33	26.0	8.1	0.10	<0
34816	540	215, −26	40.0	6.0, 8.0	0.10	<0
24912	46	160, −13	2.2	4.3, 6.0, −82.0	0.39	−5
214680	780	97, −17	12.0	−4.8, 1.4	0.28	-5
148184	150	358, 21	0.82	3.4	0.26	0
141637	170	346, 21	11.0	0.5, −0.2	0.28	0
41335	300	213, −13	3.0	1.0, 10.0	0.04	>0
156110	720	71, 36	<10.0	2.2	0.18	5
199478	2000	88, 1	8.0	5.0 to −75.0	0.21	-7
212978	520	95, −15	12.0	0.3, −12.3	0.04	-5
21278	190	148, −6	37.0	2.8	0.08	>0
37742	500	206, −16	15.0	9.5	0.03	5
42087	1200	188, 2	42.0, 32.0	4.4, 6.5, 12.4	0.13	-5
119608	3400	320, 43	16.0	−5.4	0.09	-20
205637	250	32, −45	18.4	none	0.30	5
220172	750	68, −63	2.9	none	0.33	10
38666	300	237, −27	21.5	none	0.02	5
93521	2000	183, 62	27.0	none	0.11	<0

Table 1.1: Summary of HI absorption: Column 1 gives the HD number of the star. Column 2 and 3 show the distance to the star (as listed in the SKY 2000 catalogue of bright stars) and its galactic coordinates, respectively. Column 4 gives the angular separation of the star from the radio source(s) towards which absorption has been detected. Column 5 lists the HI absorption velocities (LSR). Columns 6 shows the detection limit in τ (towards the strongest source in the field). Column 7 shows the approximate radial component of the Galactic rotation velocity at the distance to the star. < 0 and > 0 are used to indicate velocities with magnitude $<$ 5 km s^{-1}.

Field	V_{lsr}(optical, all)	V_{lsr}(HI, coincident)	V_{Gal}	Ref
	km s^{-1}	km s^{-1}	km s^{-1}	
21291	−34.0, −7.5	−31.2, −7.0, −4.9	−10	M
14143−	−62.3, −46.8, −6.3	−46.1, −50.3, −11.2	−25	M
14134	−65.3, −50.8, −10.3			
14818	−42.6, −33.6, −6.6	−3.7	−25	M
159176	3.5, −22.5	−20.8	0	A
166937	−5.5, 5.9, 25.3, 41.1	5.4, 47.2, 35.7	5	A
175754	−73.0, 5.9, 29.5	6.8	10	A
25558	10.1, 19.0	8.1	<0	A
34816	−14.0, 4.14	6.0	<0	A
24912	4.7, 20.7	4.3	−5	A
214680	−23.7, −14.7, 0.1	1.4	−5	A
148184	14.2, 2.2	3.4	0	A
141637	−22.0, 0.0	0.5, −0.2	0	B
41335	−20.8, 0.2	1.0	>0	A
156110	−19.7, 0.4	2.2	5	MZ
199478	−2.1, 8.7, 42.3, 61.2	3.8 (blend)	−7	A
212978	−73.0, 0.6	0.3	−5	A
21278	−0.2, 48.6	2.8	>0	A
37742	−21.0, 3.6	none	5	A
42087	−37.7, −4.8, 10.2	12.4	−5	A
119608	1.3, 22.4	none	−20	MZ
205637	−13.9, 1.8	no absorption	5	A
220172	−21.5, −0.8, 13.5	no absorption	10	MZ
38666	1.0, 20.2	no absorption	5	MZ
93521	−55.0, −34.0, −10.3, 6.8	no absorption	< 0	MZ

Table 1.2: Summary of coincident velocities: Column 2 lists the LSR velocities of all the optical absorption features seen in each line of sight (most of the listed velocities are from CaII observations). Velocities of the matching HI absorption features follow in column 3. Column 4 shows the radial component of the Galactic rotation velocity at the distance to the star. Column 5 has the reference for the optical absorption velocities which are from A: Adams (1949), B: Buscombe and Kennedy (1962), M: Munch (1957) and MZ: Munch and Zirrin (1961). These velocities have been corrected for solar motion, adopting in most cases the values suggested by the authors. The error on these velocity estimates vary but most tire accurate to $\pm$ 1 km s^{-1}.

Münch (1957) and Munch and Zirrin (1961). We have used later compilations of these by Takakubo (1967), Siluk and Silk (1974), and Habing (1969). The velocities have been corrected for solar motion, adopting in most cases the values suggested by the authors. The error on these velocity estimates vary but most are accurate to $\pm$ 1 km s^{-1}(Münch 1957).

We now discuss the HI absorption features at low and high velocities to highlight the emerging trend. The optical absorption spectra are likely to be accurate to $\gtrsim$1 km s^{-1}or so, but suffer from blending of features due to lack of resolution. A discusion of this and associated problems can be found in Welty, Morton and Hobbs (1996). Moreover, the correction for the solar motion adopted by different authors may slightly differ leading to errors of roughly 1 km s^{-1}(see for example Blaauw, 1952). In some cases, we have smoothed the absorption spectra to a resolution of 5 km $s^{-1}$to facilitate the convergence of the fit. Narrow absorption features are known to have widths less than this (Crovisier 1981). We have checked the unsmoothed data to ensure that there are no serious effects of blending in the estimates for velocities for the features discussed below. However, crowding in velocities inevitably causes some of the absorption widths to be suspect. The formal error on the fitting procedure for our HI absorption velocities is in most cases of the order of 1 km s^{-1}or less. The formal errors add to $\lesssim$2 km s^{-1}. However, it must be stated that the blending of features in both optical and radio could easily lead to larger errors than this formal value and *we have adopted a value of 3 km s^{-1} as our criterion for "matching" features in the optical and HI absorption.* This is roughly the same value as indicated by Habing (1969) and Howard *et al.*(1963).

1.6.1 The low velocity absorption features

As stated earlier, all lines of sight in our sample show optical absorption (CaII) at both high and low velocities. It is difficult to attribute a sharp dividing line between the "low" and "high" velocity features, but $\sim$ 10 - 15 km s^{-1}or higher random velocity features seem to invariably show no corresponding HI emission in previous studies. Moreover, the NaI/CaII ratios are systematically lower for clouds with velocities down to 10 km s^{-1}, although the effect is pronounced only above 20 km s^{-1}(Sembach and Danks, 1994). Both these characteristics, ie "missing" HI emission and low NaI/CaII ratio are typical of the so called "high velocity" population and therefore we adopt a velocity of 10 km s^{-1}as the dividing line. We

which we detect "matching" HI absorption (coincident velocities) and those for which we are unable to detect matching HI absorption (here "matching" refers to agreement with optical velocities). At this point we wish to point out that there are HI absorption features seen in many fields for which there is *no corresponding optical absorption* (for eg; the field 199478 shown in Fig 1.14 has several high negative velocity HI absorption features with no optical counterparts). In most cases these could be due to absorbing gas *beyond the star* and their velocities are probably the radial component of galactic rotation at the distance to the feature. We will not comment further on such features.

Coincident velocities

In the fields where we have detected absorption, almost all have HI absorption features "matching" the optical absorption at low velocities. HI emission is also seen at these velocities wherever measurements are available. The data is summarized in Table 1.3, listing the matching velocites, and the computed optical depths, spin temperatures (wherever an HI emission measurement is available) and the fitted widths from HI absorption.

The data clearly indicates that

1. Low velocity features in optical absorption, HI emission and HI absorption seem to arise in the same gas.

2 The derived spin temperatures are consistent with this gas being the cold diffuse HI clouds.

We show the HI absorption spectra towards three sample fields in Fig 1.5, 1.6 and 1.7, to demonstrate the coincident low velocity absorption features. *In all the following spectra, the arrows on the velocity axis indicate the position of optical absorption.* In Fig 1.5, 1.6 and 1.7, the HI emission spectrum (Habing, 1968) is shown in the lower panel; these have been digitised from Habing (1968). Fig 1.5 shows the spectra towards the star HD 34816. The optical spectrum (Adams, 1949) shows CaII absorption features at -14.9 and $+4.1$ km s^{-1}. The HI absorption profile shows low velocity features at 8.0 and 6.0 km s^{-1}. The 6.0 km s^{-1}feature could be coincident with the optical absorption. We have obtained spectra towards 2 radio sources in the field, one of which is shown here. The source is 20' away from the star. The estimated spin temperature for the 6.0 ltm s^{-1}feature is $\sim$ 26 K (Table 1.3). The higher velocity feature seen in the

Field	V_{lsr}(optical)	V_{lsr}(HI)	τ	ΔV	T_s
	km s^{-1}	km s^{-1}		km s^{-1}	K
21291	-7.5	7.0	0.60	6.2	180
14143-14134	-10.3	−11.2	0.18	11.8	283
159176	-22.5	−20.8	1.15	15.3	NA
166937	5.9	5.4	1.70	5.7	NA
175754	5.9	6.8	0.35	17.7	135
25558	10.1	8.1	1.13	5.6	73
34816	4.1	6.0	1.50	3.2	45
24912	4.7	4.3	0.80	14.9	73
214680	0.1	1.4	saturated	2.1	NA
148184	2.2	3.4	4.90	3.4	50
141637	0.0	0.5,	1.60	8.0	NA
41335	0.2	1.0	0.22	7.2	342
156110	0.4	2.2	0.28	7.5	102
199478	-2.1, 8.7	3.8 (blend)	0.60	11.4	121
212978	0.6	0.3	0.20	9.0	NA
21278	-0.2	2.8	0.18	5.1	250
42087	10.2	12.4	1.26	3.5	211
14818	-6.6	-3.7	0.43	13.7	143

Table 1.3: Summary of coincident low velocities: Column 1 lists the HD number for the field. Columns 2 and 3 give the LSR velocities for the "matching" optical and HI absorption features respectively. Column 4 and 5 lists the optical depth and width for the HI absorption derived from the fitted gaussian. Column 6 lists the spin temperature T,. These values have been derived by using the optical depth from our observations along with the emission brightness temperatures from Habing (1968). Where this was not available we used brightness temperatures from the Leiden-Green Bank survey (Burton, 1985). Those fields where emission measurements were not available are marked NA in column 6.

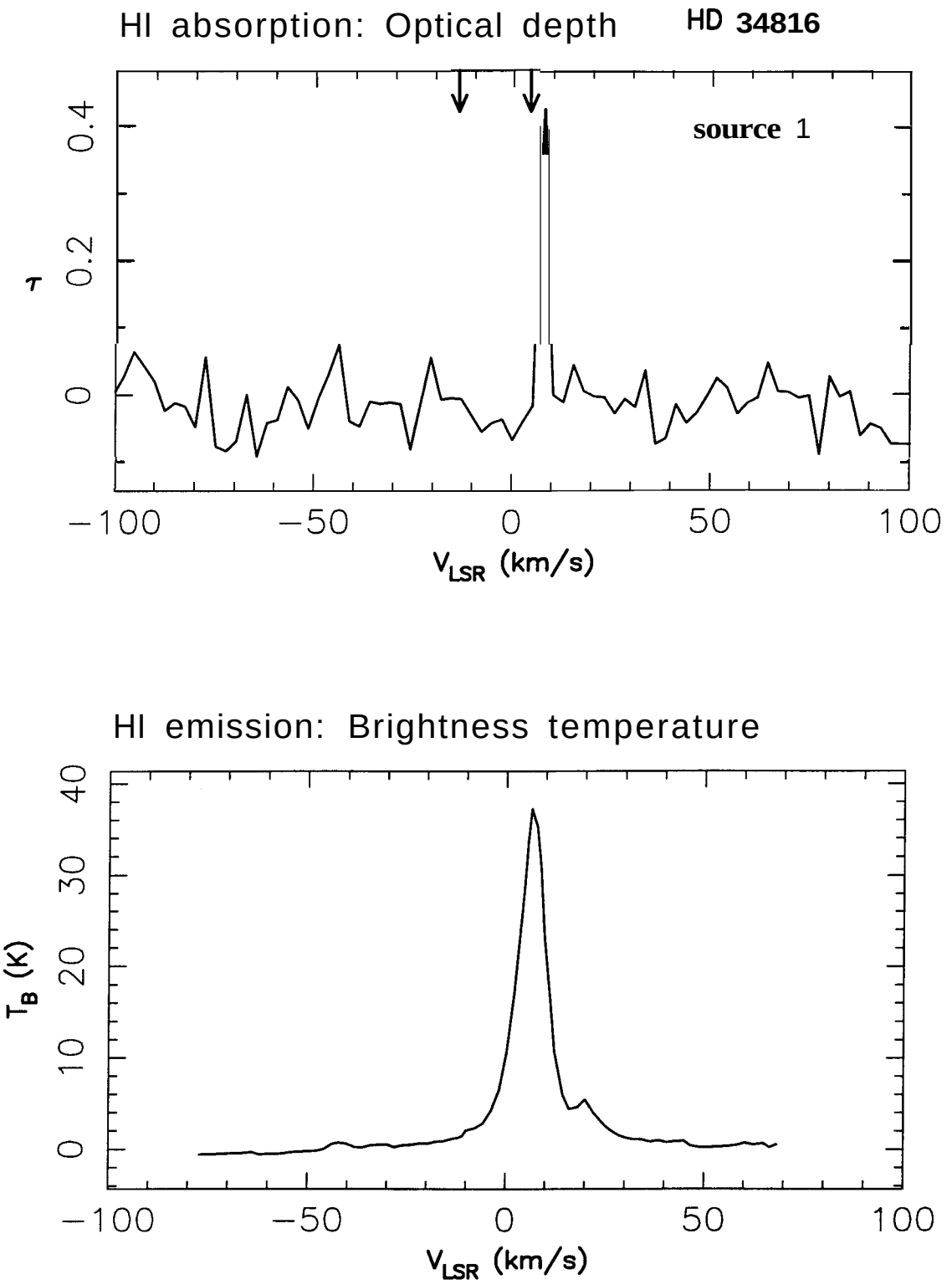

Figure 1.5: HI absorption (top) and emission (bottom) spectra towards HD 34816.

HI absorption: Optical depth HD 42087

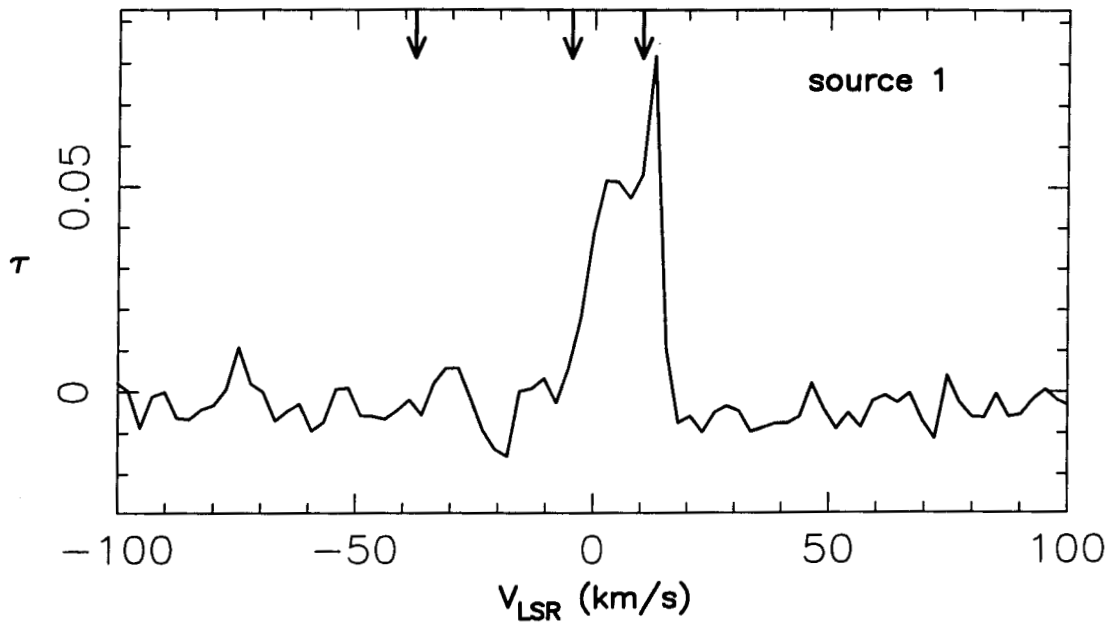

HI emission: Brightness temperature

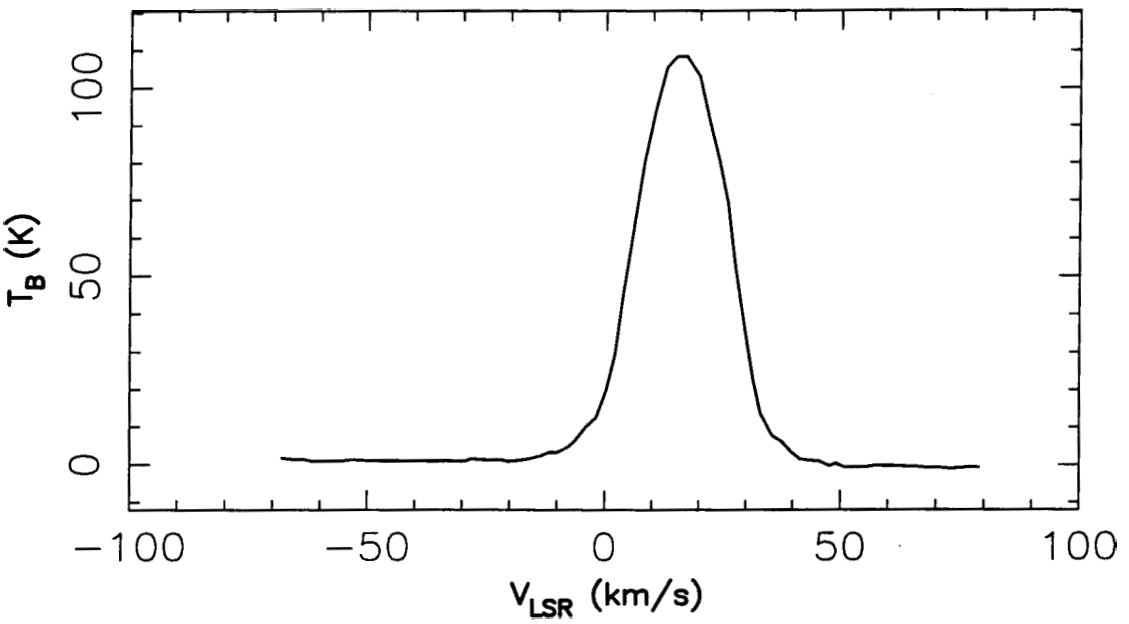

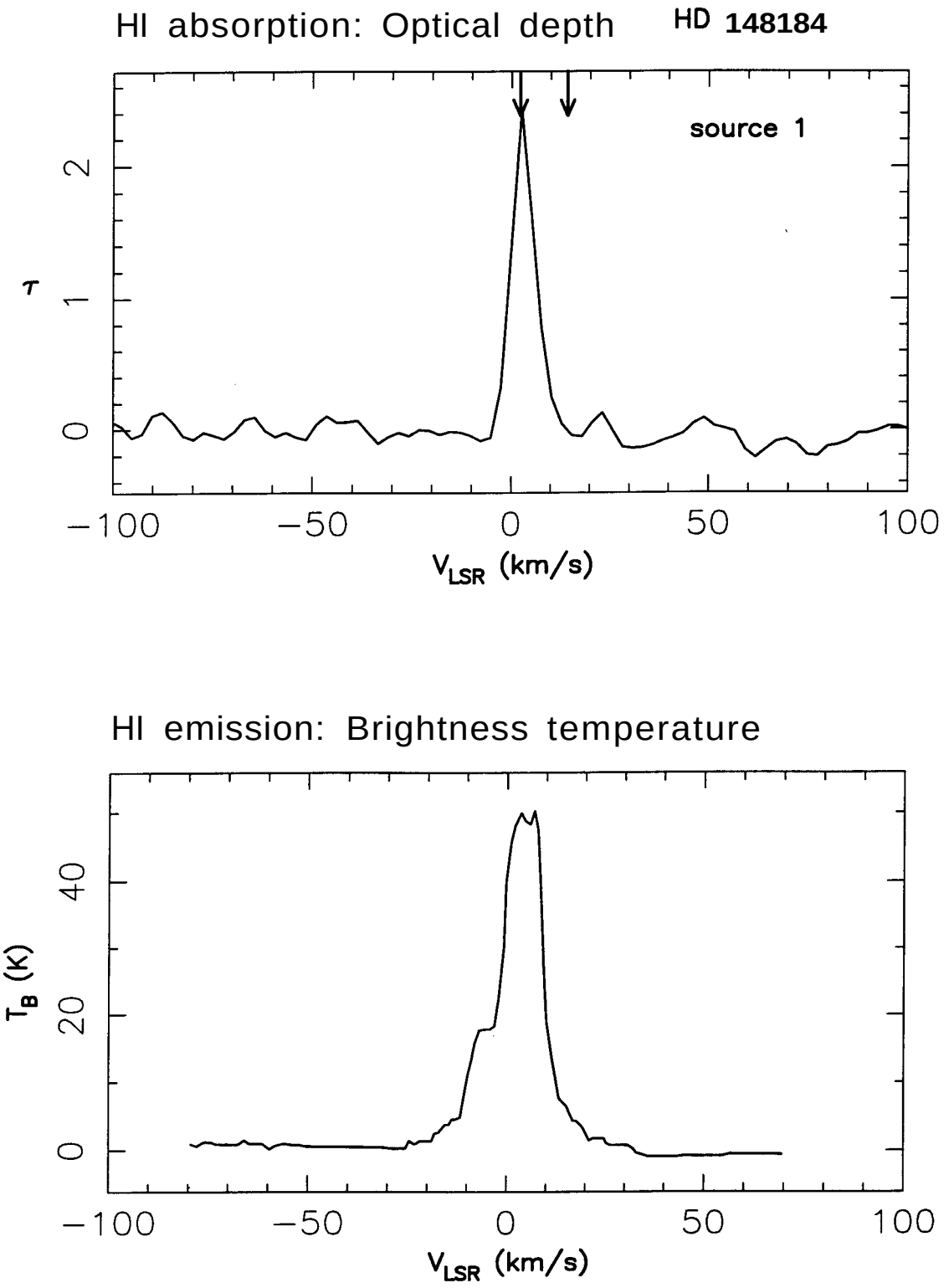

Figure 1.7: HI absorption (top) and emission (bottom) spectra towards HD

Fig 1.6 shows the HI absorption spectrum towards HD 42087. In this field also we have 2 radio sources within the primary beam. The spectrum towards one of them is shown. An absorption feature is seen at 12.4 km s^{-1}. This probably corresponds to the optical absorption feature seen at 10.2 km s^{-1}. The HI emission spectrum also shows a broad peak at $\sim$ 15 km s^{-1}. If the absorption arises in this feature, the estimated spin temperature is $\sim$ 112 K (Table 1.3). There is no HI absorption at velocities corresponding to the other optical absorption features, indicated by arrows on the velocity axis. The radio source in this case is more than 30' from the star, which is at a distance of 1.3 kpc (table 1.1). Hence it is possible that the gas we sample in HI absorption is different from the gas seen in optical absorption.

Fig 1.7 shows the spectrum towards HD 148184. Again, we detect HI absorption at low velocities coincident with the optical absorption. The HI emission spectrum also shows a peak at these velocities. The derived spin temperature is $\sim$ 50 K (Table 1.3). As in the other case, the high velocity optical features are missing in HI absorption and emission. We wish to emphasise again that we see HI absorption coincident with optical absorption at low velocities in almost all fields where we detect any HI absorption. This fact is further illustrated later in this section when we discuss high velocity features. Almost all the spectra that we show there also have coincident low velocity features.

Non-coincident velocities

In a few fields, we see exceptions to the above trend, ie, low velocity HI absorption not coincident with low velocity optical absorption. We discuss these fields below.

HD 37742

The HI absorption spectrum towards the strong source near HD 37742 (Fig 1.8) shows a deep absorption feature at 9.5 km s^{-1}. *There is no absorption at higher velocities to an optical depth limit of* 0.03. The optical features are at 3.6 km s^{-1} and -21 km s^{-1}. The difference of $\sim$ 6 km s^{-1} for the low velocity features is difficult to attribute to the errors in measurement of either the optical or the HI absorption feature. We have already discussed the case of HD 42087 (Fig 1.6). Though we do see HI absorption at 12.2 km s^{-1}, near the 10.2 km s^{-1} optical feature, there is no absorption at velocities near the -4.8 km s^{-1} optical feature. The HI emission is broad and covers the range of velocities seen in absorption

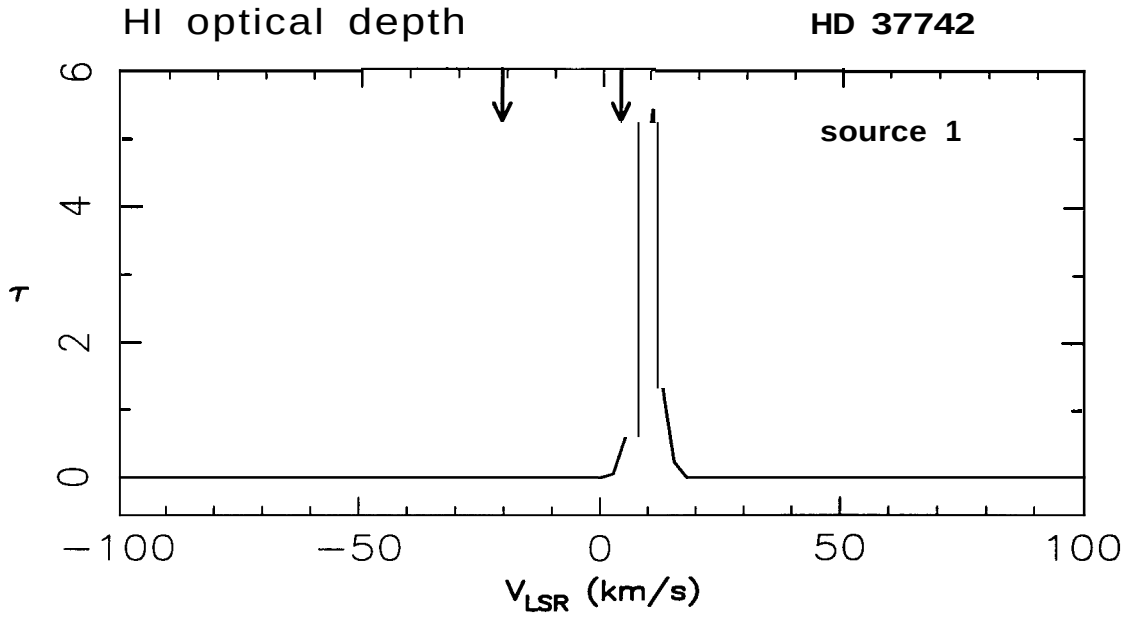

Figure 1.8: HI absorption optical depth spectrum towards HD 3742. The arrows on the velocity axis of the optical depth plot mark the velocities at which optical absorption is seen.

away from HD 42087. It could be that the gas sampled by the HI absorption is different from that seen in optical absorption. In that case the matching features seen towards HD 42087 may be a coincidence.

HD 119608

The optical absorption towards HD 119608 shows two minima at 1.3 and 22.4 km s^{-1} (Münch and Zirrin (1961). The radial component of Galactic rotation at the distance to the star is −20 km s^{-1}. Habing (1969) has observed HI emission in an extensive grid around the star. The emission spectra at many points show a similar double peaked structure with the peaks at −6 and 20 km s^{-1}prompting Habing to conjecture that the emission is in fact from the same cloud as seen in optical and that the mismatch at low velocity might be a measurement artifact. However, recent measurements towards this star by Danly et *al.*(1992) confirm this mismatch of velocities. We have 2 strong sources in this field within about 15' of the star. The absorption spectra against both these sources shows a deep feature at −5.4 km s^{-1}(Fig 1.9). This is coincident with the HI emission (seen

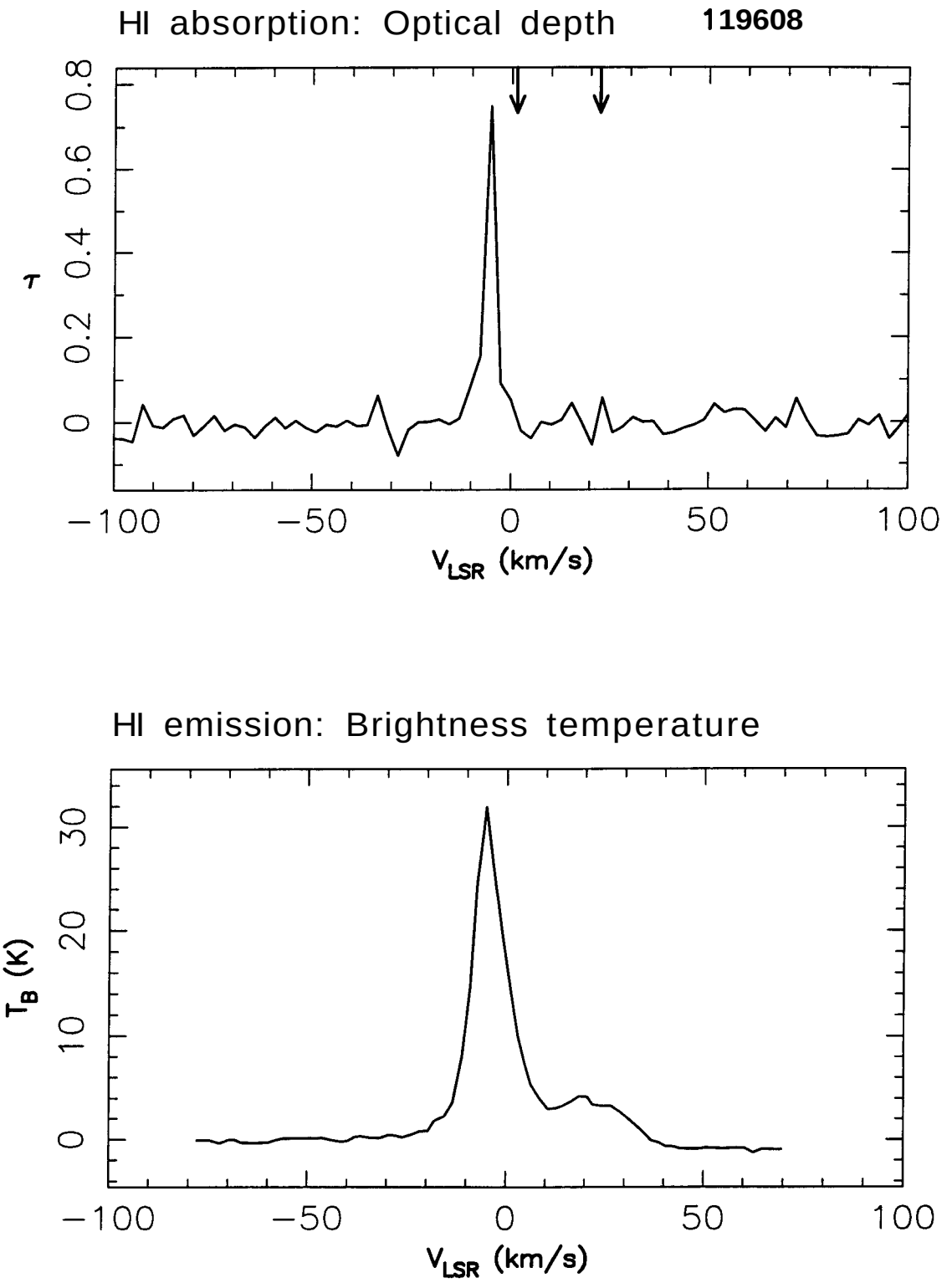

Figure 1.9: HI absorption (top) and emission (bottom) spectra towards HD

of this feature is 1 and the spin temperature 32.4 K. There is no absorption at higher velocities. This line of sight is at high Galactic latitude and samples the halo gas. Other high latitude lines of sight in our sample are discussed below and we refer to this field there as well.

1.6.2 High velocities

Here again, we discuss the absorption features under two heads, coincident and non-coincident velocities. As in the previous case the pattern of "matches" and "missing" absorption clearly emerges from the spectra.

Coincident velocities

At velocities higher than ~ 10 km s^{-1} *only 4 out of 24 lines of sight show matching HI absorption features.* Of these four, HI emission measurements exist for 2 and data from emission surveys for the others. We discuss these "coincident velocities" below. All four of these directions show $\sim$ 20 K or more HI emission temperatures at the corresponding velocities, although no distinct emission "hump" is discernible. The typical "fast" clouds are found to be missing in HI emission down to a limit of 1 K or less, as discussed earlier. *These clouds which have HI absorption features at high velocities therefore do not seem to belong to the typical fast population.* These fields which do show high velocity matches are discussed below. (Table 1.4 for details). We list the matching absorption velocities in radio and optical. The estimated optical depth of HI absorption and the derived spin temperature are also listed. For the latter we have used emision measurements from Habing (1969). In cases where this was not available, the brightness temperature seen toward the region of the star was estimated from the Leiden-Green Bank survey (Burton, 1985).

HD 14134, HD 14143

These two stars are members of the h and χ Persei cluster and seen close together in projection (Münch 1957). Both the stars are well within the primary beam and hence are included as one field (referred to as 14134-14143). There are 3 radio sources in the field all within $\sim$ 10' of the stars. The HI absorption features close to -45, -50 and -10 km s^{-1} are coincident with or near to corresponding features in the optical spectra as seen from Table 1.2. Fig 1.10 shows the HI spectra for the three sources in this field. The Galactic rotation velocity at the

Field	V_{lsr}(optical)	V_{lsr}(HI)	τ	ΔV	T_s
	km s^{-1}	km s^{-1}		km s^{-1}	K
21291	−34.0	−31.2	0.40	3.3	181
14143-	50.8	−50.3	0.30	10.0	96
14134					
14818	−42.6, −33.6				
159176	−22.5	−20.8	1.15	15.2	NA
166937	41.1	47.2	0.65	9.4	54
175754	−73.0, 29.5				
25558	10.1, 19.0				
34816	−14.0				
24912	20.7				
214680	−23.7, −14.7				
148184	14.2				
141637	−22.0				
41335	−20.8				
156110	−19.7				
199478	42.3, 61.2				
212978	−73.0				
21278	48.6				
37742	−21.0				
119608	22.4				
205637	−13.9	no absorption			
220172	−21.5, 13.5	no absorption			
38666	20.2	no absorption			
93521	−55.0, -34.0, -10.3	no absorption			

Table 1.4: Summary of coincident high velocities: Column 1 gives the HD number of the field. Column 2 lists the ***high*** velocity optical absorption seen towards the star. Column **3** is the "matching" HI absorption. Fields with no high velocity HI absorption have been left blank in this column and fields with no absorption (at high or low velocites) are marked "no absorption". Columns 4 and 5 give the fitted optical depth and width of the HI absorption features. The spin temperature is listed in column 6. As in the case for low velocity features, we have used Habing(1968) and the Leiden-Green Bank survey for the emission temperatures needed to compute the spin temperature from the optical depth.

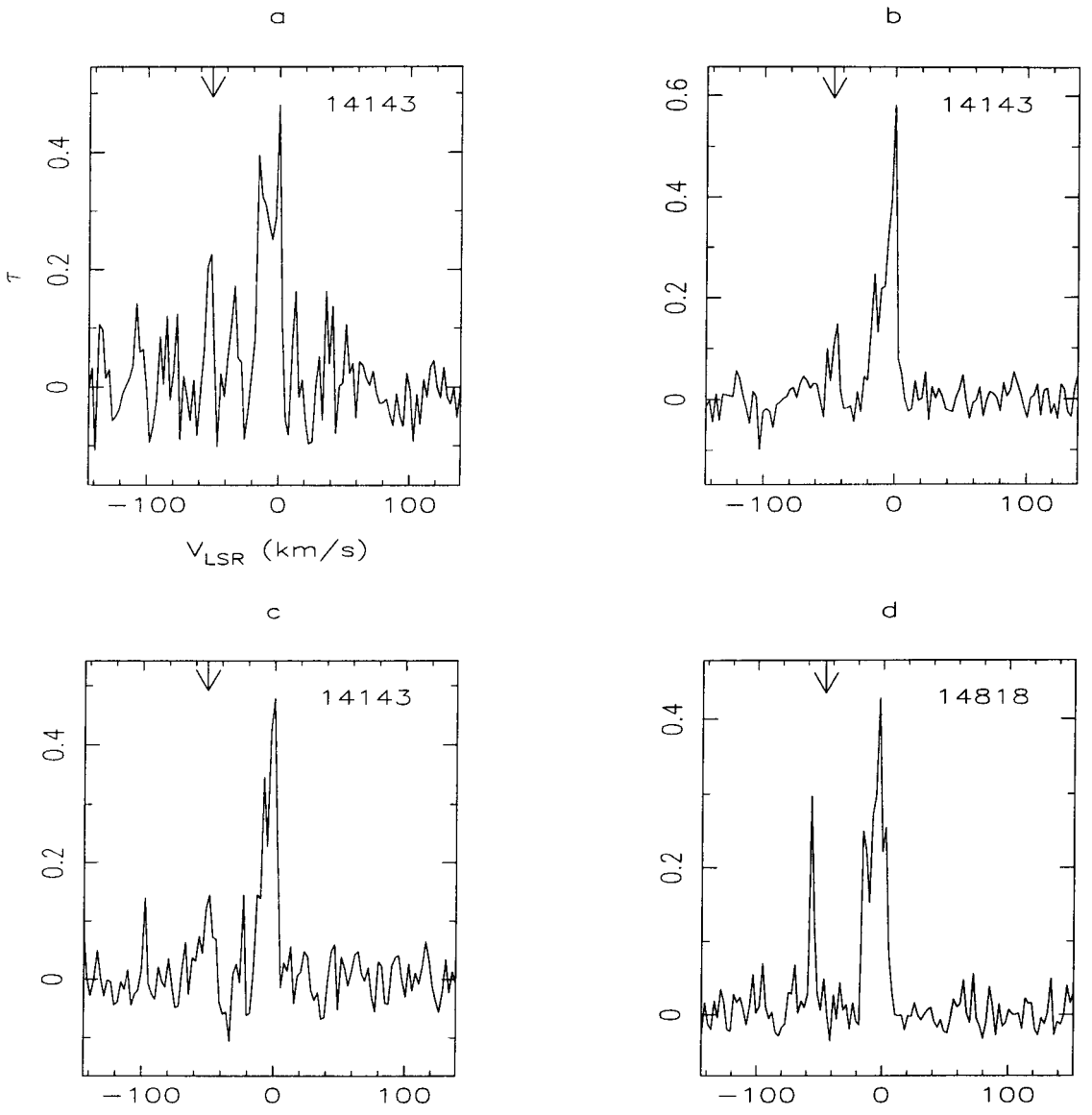

Figure 1.10: HI absorption spectra towards HD 14143 (same field as HD 14134) **(a,** b, ***c)*** and 14818 **(d).** All 3 stars are in the Perseus arm. The arrows on the velocity axis of the optical depth plot mark the velocities at which optical absorption is seen.

cannot explain the high velocity features. HI emission profiles towards this region also show a peak at ~ -50 km s^{-1}attributed to the Perseus arm. The location of the stars in Fig 1.4 also places them within the arm.The high velocity features in the optical spectra are attributed to anomalously high velocities in the Perseus arm by Münch (1957). It is known that the Perseus arm region exhibits streaming motion of the order of 10 to 30 km s^{-1}in addition to the Galactic rotation (Brand and Blitz, 1993; Blaauw and Tolbert, 1966). We conclude that the HI absorption we detect, the optical absorption, as well as HI emission all arise in this gas with anomalous motion. **Such an extended, streaming flow is not to be associated with the high velocity cloud population that we targetted in this experiment.** The derived optical depth and temperature (Table 1.3) is within the accepted range for diffuse HI gas. HD 14818 is the third star in this region of the sky that we have selected to observe. Although we do not see any HI absorption features at high velocities which coincide with those of optical lines (ref table.2), we do see a feature at -55 km s^{-1}towards more than one source in this field (Fig 1.10), as in the neighbouring field. All three stars are in the Per OB1 association (which include the h and χ clusters), a fact which may be of significance as we discuss next.

HD 21291

The spectrum of the star has a prominent Na D line at a velocity of -34 km s^{-1}(Münch, 1957). The HI absorption spectrum (Fig 1.11) shows a feature at -31.2 km s^{-1} ($\tau = 0.4$). The background source flux is 123 mJy and its angular separation from the star is $\sim$ 36'. The expected Galactic rotation velocity at the distance to the star is $\sim$ 10 km s^{-1}indicating that the absorption arises from a cloud with high peculiar velocity component. The star, however, is near the Perseus arm as seen in Fig 1.4. As mentioned in the above case of the 14134-14143 field, this region does show systematic streaming flow. HI emission from the Leiden-Green bank survey show fairly large temperatures (> 25 K) at this velocity (-31 km s^{-1}), and the temperature contours show spatially extended emission. This gas could be the same as seen in HI absorption even though the line of sight sampled is 36' from the star. The star is in the Cam OB1 association. The optical spectrum also shows a low velocity feature at -8 km s^{-1}and we see a nearby HI absorption component at -7 km s^{-1}. Absorption is also seen against two other weaker sources ($\sim$ 25 mJy) within the field, but

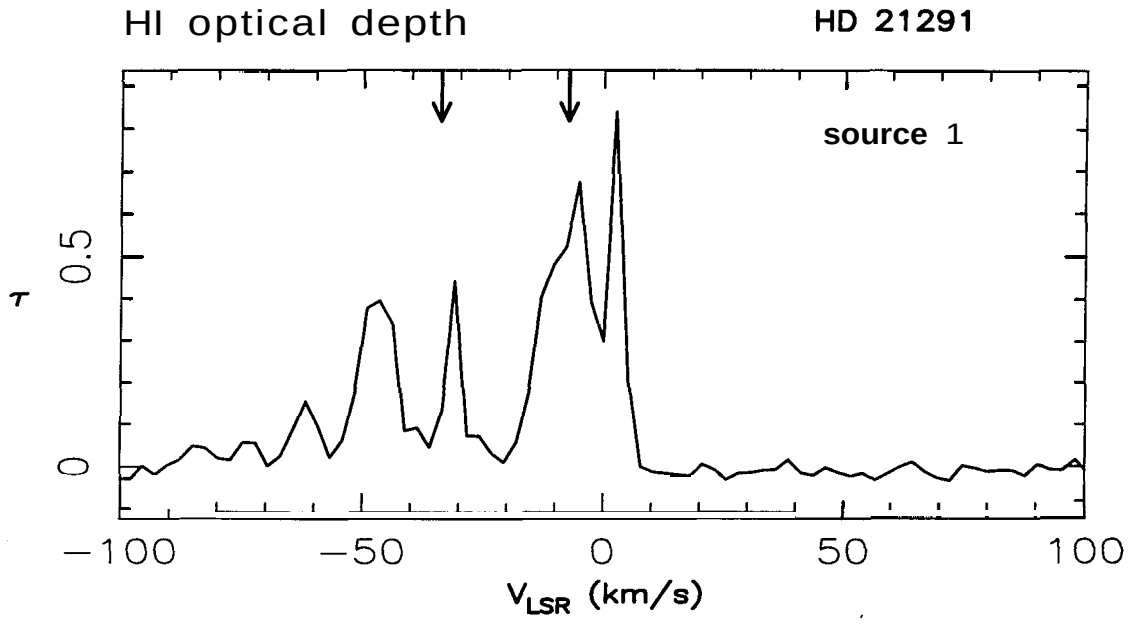

Figure 1.11: HI absorption spectrum towards HD 21291. The arrows on the velocity axis of the optical depth plot mark the velocities at which optical absorption is seen.

HD 166937, HD 159176

Both these stars are close to the Galactic center direction. The high velocities seen in opticalabsorption cannot be explained in terms of the radial component of the Galactic rotation velocities expected in this direction. The HI emission profiles (Takakubo 1967, Goniadzki 1972) show high emission temperatures at the correponding velocities. In the case of HD 166937, there is no strict coincidence (within 3 km s^{-1}) between the HI and optical absorption at high velocities. However, we see two HI absorption features at velocities close to and straddling the optical feature (Table 1.3) and so we include this field in our list of high velocity coincidences. Fig 1.12 and 1.13 show spectra towards these fields. These two fields are exceptions to the trend that clouds don't show HI absorption at high velocities. *Interestingly, they also show considerable emission levels at corresponding velocities.*

Absence of high velocity HI absorption features

The four cases listed above turn out to be the exceptions to the rule. *In all other*

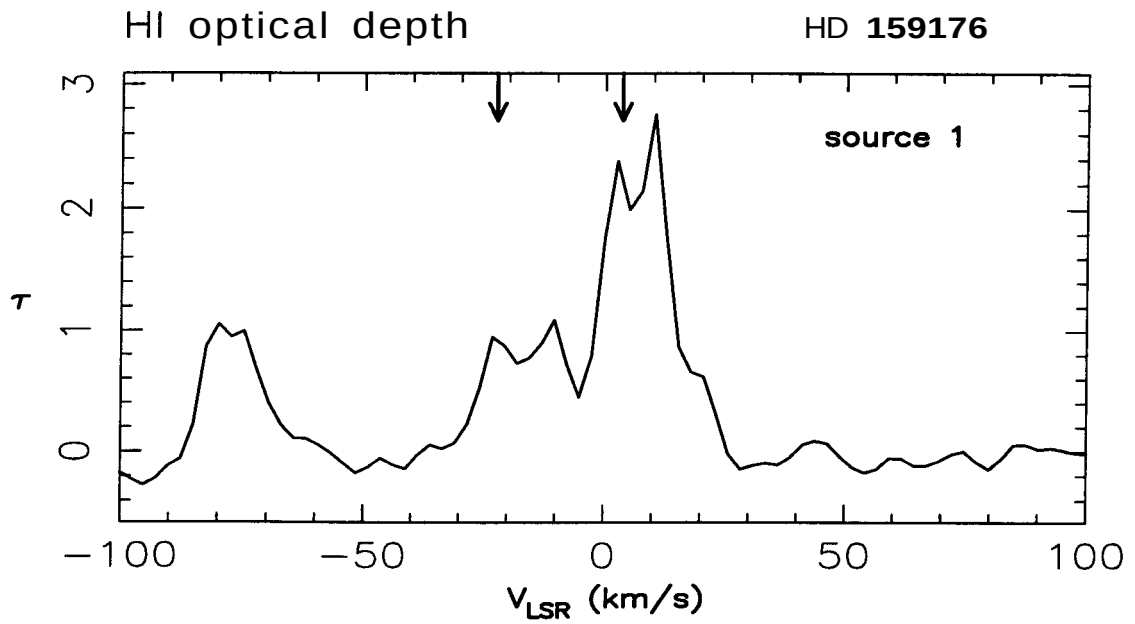

Figure 1.12: HI absorption spectrum towards HD 159176. The arrows on the velocity axis of the optical depth plot mark the velocities at which optical absorption is seen.

high velocity optical absorption. As mentioned before, we have probed to optical depths of ~ 0.1 in lines of sight less than a parsec from the star. We illustrate the typical result we see in most of our sample with 3 select spectra in Fig 1.14, 1.15 and 1.16, towards fields HD 199478, HD 175754, and HD 21278 respectively. The HI emission towards all these fields also shows no features at high velocities as can be seen from the emission spectra from Habing (1968) which have been reproduced for comparison.

1.6.3 Fields with no measured HI absorption

In the fields containing the stars HD 38666, HD 93521, HD 205637 and HD 220172, **we do not detect any HI absorption at all, even at low velocities.** These are all high latitude stars. Typically, the emission spectrum shows weak emission at low velocities coinciding with the low velocity optical absorption. The high latitude lines of sight sample gas which differs considerably from the gas in the disk. This has been the conclusion from previous investigations as well. For example the star HD 93521 is a distant halo star and has been extensively

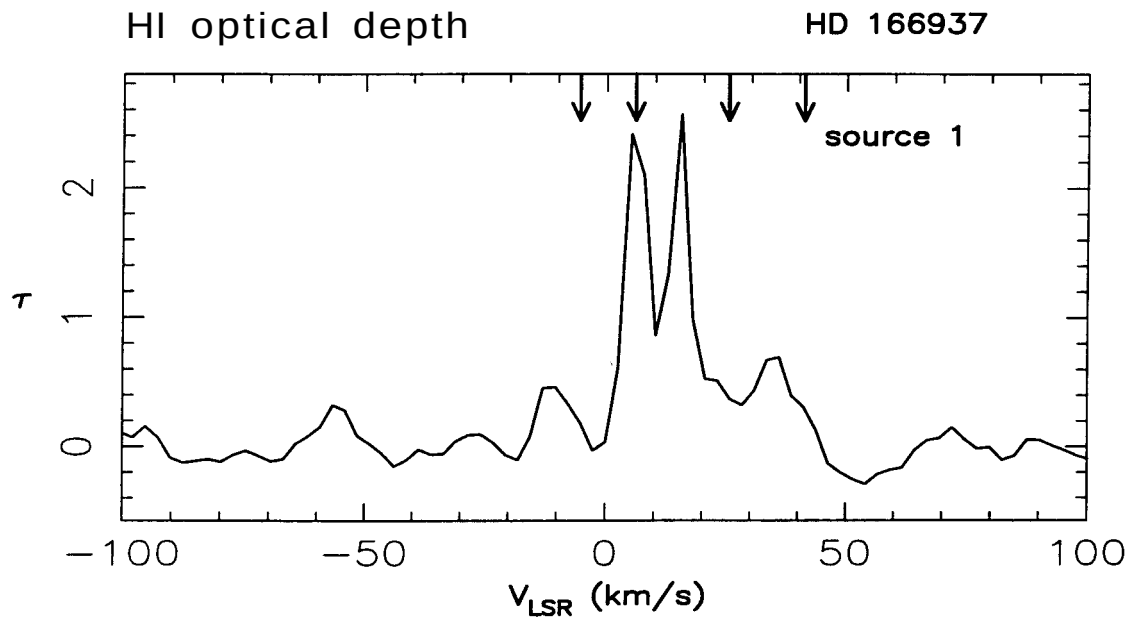

Figure 1.13: HI absorption spectrum towards HD 166937. The arrows on the velocity axis of the optical depth plot mark the velocities at which optical absorption is seen.

these previous investigations are summarized below.

HD 93521

HD 93521 shows optical absorption at velocities as high as -54.6 km s^{-1}. Habing (1968, 1969) detected HI emission at velocities ranging from -40 to -60 km s^{-1} in a grid of points around the direction of the star which he attributed to a gas complex in the region (Blaauw and Tolbert 1966). We have 2 sources in the field within 30' from the star. There is no absorption feature seen towards either of these to a detection limit in optical depth of 0.2. Fig 1.17 shows one of the absorption spectra along with the weak emission towards this star from Habing (1969). HD 93521 is a well studied star since it offers a line of sight through the warm gas in the halo. There is evidence for a large number of high negative velocity CaII components (Welty, Morton and Hobbs 1996) towards this distant halo star. A detailed study of UV absorption lines and comparison with optical absorption and HI emission data (from Danly et *al.*1992) has been done towards this line of sight by Spitzer and Fitzpatrick (1993). They identify nine absorption

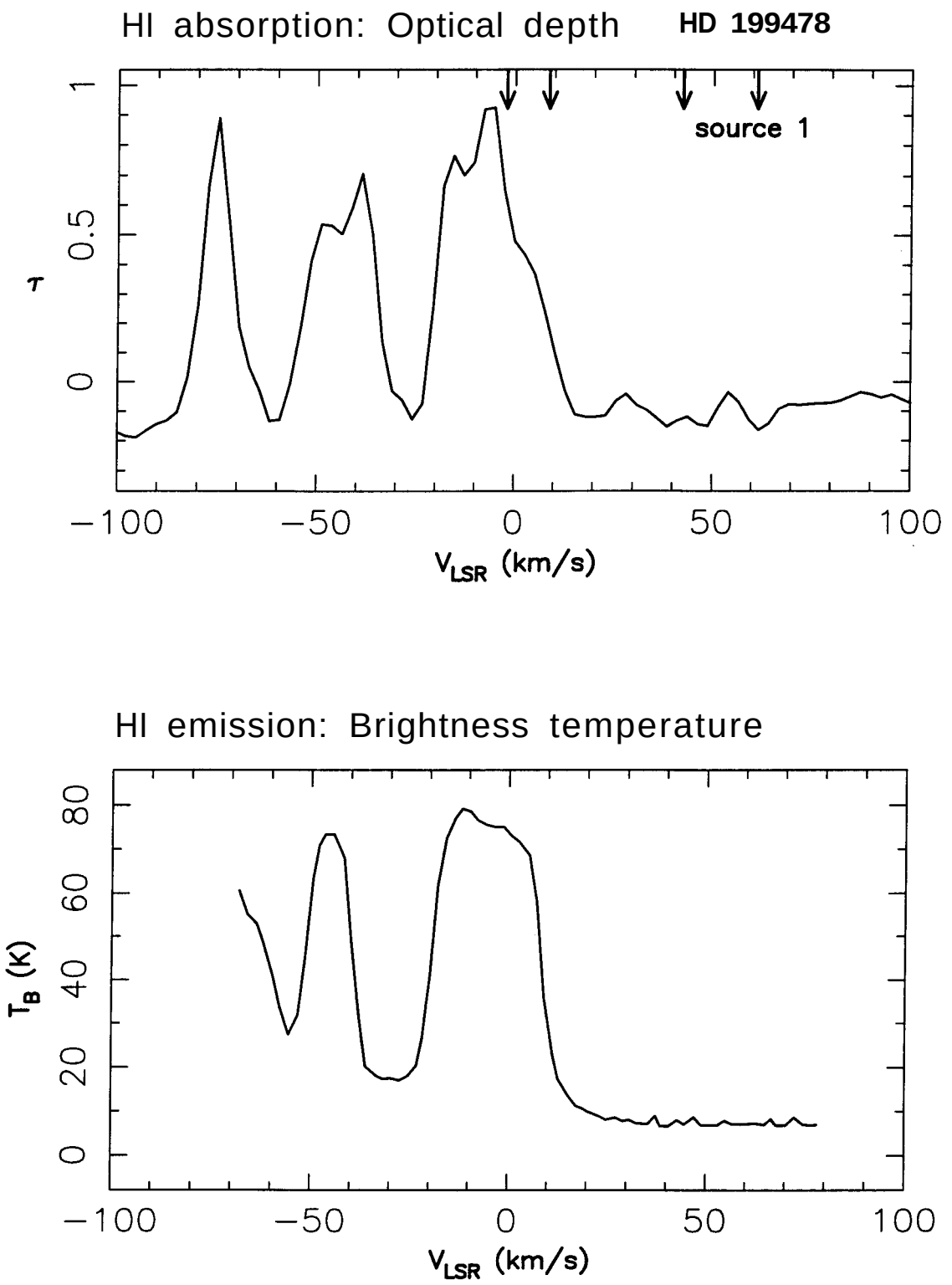

Figure 1.14: HI absorption (top) and emission (bottom) spectra towards HD

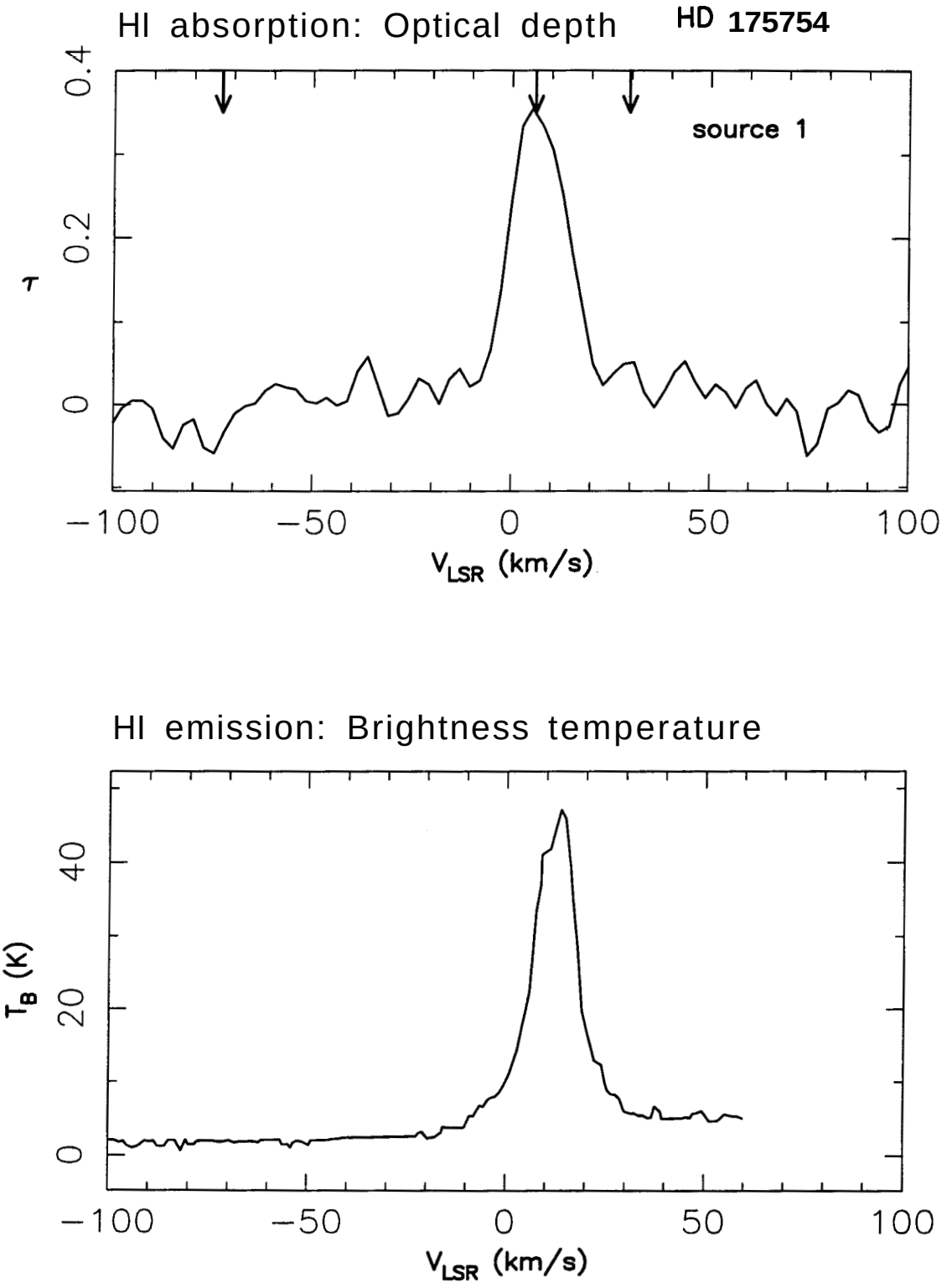

Figure 1.15: HI absorption (top) and emission (bottom) spectra towards HD

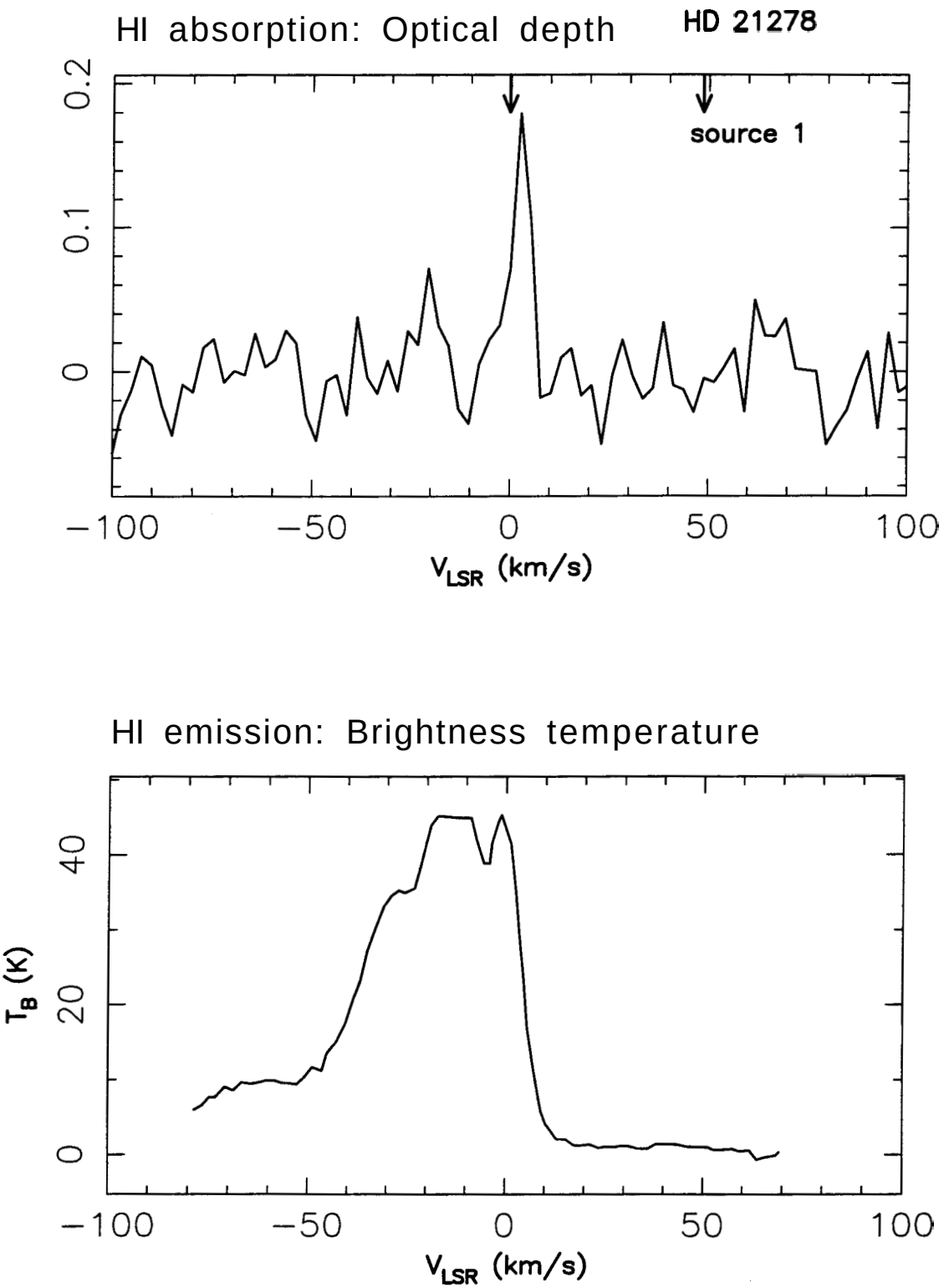

Figure 1.16: HI absorption (top) and emission (bottom) spectra towards HD

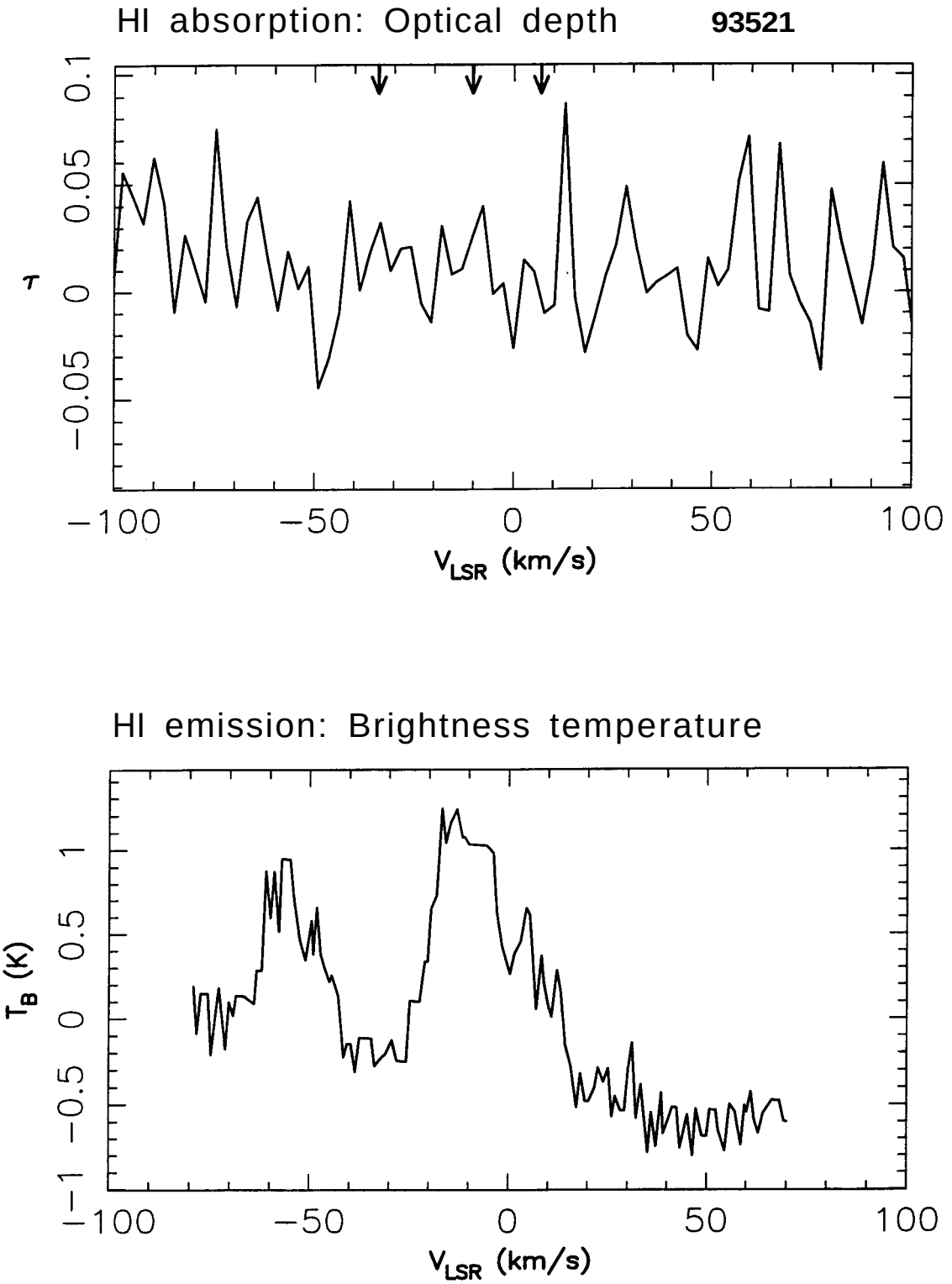

Figure 1.17: HI absorption (top) and emission (bottom) spectra towards HD

Warm Neutral Medium (also consistent with HI emission). Depletion of metals in these clouds is low. The absence of cool diffuse clouds towards this star is remarked upon in this study. Their temperature estimates for the gas in this line of sight is of the order of 6000 K and optical depths would be well below our detection limits. This field is atypical and the interstellar gas towards this star differs in nature from that in the disk.

These fields then sample some component of the halo gas and/or local gas at high latitudes. The fact that we do not detect any HI absorption towards even the low velocity components towards these directions is peculiar and may indicate the atypical nature of the gas as compared to the in-disk lines of sight.

1.6.4 Summary and Conclusions

In the preceding section we described *the first attempt to directly compare HI absorption with optical absorption features arising in the ISM*. We summarize below the main results:

1. *HI absorption measurements were carried out towards 24 fields. Each field has existing optical absorption spectra towards a bright star in the field. In 20 of these fields we detect HI absorption features.*

2. *In all but 4 of these 20 fields, we detect HI absorption features at low (< 10 km s^{-1}) velocities coincident with the optical absorption features.*

3. *Most of the low velocity optical features are also seen in HI emission.*

4. *The spin temperatures derived by us for the low velocity gas is consistent with that of cold diffuse HI clouds. In short, our results confirm that the low velocity features arise in the cold component of the ISM and that this population of HI "clouds" is to be identified with the "clouds" of Adams, Blaauw, Munch et al..*

5. *While comparing the low velocity features seen in the radio with those in the optical, it must be kept in mind that some of the "matches" could be chance coincidences. Some of the low velocity gas is likely to be from the local ISM and is seen in most lines of sight at low to intermediate latitudes. Given the ubiquitous nature of the low velocity gas, this eventuality cannot be ignored, especially in a limited sample. Nonetheless, it is clear from statistical tests (Habing 1969) that a significant fraction of the low velocity "matches" are*

6. *In 20 out of 24 fields surveyed, we see no HI absorption corresponding to optical absorption at high velocities. In most of these fields, previous emission measurements also failed to detect emission at high velocities. We have sampled lines of sight as close as .03 pc to the star and to optical depth limits of 0.2 or better. The column density of HI towards these directions deduced from the Leiden-Green Bank emission survey is typically very low or not detected at all. For e.g. the N_{HI} is often $<10^{18}$ cm^{-2} over a 2.5 km s^{-1} interval centered at the optical absorption velocities (this velocity width is typical for HI absorption in the ISM).*

7. *The lack of HI emission at high velocities could possibly have been attributed to beam dilution efects. Our absorption experiment rules out this as a generic explanation, since we have sampled gas very close to the star with resolution comparable to the optical observations. Small dense clumps are thus unlikely unless they have very little HI content and/or sizes much less than a parsec.*

8. *At velocities higher than 10 km s^{-1}, only 4 out of the 20 fields show HI absorption at velocities coincident with the optical absorption. In each of these 4 fields, existing measurements show HI* **emission** *at these high velocities as well. There are indications that these features arise in large scale streaming motion associated with spiral arms rather than from random motions and are therefore distinct in nature from the rest of the high velocity features.*

1.7 Discussion of the low velocity population

As summarized above, our study clearly indicates that the low velocity clouds seen in optical absorption are to be identified with the standard HI clouds seen in 21 cm emission and absorption. This section is devoted to a discussion of this finding.

Clouds seen at low velocities in optical absorption usually have HI emission counterparts (for e.g., Habing 1969). The column densities suggested by the emission measurements are of the order of 10^{20} cm^{-2}, which is the range of column densities seen in the usual diffuse HI clouds. Independent measurement of the HI column densities can be arrived at from the optical and UV absorption features. This is, however, a difficult task for two reasons. In the optical, the large scale

(and will discuss in detail in the next section), the relative abundances of these elements are known to be affected by depletion into dust. To further comlplicate matters, the depletion has a strong velocity dependence. As for the UV lines, poor velocity resolution hampers any effort to identify individual components and establish column densities. To our knowledge, the only attempt to circumvent these difficulties has been by Martin and York (1982). These authors have looked at 18 selected UV absorption lines of H_2, CII, NI, NII, OI, SII, PII and ArI. The method involves using the weaker transitions (which are unlikely to be saturated and therefore less corrupted by blending) to identify the velocities of the main components, and using these velocities as initial guesses to fit the profiles from the stronger transitions. Additional components were introduced if and only if the fit refused to converge. Once the components were identified, the line widths and column densities of elements which are known to suffer the least depletion were used to determine the HI column densities. Thus they establish models for the absorbing clouds in the line of sight which best fit the profiles. These then lead to HI column densities. Unfortunately, this attempt has been made only for two lines of sight towards Perseus. The results from this study indicates that for the low velocity clouds, the derived HI column densities are in the range of a few times 10^{18} to 10^{20} cm^{-2}. Clearly this is consistent with the values mentioned earlier.

The optical low velocity clouds are known to follow galactic rotation. Their longitude - velocity diagrams indicate the "double sine" curve (section 1.3) which is the signature for Galactic rotation (Siluk and Silk, 1974; Welty, Morton and Hobbs, 1996). The same is true for the clouds seen in 21 cm emission and absorption.

The clinching piece of evidence comes from our study, where we look at absorption from optically identified couds for the first time. Using existing emission measurements we derive spin temperatures for these clouds. These values for the spin temperatures have to be viewed with caution since they represent a harmonic mean of the HI temperatures in the line of sight and the low velocity spectral features suffer from blending effects. The range of temperatures (see table 1.4) is roughly

1.8 Discussion of the high velocity population

As briefly summarised in section 1.1.1, there exists clear evidence for the existence for two populations of interstellar clouds as seen in optical absorption. Surveys of CaII and NaI absorption lines towards bright stars (at distances upto 2 kpc) in all directions reveal low ($<$15 km s^{-1}) and high ($>$15 km s^{-1}) velocity features. In a study of the velocity distribution of these features, Blaauw (1952) fitted an exponential distribution of the form $e^{|v|/\mu}$ where μ is the mean radial velocity without sign. The best fit was obtained for a value of 5 km s^{-1} for μ for stars within 500 parsecs. This work ignores the possibility that there may be two distinct populations of clouds and therefore two different distributions. As we have stated, there is evidence for differing physical parameters for the low velocity clouds as compared to the high velocity ones. Whether one fits a single distribution or appeals to two distributions, the existence of the high velocity tail in the distribution of velocities cannot be questioned. In the radio wavelengths, some evidence for the existence of a fast population seen in both HI absorption (Radhakrishnan and Sarma, 1980; Anantharamiah Radhakrishnan and Shaver, 1984) and emission (Kulkarni and Fich, 1985) were summarized in Section 1. The picture is less clear than in the optical and the correspondence between the HI clouds and the optical clouds is a wide open question.

Previous studies reveal that HI emission towards the high velocity clouds is weak or non-existent. Our investigation shows that there is little or no HI absorption either. This prevents us from making a meaningful estimate of the spin temperature of the gas, except to comment that it is probably a warm component. Several scenarios have been proposed by previous investigators to account for the clouds "missing" in HI emission. We review some of them in the light of our new results.

1.8.1 Are high velocity clouds circumstellar?

The high velocity clouds show an apparent excess of negative velocities as noted by Blaauw (1952), Searle (1952) and Schlüter, Schmidt and Stumpff (1953). The distribution of velocities from Adams' sample is shown in Fig 1.18 (Spitzer, 1968). Of 64 stars with high velocities ($>$ 15 km s^{-1}), 41 show negative residual (LSR) velocities, 18 are positive and 5 show both negative and positive velocities. This effect prompted Schliiter, Schmidt and Stumpff (1953) to conjecture that these

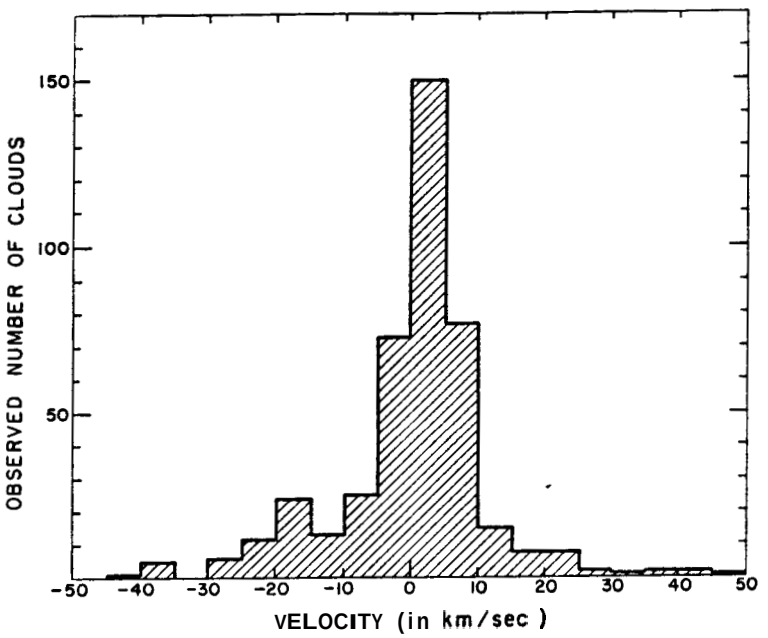

Figure 1.18: Histogram of absorption velocities of CaII from Spitzer (1968), showing the apparent excess of negative velocity components. The velocities (LSR) are from Adams (1949). Each vertical bar shows the number of such components within a velocity interval of 5 km s^{-1}.

stars which are being accelerated away from them by the effects of stellar winds and radiation. Mechanisms for accelerating clouds in the vicinity of hot stars include the "rocket effect" proposed by Oort and Spitzer (1955). The ionizing radiation from the star causes a stream of ionised particles to stream away from the cloud surface facing the star. The momentum imparted by this flow causes the cloud to accelerate away. Such clouds would appear to be approaching the observer when seen in absorption against the star. This scenario cannot explain the presence of positive velocities seen in absorption. It could be argued that the positive velocities occur in cases where the gas is being accelerated by a star near the line of sight and seen in absorption against the target star. In our sample, there are 8 cases of ***positive*** velocities which cannot be explained by Galactic rotation. Only one out of these stars is in the vicinity of an OB association, making the above hypothesis unlikely. In addition, given the fact that most of the stars in our sample were selected not to belong to star forming regions like Orion, anomalous velocities seen in circumstellar environments are not likely to explain all the high velocity components. The excess of negative velocities is inferred from a small sample and it is only marginally significant. Hence any interpretation is to be viewed with caution. Moreover, velocities in excess of 50 km s^{-1} are not easily generated by the rocket effect. Following Spitzer (1968), the acceleration of the cloud is given by

$$M_c \frac{dv}{dt} = -V \frac{dM_c}{dt}$$

where M_c is the mass and v the velocity of the cloud, and V is the velocity of the outflow of mass. This velocity is equated to the sound speed in the ionized region of the cloud. Given reasonably uniform distribution of masses and other quantities, the number of components in the velocity interval v to v + dv can be shown to be proportional to $e^{-v/V}$. Comparing this to the distribution of high velocity components in Adams' data, Spitzer came to the conclusion that the sound speed would have to be as high as 20 km s^{-1} to explain the observations. This would be close to the limit for the velocity of sound in HII regions (Spitzer 1978). Based on the premise that the high velocity clouds are ionized, Pottasch (1972) came to the conclusion that the energy requirement to accelerate and ionize the cloud is unlikely to be provided in the lifetime of an O star. These arguments to the contrary notwithstanding, the circumstellar scenario cannot be ruled out. Indeed, the rocket mechanism is known to operate in clouds seen in the vicinity of bright stars (see for e.g. Spitzer 1968). One would expect a subset

We wish to point out that earlier studies have also considered the possibility that the clouds could be almost completely ionized. Heiles (1974) examined the HI distribution near some of the stars in Habing's list at higher sensitivity levels. This study revealed weak broad HI features at or close to the optical velocities, which appear nearby in the sky but not at the postion of the star, suggesting ionized gas. An attempt by Reynolds, Scherb and Roesler (1973) to look for Hα emission from five clouds in Habing's list failed to reveal their presence. This study, however, does not go down to the emission measure levels estimated by Heiles, which are of the order of 0.2 cm^{-6} pc. As stated before, Pottasch (1972) had concluded that it was unlikely that a cloud could be completely ionised and accelerated to high velocities by an O star during its lifetime, making this scenario improbable.

1.8.2 Are the fast clouds old Supernova Remnant shells?

In one of the early studies of the optical high velocity features, Siluk and Silk (1974) attributed them to very old SNRs in the line of sight. In order to examine this proposition, we briefly recall the evolution of a supernova remnant in the ISRI. Assuming spherical symmetry, and hydrodynamic behaviour (i.e, the mean free path of the particles constituting the expanding remnant is much lesser than the size of the remnant thereby allowing the approximation to a fluid), SNR evolution in a homogeneous medium follows four stages (for a comprehensive review see Woltjer 1972).

Phase I: Free expansion

At time t_0, let a mass M_0 be injected into the cold ISM at density ρ_0 by the supernova explosion. The total energy injected (both thermal and kinetic) is ϵ_0. R is the radius of the shock wave and $\frac{d\epsilon}{dt}$ is the radiative loss from the remnant. Initially, $M_0 \gg \frac{4}{3}\pi\rho R^3$ and the remnant expands freely in the ambient medium.

Phase II: Adiabatic expansion

During this stage,$M_0 \ll \frac{4}{3}\pi\rho R^3$. For a strong adiabatic shock, $\rho_{shocked} = 4\rho_0$ and $P_{shocked} = 3/4\ \rho_0 V^2$, implying the temperature behind the shock,

$$T_{shock} = \frac{3}{16}\frac{m}{k}V^2 \tag{1.9}$$

where m is the mean mass per particle behind the shock front moving with a

K, the radiation from interstellar gas is primarily through free-free emission from H and He atoms. This is the condition during phase II. The radiated energy is negligible compared to ϵ_0. A self-similar solution (Taylor, 1950; Sedov, 1959) describes the evolution as,

$$R = 1.17(\frac{\epsilon_0}{\rho_0})^{1/5} t^{2/5} \tag{1.10}$$

giving

$$V = \frac{2}{5}\frac{R}{t} \tag{1.11}$$

The above two equations show that $\mathbf{R^3V^2}$ is a constant, i.e the kinetic energy is conserved. Thus, both kinetic and thermal energies are separately conserved during the adiabatic or Sedov phase. Nearly half of the mass inside the remnant is concentrated in a shell of thickness aproximately 10% of the radius of the remnant. The temperature increases towards the interior, since the gas progressively further inward was shocked when the shock velocities were higher.

Phase III: **Snow** plow phase

As the shell slows down further, $T_{shocked}$ continues to decrease. Since the entire T_{shock} profile drops as V^2_{shock} or $t^{-6/5}$, the temperature of the shocked gas eventually falls to -- 2 x 10^5 K in 10^5 years. Below 10^6 K, line radiation from heavier elements start to dominate and radiative losses become important. Following Woltjer (1972), the integrated radiative loss becomes $\sim 0.5\ \epsilon_0$ when V = 200 km s^{-1}assuming standard parameters. For t greater than this time t_{rad}, the radiative cooling time is short. The shell is no longer driven by the thermal pressure behind the shock. The gas behind the shock cools rapidly and is compressed to high densities. The density contrast behind the isothermal shock can be as high as 100 and the shell is much thinner than before. The shell moves with constant momentum in this "snow plow" phase. The radius,

$$R = R_{rad}(\frac{8}{5}\frac{t}{t_{rad}} - \frac{3}{5})^{1/4} \tag{1.12}$$

where the subscript *rad* stands for the transition between phases II and III.

Phase IV

By the time the shell slows down to velocities of the order of the interstellar velocity dipsersion (*i.e.*, $\sim$ 10 km s^{-1}), it completely loses its identity.

The above description does not account for the magnetic pressure in the shell

starts to affect the evolution in phase II. The cosmic ray pressure cannot be neglected by the time the SNR is in phase III. We discuss these effects later in this section. With this brief summary of SNR evolution as background, we now examine the conjecture of Siluk and Silk(1974), namely that the optical absorption features arise in old SNR shells that have lost their identity in the ISM.

For the optical absorption features, Siluk and Silk fit a distribution of velocities of the form

$$N(> v) = Av^{-\alpha} \qquad v > 20 \text{ kms}^{-1}$$

where v is the velocity corrected for Galactic rotation, N(>v) is the number of CaII components in Adams (1949) data with velocities greater than v, A and α are constants. Their best fit value for a was 2. If the gas is located in supernova shells, the relation can be rewritten in terms of the diameter of the expanding shell, i.e $N(< D) = D^{\beta}$. For example, in the Sedov phase, from equation 1.10

$$N(> V) \longrightarrow N(< D) \longrightarrow N(< t) \propto t \propto D^{5/2}$$

β can be related to a in the following fashion. From equation 1.11 it follows that

$$V \propto D^{1-\beta}$$

Therefore,

$$N(< t) : N(< D) : N(> V) \propto D^{\beta} = V^{\beta/1-\beta}$$

Since we have defined $N(> v) = Av^{-\alpha}$, it follows that the index $\alpha = \frac{\beta}{\beta-1}$. If the gas seen in absorption is associated with SNR shells in the Sedov phase then α would be $\frac{5}{3}$, not very different from 2, the best fit obatined by Siluk and Silk. But they did not make this association. As stated previously, in the adiabatic phase the shell is at temperatures $> 10^5$ K and *cannot be seen in line radiation.* According to numerical computations by Chevalier (1974) much older SNRs in the radiative phase evolve according to the relation $R \propto t^{1/3.2}$, or $t \propto R^{3.2}$. In an ambient density ~ 1 cm^{-3}, these SNRs would have a velocity less than ~ 90 km s^{-1}and would be $\sim 5 \times 10^4$ years old. If the gas seen in absorption is associated with such old remnants then it would imply a velocity distribution which can be approximated by

$$N(> v) \propto v^{-3/2}$$

Although this is not the best fit they obtained, Siluk and Silk identified the high

An implicit assumption in the foregoing discussion is that the SNR shell has a large enough column density when it is in the radiative stage to be detected in the optical lines of Ca and Na. The minimum detectable column density in optical absorption is of the order of $10^{19} cm^{-2}$ (this is the equivalent HI column density). This is almost two orders of magnitude larger than the estimated column density accumulated behind a shock when it becomes radiative ($\sim 10^{17}$, Cowie and York 1978). UV absorption lines of abundant elements are sensitive to much lower column densities ($>10^{16} cm^{-2}$) than optical lines because of their larger oscillator strengths. These lines are therefore better probes than optical absorption lines to study gas in the radiative SNR shells. If indeed the lines seen in UV and optical arise in the shells of old SNRs, they form a powerful probe of the density of the medium into which the SNRs evolve. This information is of great importance to any model of the ISM. The discussion below examines the implication of this claim for two of the popular models.

A detailed comparison of interstellar UV lines of heavy elements with CaII absorption lines by Cowie and York (1978) leads to the conclusion that the velocity distributions of both sets of lines are very similar. The oscillator strength of the UV transitions they have observed are higher than those of the Ca and Na lines and so the sensitivity is higher, implying that lower gas column densities can be detected. Despite this superior sensitivity of UV over the optical absorption, the two distributions appear to be similar. This has, however, been contested by Hobbs (1984). Regarding the contribution to this distribution from SNRs, Cowie and York come to the following conclusion. If the UV and optical features are from the blast waves of SNRs in the radiative phase, the observations indicate that the interstellar density into which these SNRs evolve must be $\sim 0.1\ cm^{-3}$. The velocities and filling factor of SNRs in such ambient densities (assuming a birthrate of one per 50 years in a disk of radius 15 kpc and thickness 200 pc) are consistent with the number of absorption features seen towards stars and their velocity distribution. This is the ambient density proposed in the earlier two phase models of the ISM (Field, Goldsmith and Habing, 1969) in which cool dense HI clouds are in pressure equilibrium with a warm intercloud medium.

Are the fast clouds then surviving shells of old SNRs in the standard intercloud medium? To answer this we need also to examine the *longevity* of SNR *shells i.e.*, whether they will survive long enough (say $>10^5$ to 10^6 years) to be seen as "clouds" with velocities of the order of 50 km s^{-1}or so. In order to assess the

considered. If the energy density of the field $B^2/87r$ is comparable to the thermal energy density nkT, the field will play a significant role. The current estimates seem to suggest that the field pressure is comparable to if not more than the thermal pressure. For an rms field of 5 μG the field pressure is estimated at 7500 cm^{-3} K as compared to the usual estimate of 3000 cm^{-3} K for the thermal pressure (Boulares and Cox, 1990; Lockman and Gehmann 1991). As the ejecta expand into the ISM the ambient field lines of force will be compressed into a thin layer. The resultant high pressure tends to slow down the ejecta, causing instabilities and possible break up of the shell (Slavin and Cox 1993; Spitzer 1990). The field also affects the evolution during the "snow plow" phase. The density contrast in the swept up shell is much lower in the presence of a strong magnetic field than otherwise. For example, when the shock velocity is $\sim$ 40 km s^{-1}(implying that the shock is well into the isothermal phase for usual parameters), the density contrast i.e, $\rho_{shocked}/\rho_{unshocked}$ is $\sim (V_{shock}/C_s)^2$ where C, is the sound velocity in the ambient medium. This is $\sim$ 43 when there is no field or if the field is parallel to the shock propogation. However this is reduced to the order of $2^{1/2}V_{shock}/V_A$ (Spitzer 1990), where V_A is the alfven velocity in the ambient medium, in the presence of a magnetic field transverse to the shock such as in the remnant shown in Fig 1.19. Again, for standard parameters this value is $\sim$ 3.4. Thus the shell tends to be *significantly rarer* in the presence of a B field. The magnetic field in older SNRs as mapped by radio polarization shows a tangential configuration (Fig 1.19) (Milne, 1987). This is the configuration which reduces the density contrast. Moreover, the energy stored in compressing is released in re-expansion when the confining pressure reduces. This happens in the late stages of the SNR when the interior pressure falls due to radiative losses and the external ram pressure drops as the shell decelerates. Thus the shell tends to re-expand back to ambient densities. To illustrate this, a model of the ISM with an *isotropic* field has been considered by Slavin and Cox (1993) with a 0.1 cm^{-3} ambient density. They show that the density contrast of the shell would at most be $\sim$ 4, decreasing to 2 in 6×10^5 years. This model exagerates the role of the field. Realistically some compression occurs along the field lines and the density contrast is between the two limits mentioned above (for a summary of B field configuration following a shock and its effect on the swept up ISM we refer to a review by Spitzer, 1990). In any case, the field has a significant effect on the SNR shell. *It reduces the density of the shell, limits its lifetime, and by inhibiting the expansion rate it considerably reduces the filling factor of SNR shells in the*

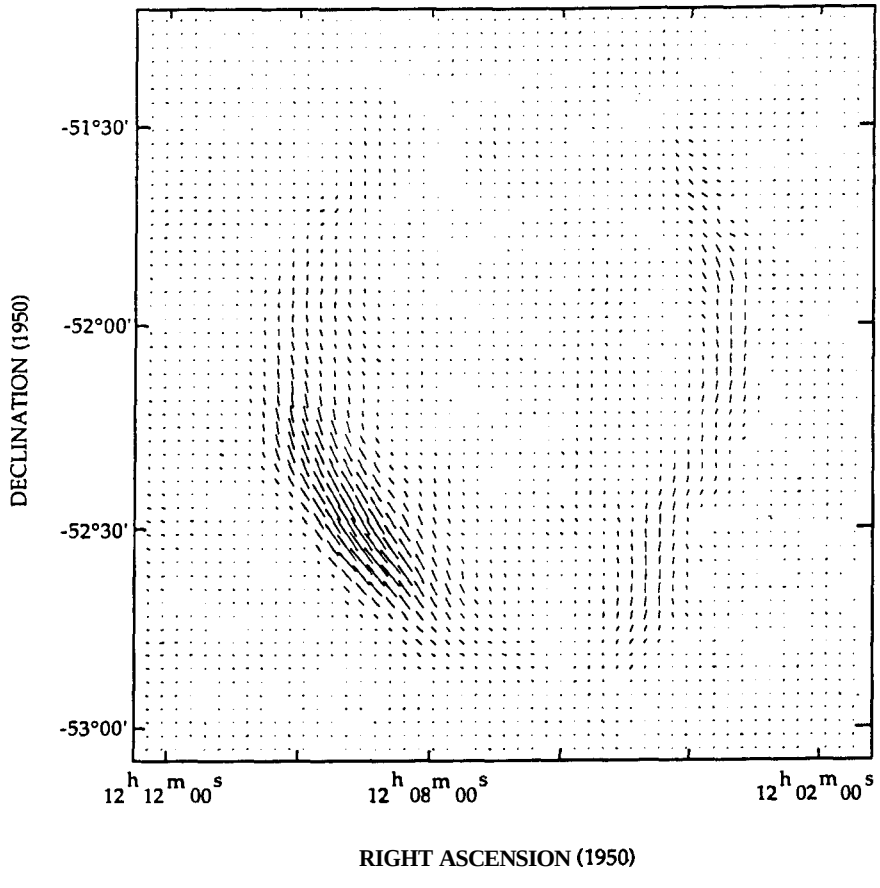

Figure 1.19: The observed magnetic field in SNR G 296.5 + 10.0 as deduced from radio polarization measurements. The magnitude of the vectors shown is proportional to the mean value of the polarization at 4.8 and 8.4 GHz. The tangential nature of the field is evident. From Milne and Haynes (1994).

ISM. These possibilities were neglected in the analysis of the UV and optical absorption measurements mentioned above, and therefore cast serious doubt on the origin of the high velocity features in SNRs.

The above discussion was on the fate of an SNR shell in the ambient densities corresponding to the standard raisin-pudding or the two phase model. Later models of the ISM, with a third phase, suggest much lower ambient densities (McKee and Ostriker 1977). In this model most of the ISM is pervaded by hot gas ($T \sim 5 \times 10^5$ K), *the Hot Ionised Medium.* Observational evidence for such a component, at least in the solar neighbourhood, comes from interstellar absorption lines of the OVI atom and diffuse soft X-ray background (0.1 to 1 KeV). The main energy source in the McKee-Ostriker model are SNRs. The two phase ISM of Feld, Goldsmith and Habing is found to be unstable to the mechanical stirring caused by SNR explosions resulting in the formation of the Hot Ionised Medium. That the filling factor of SNR bubbles may be significant was already anticipated by Cox and Smith (1974). The SNRs sweep up shells as they expand. These shells overlap forming tunnels of hot gas. Cold clouds condense at the periphery of the shells and the hot interiors form the intercloud medium. McKee and Ostriker assume energy balance between the input energy of the supernovae and the losses, mainly radiative in nature. The formation of cold clouds is offset by the destruction of clouds caught up in the SNR interior, crushed and evaporated (Fig 1.20). Thus mass balance is postulated. The velocity dispersion of cold clouds is achieved through cloud-shell collisions and is another source of dissipation. The global equilibrium of mass and energy input-output is maintained. The model predicts a spectrum of clouds with ionized edges and an onion skin structure (Fig 1.20). The ionisation is a consequence of the immersion of the cloud in the UV background from the *Hot Ionised Medium* and stars. Soft X-rays from the *Hot Ionised Medium* penetrate deeper into the cloud giving rise to a warm neutral layer interior to the ionized edge. This constitutes the *Warm Neutral Medium.* The larger clouds have a cold neutral core, the *Cold Neutral Medium.* In the McKee and Ostriker model the *Warm Neutral Medium,* the intercloud phase in the two phase model, is confined to the outer layers of cold clouds. The *Hot Ionised Medium* is the pervasive medium. Neither the classical Field, Goldsmith and Habing model nor the McKee and Ostriker model fully satisfy observational constraints (see review by Cox and Reynolds, 1987). We have already discussed a serious difficulty with the high filling factor of SNR

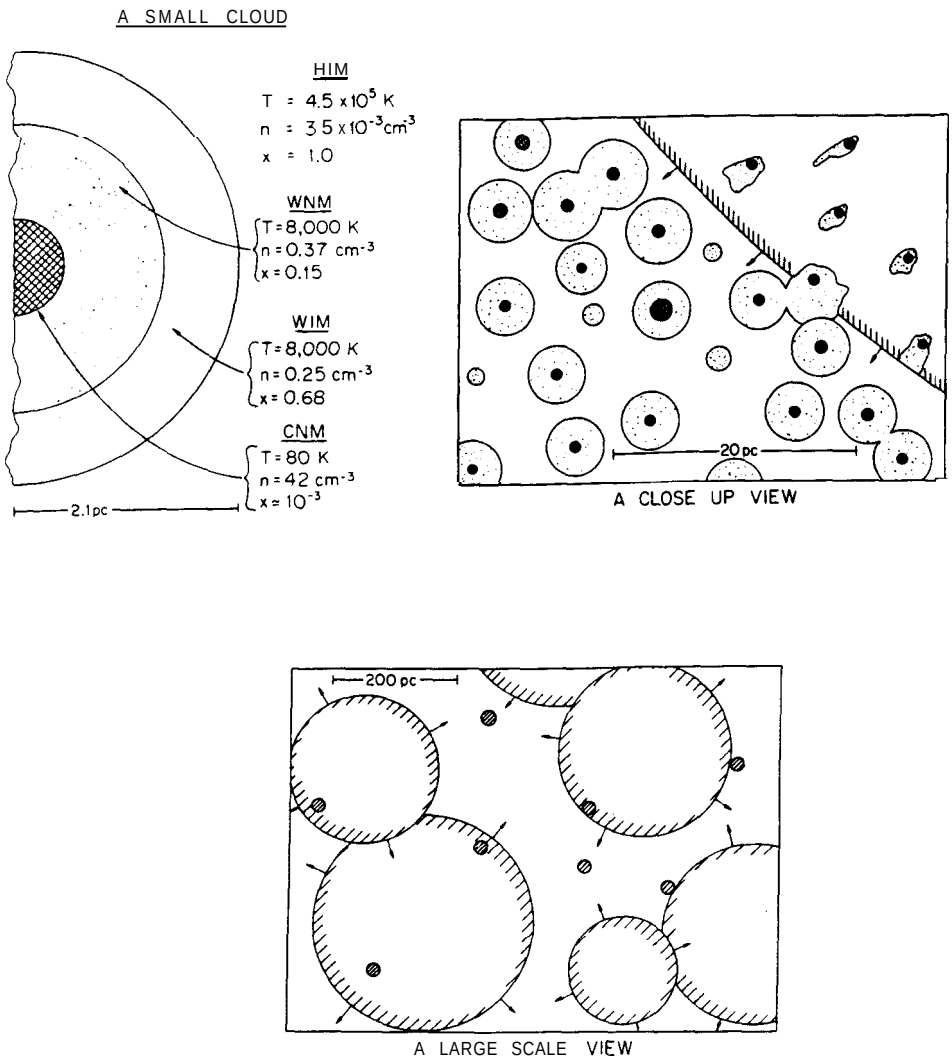

Figure 1.20: Reproduced from McKee and Ostriker (1977). a: Cross section of a characteristic small cloud. The hatched lines show the core, which gives rise to the optical lines. The next layer is the Warm Neutral Medium produced by the soft X-ray background. The outer layer is the Warm Ionized Medium produced by stellar UV radiation. Typical values of hydrogen density n, temperature T and ionization fraction x are shown. **b:** A cross section of a representative region of the ISM 30pc x 40pc in size, with area of the features approximately equal to the filling factor. A supernova blast wave is expanding into the region from the upper right. The size of the hatched cores of the clouds is $\sim$ 0.4 to 1 pc. The warm envelopes are $\sim$ 2.1 pc. A few clouds are too small to have cores. The envelopes are distorted inside the SNR. ***c:*** A region of the ISM 600 x 800 pc in size. Only SNRs with R $<$ 180 pc and clouds with a $>$ 7 pc are shown.

ambient medium into which the SNR shell expands, we once again discuss the possible origin of the high velocity optical and UV absorption features in these shells.

If SNRs are expanding into the *Hot Ionised Medium* whose density is ~ 0.003 cm^{-3} and temperature $\sim 5 \times 10^5$ K, and were to be seen in absorption in optical and UV in their isothermal phase, the observed distribution would fail to match the predicted one (Cowie and York, 1978). The high filling factor would imply that a larger number of remnants would appear in a given velocity range than is seen. This difficulty can be overcome if the ambient density is low enough for the blast waves to remain non-radiative till they intersect or escape from the Galaxy. If this is true, *none of the observed features can arise in SNR shells.* The density limits derived from such a constraint are consistent with the Hot Ionised Medium density (~ 0.003 cm $^{-3}$). Indeed Cowie and York concluded that if the coronal gas (or Hot Ionised Medium) has a large filling factor, then the optical and UV absorption lines cannot be attributed to absorption in old SNR shells.

To summarize the above discussion,

- *It is unlikely that the interstellar aborption lines arise in old SNRs that have lost their distinct identity.*

- *If the SNRs expand in the standard, relatively dense intercloud medium then it is very likely that the compressd shells will re-expand due to the pressure of the amplified magnetic field in the Shell. If so, the dense SNR shells with HI column densities* $\sim 10^{19}$ cm^{-2} *will not survive for times* $\sim 10^6$ *years which would be necessary for this scenario to be viable.*

- *If the coronal gas predicted by Spitzer has a large filling factor, as envisaged by McKee and Ostriker, then they will become radiative and develop dense shells only at much larger radii than their counterparts expanding in the dense intercloud medium. Such SNR bubbles will therefore have a much larger filling factor. Again, on account of this, the scenario proposed by Siluk and Silk is untenable.*

Unfortunately our observations cannot impose constraints on this hypothesis for the origin of high velocity absorption features. The column densities swept up by the SNR shells in the radiative stage are expected to be of the order of 10^{19} cm^{-2} or less. Given such a column density, even if the temperature of this gas is ~ 100 K the resultant optical depth would be below the limits upto which

1.8.3 Shocked clouds

The preceding discussion leads us inescapably to the conclusion that the most plausible explanation for the high velocity features are that they are clouds engulfed and shocked by expanding SNRs. As noted in the Introduction (Section 1.1.1), this scenario has been suggested by previous investigators as well. In the preceding sections we argued that the other alternatives, like circumstellar clouds or old SNRs are unlikely to account for all the absorption features, although they are certainly likely to contribute in some measure. In this section we present detailed arguments for the shocked cloud hypothesis and describe how interstellar clouds are affected by an SNR blast wave.

1. The "shocked cloud" scenario has support from several quarters. The earliest indication for a "shocked" population of clouds is the well known *Routly-Spitxer effect.* The NaI/CaII ratios seen for the fast clouds is lower (sometimes by several orders of magnitude) than that in the slow clouds. Based on the assumption that this is due to the ionisation of NaI (implying higher temperatures) in the fast clouds, Pottasch(1972) attempted to model the physical conditions in these clouds. He however arrived at the unlikely conclusion that most of the gas must be at a temperature in excess of 10^4 K. *The present view is that the variation in NaI/CaII ratio is primarily due to the variable gas phase abundance of Ca in these clouds.* Calcium depletion is also found to be correlated to the HI density, decreasing as the gas becomes less dense. Considering the correlation between low NaI/CaII ratio and high velocities, Spitzer speculated that the mechanism involved in accelerating these clouds would also release calcium back to the gas phase, a view which has found further support since then. *A shock wave propogating in the cloud causing sputtering of the grains is a favoured candidate for accelerating the cloud as well as releasing calcium back into the gas phase.* However, caution is to be exercised in using the sodium and calcium abundance ratios to study the cloud conditions. Since the ionization potential of CaII (11.9 ev) is smaller than that of HI, CaII is typically a trace ionization stage in diffuse neutral clouds. It can, however be the dominant ionisation stage in colder denser clouds because of its small photoionization cross section. In the high velocity clouds, CaII seems to be returned to the gas phase perhaps by the action of interstellar shocks (Routly and Spitzer, 1952; Siluk and Silk, 1974), in part offsetting the effect of it becoming the trace ionization stage (Welty, Morton and Hobbs 1996; Sembach and Danks, 1994).This intricate balance between ionization and deple-

prevailing inside the cloud. However, there does seem to be strong evidence that these clouds could have been subjected to shocks.

2. In the line of sight towards the Galactic center, the radial component of the Galactic rotation velocity is zero (section 1.3). This direction is therefore ideal to probe the random velocities. If a weakly absorbing population of clouds exists, they would appear as a low optical depth feature in this direction. Such a broad, low optical depth feature was indicated in the HI absorption profile towards the Galactic center obtained by Radhakrishnan et *al.*(1972a) and analysed in detail by Radhakrishnan and Sarma (1980). All the individual features in the line of sight would blend to form the absorption dip centered at zero velocity, the width of which would indicate the spread in random velocities of the clouds. As summarised in Section 1.1.1, Radhakrishnan and Srinivasan postulated a high velocity dispersion ($\sim$ 35 km s^{-1}), low optical depth (peak of 0.3) component seen in HI absorption towards the Galactic center. This was attributed to warm, low optical depth clouds resulting from shocked condensations of the ISM within SNRs, almost identical to the conjecture of Cowie and York described in the previous section.

While conjecturing that the high velocity optical absorption features might arise in shocked clouds, Radhakrishnan and Srinivasan (1980) had remarked on the distinct dependence of temperature on velocity dispersion seen by Dickey, Salpeter and Terzian (1978) in their HI absorption study. High temperature HI seems to have higher velocity dispersion. A correlation between optical depth and temperature is also seen for low optical depth features in this study with low optical (< 0.1) depth features having higher temperatures. Clouds of higher optical depth, on the other hand, seem to show no significant empirical relationship with temperature. These two facts prompted Radhakrishnan and Srinivasan to conjecture that there could be a dividing line in optical depth between the unshocked and shocked population. The clouds with low optical depth and high temperature forms the latter and the higher optical depth features, with no correlation with temperature or velocity forms the former.

3. Several investigators have proposed that the fast clouds seen in radio and optical observations arise in a *"Not* Strongly Absorbing" medium, a component of the ISM proposed by Dickey, Salpeter and Terzian (1979) in their absorption/emission study. Both our observations as well as the Galactic center absorption experiment clearly reveal that the fast population is indeed a weakly absorbing one at

shocked clouds as an important constituent of this component. Hence this hypothesis is very much in line with our contention that the high velocity features seen in optical absorption arise primarily in a shocked population. The investigations leading to the picture of the *Not Strongly Absorbing* medium as origin for the high velocity features both in 21 cm and in the optical are summarized below.

Towards the inner Galaxy, the expected radial component of Galactic rotation has a clear maximum for any line of sight. This velocity occurs at that point along the line of sight where the line of sight is perpendicular to the Galactic radius vector (*i.e.*, the tangent point). Fig 1.21 shows a schematic emission profile for a line of sight towards the inner galaxy. The maximum radial velocity occurs at the tangent point. The amount of gas seen at velocities beyond this is a measure of the velocity dispersion of the gas. Kulkarni and Fich (1985) examined HI emission at such "forbidden velocities" occuring along selected lines of sight. The tail of HI emission velocities occurring outside allowed Galactic rotation was best fitted by two Gaussians, a narrow and a wide component (see Fig 1.22 reproduced from Kulkarni and Fich). Kulkarni and Fich (1985) proposed that the high velocity dispersion component is to be identified with the *Not Strongly Absorbing medium.* This medium is believed to be made up of three components:

i the wings of HI absorption features,

ii low optical depth, low brightness temperature HI and

iii the truly warm ($\sim$ 8000 K) gas.

Kulkarni and Fich attributed the fast population to component (iii). As discussed below, optical studies do not validate this hypothesis that the fast population arises in gas at such high temperatures ($\sim$ 8000 K).

A recent high resolution survey of CaII towards 42 stars (Welty, Morton and Hobbs 1996) has led to a detailed study of the CaII linewidths. Their study places the percentage of CaII absorbing gas at $T > 6000$ K at less than 40%. This is assuming that the linewidth is entirely thermal in origin, neglecting turbulence. Thus this is an overestimate and makes it likely that most of the CaII arises in the intermediate temperature component of the so called Not *Strongly Absorbing medium.* We digress here to point out that another interesting result from the Welty, Morton and Hobbs study is that CaII may originate from a larger region in space than NaI. A cool core-warm envelope model for the clouds, with CaII

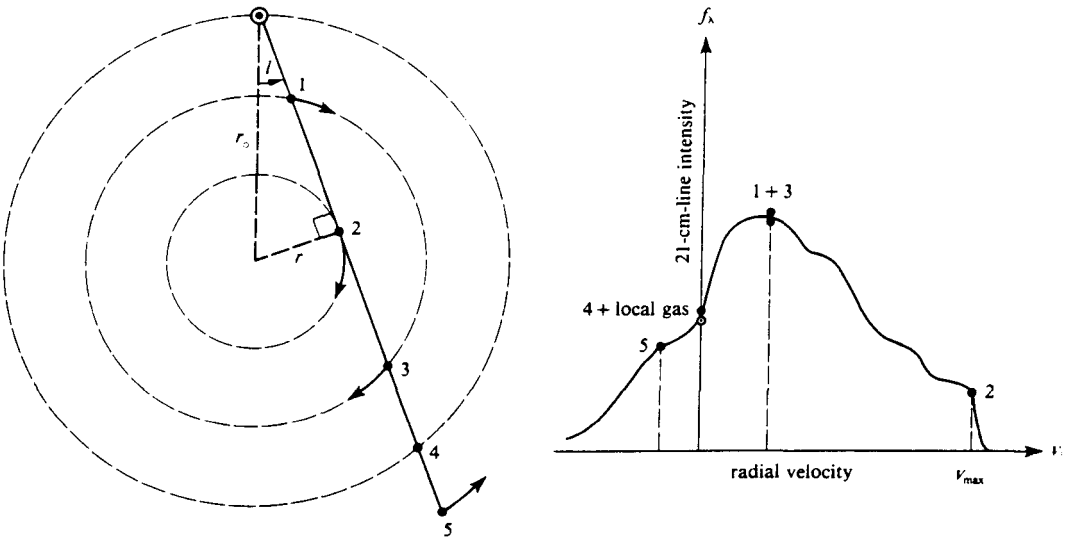

Figure 1.21: A schematic of the expected HI emission velocities towards the inner Galaxy. The gas at the numbered regions on the left gives rise to features marked by the same numbers in the spectrum on the right. The gas at the tangent point (point 2) in the line of sight is at the maximum velocity V_{max} in the spectrum. The tail beyond V_{max} in the spectrum is produced by the random velocities of the gas at **2** and can be used to measure the velocity dispersion of the gas.

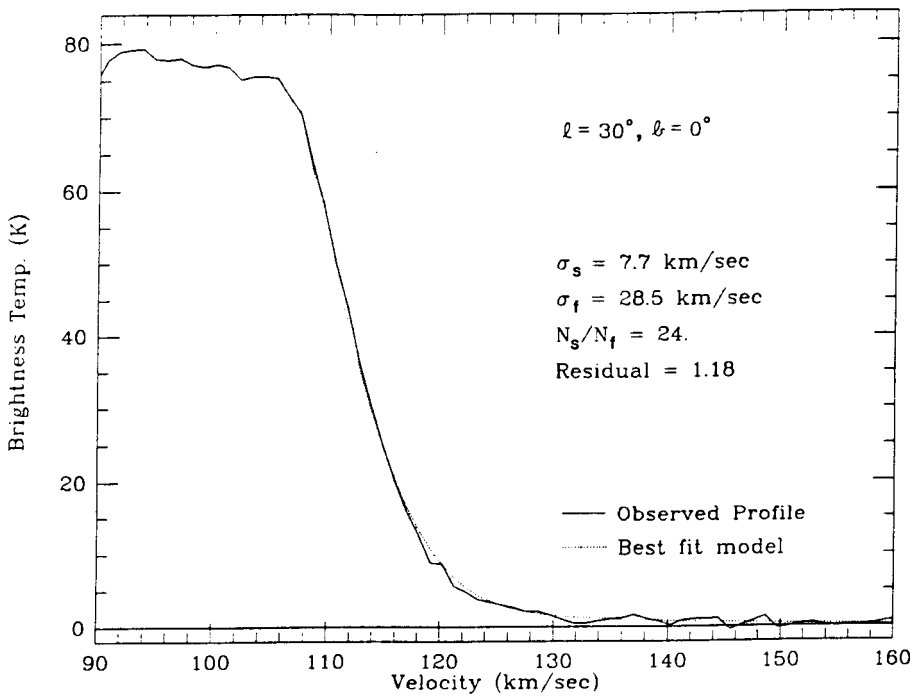

Figure 1.22: The observed HI emission (thick line) towards l=30°, b=O°, and a two-component gaussian model (dashed line) from Kulkarni and Fich (1985). The velocity dispersion for the slow component (a,) and fast component (σ_f) along with the ratio of their column densities (N_s/N_f) used for the model are indicated.

This hypothesis has further support from a study of "CaII only" local fast clouds by Vallerga *et* al.(1993).

More evidence for a high velocity population comes from the recent study of CaII and NaI clouds towards $\sim$ 60 stars by Sembach and Danks (1994). The Routly-Spitzer effect is seen down to velocities as low as 10 km s^{-1}. On an average 10% of the CaII column densities occur at "forbidden" (non-Galactic rotation) velocities. Using a normalized column density for CaII (normalized to the column density at zero velocity), they postulate a two component model, with velocity dispersions of 8 and 21 km s^{-1} respectively. The fast component is conjectured to arise in the *Not Strongly Absorbing* medium. Sembach and Danks identify the CaII features with the warm, intermediate velocity clouds and the intercloud medium which makeup the *Not Strongly Absorbing medium.*

Our HI absorption study supports these earlier investigations which point to the existence of a fast, weakly absorbing, warm component of the ISM. Various studies differed in the estimates for velocity dispersion and amount of this component. For example, Sembach and Danks (1994) find no conclusive evidence for velocity dispersions as large as 35 km s^{-1} proposed by Kulkarni and Fich (1985). However, it is clear that the investigations described thus far clearly seem to favour warm tenuos gas as being the origin for most of the high velocity CaII and HI features. At this point we wish to comment on the discrepancy in the number of clouds seen in the optical and radio. As mentioned earlier, the number of clouds seen per kiloparsec in the optical absorption seem to be greater than that seen in HI absorption. Clearly, the high velocity clouds have been shown to be below the optical depth limits of existing HI absorption surveys. Hence the estimate of the number of HI clouds based on absorption experiments do not take into account these clouds. This could account for the aforesaid discrepancy. A statistical study has to be done to see if the actual number of high velocity clouds support this hypothesis.

The investigations summarized above have been presented as support for the shocked cloud origin for the high velocity features seen in the ISM. Since these are the products of the interaction of SNRs with interstellar clouds in the ambient medium, an overview of the evolution of such a cloud, as gleaned from theoretical

Qualitative description of an interstellar cloud engulfed by shock

There have been detailed investigations of the fate of an HI cloud hit by a blast wave (McKee and Cowie, 1975; Sgro, 1975; Woodward, 1976). The subject has also received attention in the context of SNR evolution in a "cloudy" ISM (Cowie, McKee and Ostriker, 1981). We shall now attempt to argue how interstellar clouds hit by SNRs could lead to the population of clouds with the characteristics discussed above.

We start with a description of an HI cloud hit by a strong adiabatic shock wave in the Sedov or adiabatic phase. Some of the important phases of evolution of such a cloud are sketched in Fig 1.23 from Heathcote and Brand (1983).

1. The SNR shock increases the ambient pressure and drives a shock into the cloud. The greater density of the cloud usually causes the cloud shock to be radiative, even if the SNR shock is not.

2. The external shock then sweeps around the cloud and moves on, leaving the cloud immersed in the flow of hot intercloud medium behind it.

3. The high thermal pressure in the sorrounding medium can now drive secondary shocks into the clouds from the sides and rear.

The acceleration of the cloud occurs in two phases.

a) The impulse or shock acceleration by the cloud shock

b) Smooth acceleration by the flow of hot material inside the SNR.

The cloud shock is usually assumed to be isothermal. Given the jump conditions for such shocks, the velocity of the shock inside the cloud is related to the velocity of the external shock as $\frac{V_{cl}}{V_b} = (\frac{\rho_b}{\rho_{cl}})^{1/2}$, where subscripts b and cl denote the blast wave (external shock) and cloud, respectively, and ρ is the mass density. A 100 km s^{-1} blast wave would induce a 10 km s^{-1} cloud shock velocity given a density contrast of 100. For more diffuse clouds, the shock velocity could be of the order of the high velocity absorption features ($\sim$20 km s^{-1}). The cloud is accelerated by this shock to a velocity close to V_{cl}. In addition, the shock would also compress and flatten the cloud considerably as shown in Fig 1.23 (Woodward, 1976; Sgro, 1975). Compression as high as by a factor of 100 (ignoring magnetic and cosmic ray preseeures!) over the preshock density is achieved in

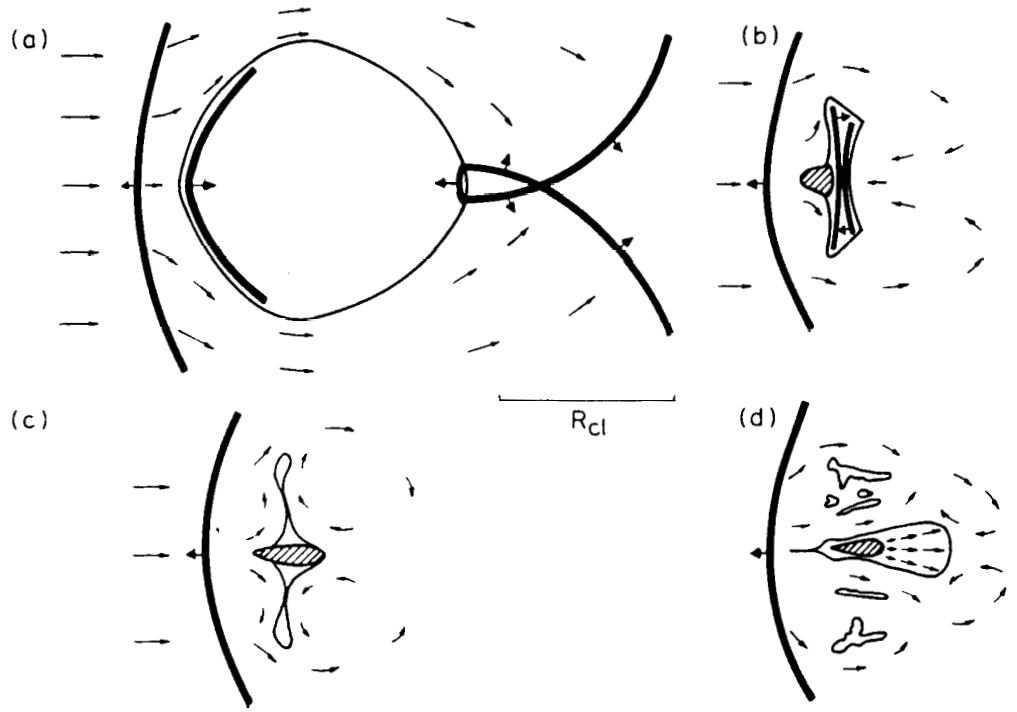

Figure 1.23: The various stages of evolution of an interstellar cloud engulfed by an SNR blast wave. Heavy lines represent shocks; the broad tipped arrows attached to these indicate the downstream side of the shock. The cross-hatched areas indicate the zone of enhanced density. Narrow tipped arrows depict the flow of the gas around the cloud. a: The external shock has swept past the cloud and just met at the back of the cloud. The cloud shock is beginning to propogate inside the cloud. b: The shocks driven into the front and back sides of the cloud are about to collide. ***c:*** The re-expansion of the cloud in the downstream direction has commenced. **d:** A typical stage during re-expansion. From Heathcote and Brand (1983).

In the second phase, the shocked cloud is further accelerated by the post-shock flow of the ambient hot gas inside the SNR. Most of the gas within the SNR is concentrated in a fairly thin shell of approximately 10 % of the SNR radius behind the shock wave. The extent of further acceleration of the cloud through momentum transferred from this shell critically depends on whether the time required to completely shock the cloud (traversing time for the cloud shock) is comparable to the time required for this shell to sweep past the cloud (McKee, Cowie and Ostriker, 1978). See Fig 1.24 for a schematic of the cloud shocked by a blast wave which has swept past. If **the shock crossing time is large compared to the shell crossing time across the cloud then the cloud does not undergo significant additional acceleration by the hot gas, since there is little of it flowing past.** The momentum transfer rate is

$$N_{cl}.\frac{dV_{cl}}{dt} = \rho_i(V_i - V_{cl})^2 sign(V_i - V_{cl})$$

where subscript i stands for the interior, hot gas. N_{cl} is the cloud mass divided by effective area of the cloud normal to $V_i - V_{cl}$. The net velocity imparted to the cloud depends on the coupling between the cloud and the hot gas. Following McKee, Cowie and Ostriker (1978), this can be parametrized by the coupling strength

$$\chi = \frac{9}{16}.\frac{\rho_b.R_b}{N_{cl}}$$

Subscript b is again used for the blast wave. For a density contrast of 10 and shock velocities of $\sim$ 300 km s^{-1}, this post shock acceleration can lead to cloud velocities as high as 300 km s^{-1}. For strong coupling, the cloud can possibly overtake the decelerating SNR shell itself!

SNRs in the isothermal phase with cool dense post-shock shells can also accelerate interstellar clouds. The ages of these remnants are of the order of 10^5 years or more, and the shock velocities are less than 100 km s^{-1}. The cloud shock in this case has a velocity of $\sim V_b/2$, which will again be the extent to which the cloud itself will be accelerated (Chevalier 1974, Cowie, McKee and Ostriker 1978).

Observational evidence

The shocked cloud hypothesis has been used to explain the shell and filamentary structure seen in SNRs recognizable as being in the Sedov phase. The Cygnus Loop SNR (e.g., McKee and Cowie, 1975; McKee, Cowie and Ostriker, 1978;

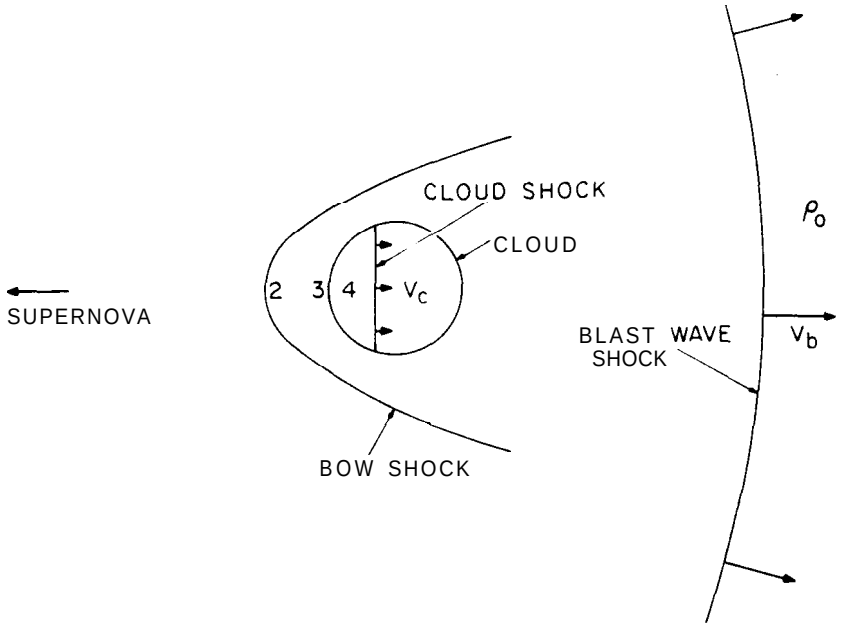

Figure 1.24: Schematic showing an interstellar cloud inside a blast wave. The blast wave (of velocity v_b) has swept past the cloud and is expanding into the ambient medium of density ρ_0. The cloud shock is propogating at velocity v,. The bow shock is also indicated. The regions 1, 2, **3** and 4 indicate the interior of the SNR, the region of enhanced pressure between the cloud and the standing bow shock, the stagnation point of the flow past the cloud, and the shocked cloud respectively.

.Jenkins, Silk and Wallerstein, *1976)* are two such cases. In the Cygnus Loop, optical emission (e.g., *Ha)* is seen at velocities of *100-300* km s^{-1}. Some of this emission can be explained as being from the radiative shock ($V_{shock} \sim 100$ km s^{-1}) traversing clouds inside the SNR. The *300* km s^{-1}emission is difficult to attribute to cloud shocks, since the implied blast wave velocity will be higher than that derived through intensity of X-ray emission from the SNR interior. These have been conjectured (McKee, Cowie and Ostriker, *1978)* to be clouds shocked early on in the evolution of the SNR when it was half its present radius, and subsequently accelerated by the flow of hot gas. The recombination time for these clouds after being shocked to temperatures of the order of 10^4 K is a few hundred years for a density of ~ 100 cm^{-3}. Hence these clouds are largely neutral presently. To account for the Ha emission, ionizing photons from a conductive interface penetrating the cloud from the hot SNR interior is invoked by McKee, Cowie and Ostriker *(1978)*. Mckee and Cowie *(1975)* argue that the thin shell appearance of the Cygnus Loop implies that the average size of clouds engulfed by the SNR is $\lesssim 0.2$ pc or less. This figure is not consistent with X-ray and optical emission from the Loop which require cloud sizes of around *1* pc or so (Hester and Cox *1986)*. However, the overall picture of optical emission from the Cygnus Loop as being from clouds shocked and crushed by the blast wave has much observational support.

Evidence for clouds inside an old SNR is seen in recent HI observations of the SNR CTB *80* (Koo *et al.*(1993) and earlier work). High resolution HI emission maps of this faint remnant reveal clumps of HI emission which are likely to he from HI clouds overtaken by the SNR shock. This remnant is $\sim 10^5$ years old *as* deduced from the expansion as well the age of the pulsar associated with it (Kulkarni *et al., 1988)*. The clouds are seen at $V \gtrsim 50$ km s^{-1}. The shell itself is moving at ~ 72 km s^{-1}. Lower velocity clouds are dificult to detect because of confusion with background features at these velocities. These clouds have sizes of 2-4 pcs and are at a distance of 2 kpc. The high resolution (~ 40 ") achieved with synthesis imaging is required to detect such features in emission.

Cloud survival

The preceding discussions dealt with theoretical and observational grounds for believing in the existence of interstellar clouds shocked by SNRs. To relate them to the high velocity absorption features seen in the ISM we have to consider two

1. What are the survival chances of clouds inside SNRs?

2. Why are the high velocity features deficient in HI?

The survival of a cloud after being engulfed by a blast wave depends primarily on whether it can cool effectively (through radiation) in the time taken for the shock to traverse the cloud (Woltjer 1972). If not, the cloud heated by both the primary and secondary shocks will expand and dissipate. This would be the likely scenario for clouds hit very early on in the evolution of an SNR and heated to temperatures of the order of 10^8 K. However, as seen in the previous section for clouds with densities in the range of a few atoms per cm^3 accelerated in the later phases of SNR evolution (the adiabatic and the subsequent isothermal phases), the post-shock recombination time is fairly short, being a few hundred to a thousand years. In the case of a cloud engulfed by a blast wave in the Sedov phase, its survival depends on its size and the stage of the SNR when it is engulfed. For a spherical cloud of radius a, engulfed by a shock of radius R, three relevant time scales can be identified (McKee, 1988): (i) The cloud-shock crossing time t_{cl}, (ii) the blast wave crossing time t_{sh} and (iii) the SNR age t. In the adiabatic phase, $R \propto t^{\eta}$, where $\eta = 2/5$. In this phase, assuming the density contrast $\rho_{cl}/\rho_0 = \chi$, (where subscript *0* is for the initial density of the intercloud medium),

$$t_{cl} = a/v_{cl} = \frac{\chi^{1/2} a}{v_b}$$

$$t_{sh} = \frac{2a}{v_b}$$

$$t = \frac{2}{5}\frac{R}{v_b}$$

t_{cl} depends on 'a' rather than '2a' in an attempt to account for the fact that the cloud is shocked from both sides.

For small clouds $t > t_{cl}$ i.e, $a < \eta R/\chi^{1/2} = 0.4R/\chi^{1/2}$. This implies that the SNR does not evolve much while the cloud shock traverses the cloud. The driving pressure for the cloud-shock (which is the pressure of the hot interior) remains constant and the shock progresses with constant velocity. The SNR shock (blast wave) sweeps around and converges behind the cloud, driving a shock into the cloud from the rear. The shocks from rear and front are stronger than the shocks from the sides since the pressure in a flow around an obstacle is a minimum at the sides (Nittman etal., 1982). The cloud is thus flattened into a pancake.

When the cloud shock has traversed the whole cloud, a strong rarefaction wave is reflected into the cloud causing it to expand downstream (Woodward, 1976) as seen in Fig 1.23 The low pressure at the sides causes it to expand sideways as well. The survival of these small clouds is not certain, with hydrodynamic instabilities developing as the hot SNR interior flows past. As stated earlier the cooling time for the shocked gas is important and for cloud shock velocities greater than 200 km s^{-1} or so, the shocked gas is usually non-radiative.

For medium sized clouds $t_{cl} > t > t_{sh}$ i.e, $\eta R/\chi^{1/2} <$ a $< \eta R/2a$. Hence in this case, the SNR does not evolve much while the blast wave sweeps past the cloud, but does evolve over the time taken to shock the cloud. As the SNR evolves over the cloud shock traversing period, the thermal pressure in the interior of the SNR which drives the cloud shock drops and the cloud shock decelerates leading to lower post-shock temperatures. For large clouds, $t_{cl} > t$ i.e, a $> \eta R/2$. In this case, the SNR evolves even in the time taken for the blast wave to sweep past the cloud and the ambient pressure decreases considerably. Thus in both medium and large clouds the blast wave leads to an impulsive pressure whereas in small clouds the pressure driving the shock is continuos and constant. As a result the large and medium clouds are likely to survive as coherent entities. We can estimate the typical numbers for the sizes of these medium and large clouds for an SNR like the Cygnus Loop. We assume the radius R of the SNR to be $\sim$ 20 pc, the cloud density n_c to be $\sim$ 10 cm^{-3} and the density in the interior of the SNR to be $\sim$ 0.2 cm $^{-3}$. These values are obtained from observations of the Cygnus Loop in the optical and radio (Lozinskaya, 1984). For these parameters a "small cloud" is $<$ 0.16 pc, a "medium cloud" is between this and 4 pc, while a "large cloud" is $>$ 4 pc. *Hence clouds which survive the shock will be* > 4 *pc or so in size.*

For medium sized and large clouds the threat for long-term survival is from *evaporation of the cloud by conduction of heat from the hot intercloud gas it finds itself immersed in.* Cloud evaporation under such conditions has been treated in detail by Cowie and Mckee (1977) and McKee and Cowie (1977) taking into account the conductive heat flux and the effects of radiation. The evaporation rate depends on cloud size and density. In particular, if the mean free path of the conducting electron is comparable to the cloud size, the heat flux is no longer given by the classical conduction equation *i.e.,* q $= -\kappa.\nabla T$. Cowie and McKee (1977) introduce a saturation parameter σ_0 to quantify this. $\sigma_0 > 1$ implies that

values. *Whether the cloud is destroyed by evaporation or not depends on whether the heat flux due to conduction is balanced by the radiative losses.* If not, the cloud eventually loses all its mass. Given the parameters of the hot gas, the balance between the two is achieved at a critical radius for the cloud. Smaller clouds are completely evaporated, and larger clouds have the ambient medium condensing on to them.

Given these factors, it is possible to estimate the lifetime of a typical cloud inside an SNR. Taking the Cygnus Loop as an example, McKee, Cowie and Ostriker (1978) show that clouds (size < 1 pc, density ~ 10 cm^{-3}) which entered the SNR when it was about half its present size will have already suffered large evaporative loss with as little as 10% of the original mass surviving and are unlikely to exist for much longer. These clouds would also have been accelerated to velocities as much as 300 km s^{-1}by now. It is clear that these are not the clouds that we see in optical absorption. Clouds which enter the SNR *at present* have *a* chance of surviving for 10^5 years or more and since the SNR has decelerated (to $\sim$ 100 kms^{-1}), these clouds are unlikely to be accelerated to velocities as high as in the previous case. Clouds surviving inside very old SNRs are therefore unlikely to have velocities higher than this value $\sim$ 100 kms^{-1} or so. Indeed, in our population of high velocity features, velocities higher than 100 km s^{-1}are not observed. This further strengthens the shocked cloud scenario. Using the estimate of 4 pc for a surviving cloud of density ~ 10 cm^{-3}, and assuming a temperature of 100 K (a conservative value, since the cloud after being shocked and immersed in the hot interior is likely to be at higher temperatures), the estimated optical depth is < 0.1, which is well below our detection limit. **To sum up, the fact that we don't see "high velocity" absorption at 21 cm is entirely consistent with the expectation if the high velocity is to be understood in terms of acceleration of clouds by supernova remnants.**

In discussing survival of clouds, we have so far ignored the severe deformation that these clouds are subjected to during the shock traversal and in the post shock phase due to developing instabilities. Although these deformations may not affect the momentum transfer and hence the cloud acceleration, they are likely to seriously affect the *observed* properties of the cloud. In particular if the clouds are flattened into thin sheets and eventually separate clumps, HI emission measurements towards these are likely to be beam diluted. This would explain

1.8.4 Summary

The answers to the questions posed at the beginning of the previous section are inter-connected. The period for which a cloud inside an SNR can be detected is decided, among other factors, by the rate of evaporation it suffers, which in turn decides the column density. Since the cloud is being accelerated for the period it is immersed in the flow of hot gas, the velocity of the surviving cloud is also related to the amount of time spent in this phase and hence to its column density. Thus, depletion of HI column density in high velocity clouds is a consequence of the mechanism of acceleration.

Is there evidence for such a correlation between velocity and column density? UV absorption lines can be detected at column densities much lower (2 orders of magnitude or more) than the optical lines. If the correlation between velocities and column densities exists, the velocities seen in UV absorption should extend to higher values than in the optical. There does seem to be some indication of such a trend as pointed out in a study by Hobbs (1984). For example, in 41 lines of sight that Hobbs has explored almost all show UV absorption features at velocities $|v| > 25$ km s^{-1}, whereas in the correponding optical profiles only 10 stars show optical features > 25 km s^{-1}. Earlier we referred to the direct estimate of HI column densities from UV absorption lines by Martin and York (1982). For the two lines of sight of sight that they studied, there is a clear indication of increasing velocities showing decreasing N(HI), as seen in the histogram (Fig 1.25) reproduced from their work. The column densities at higher velocities ($|v|$ >15 km s^{-1}) are $< 10^{19}$ cm^{-2} consistent with the expected column densities for clouds which survive SNR shocks (refer previous section).

There exists ubiquitous high velocity optical absorption features in the ISM with velocities ranging upto 100 km s^{-1}. We have argued that these are most likely clouds engulfed and accelerated by SNRs which have subsequently become undetectable or at least unrecognizable. In the preceding section we have highlighted the different aspects of evolution of such clouds. The consequence of shocking and subsequent evaporation inside the SNR has been to make these clouds progressively more difficult to detect as we go from UV to the radio. The HI emission measurements uptill now have been sensitive to column densities of the order of 10^{19} cm^{-2} at best, neglecting beam dilution effects. Observational evidence and theoretical predictions point to column densities of this order or less for clouds surviving inside SNRs. Greater resolution and sensitivity are called for

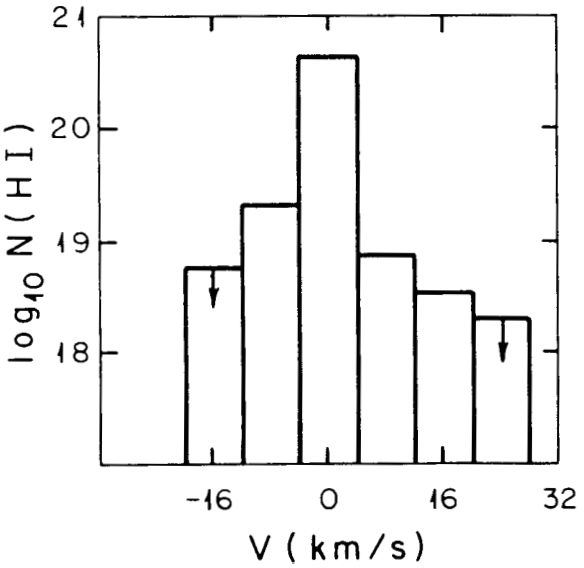

Figure 1.25: Histogram from Martin and York(1982), showing the trend of decreasing N(HI) with increasing velocities. The HI column density is inferred from an analysis of ultraviolet interstellar lines towards ϵ and δ Persei.

Supernovae figure prominently as the plausible source of energy for these clouds. It has long been recognized that supernovae provide most of the kinetic energy for the observed high velocity clouds. The importance of identifying the nature and extent of the fast clouds as well as establishing their energy source is evident. It seem unavoidable that one needs to appeal, at some level, to supernovae to provide this input. If the quantitive estimates for the velocity tlispersion and mass fraction of the fast population made by Radhakrishnan and Srinivasan is true (several indications that this may not be the case have already been mentioned) then this component is the *major resevoir* of *kinetic energy* in the ISM. Even if one were to accept the smaller figures (for e.g., Sembach and Danks 1994) the fast population is more than a minor player on the scene.

References

Adams, W.A. 1949, Ap.J., **109**, 354.

Ambartsumian, V.A 1940, Bull. Abastumani Obs., 4, 17.

Ambartsumian, V.A., Gordeladse, Sh. G. 1938, Bull. Abastumani Obs., **2**, 37.

Ananthramiah, K.R., Radhakrishnan, V., and Shaver, P.A. 1984, Astr. Astrophys., **138**, 131.

Beals, C.S., 1936, Mon. Not. R. astr. Soc., **96**, 661.

Blaauw, A. 1952, B.A.N., **11**, 459.

Blaauw, A. 1985, in IAU Symp. 106, The Milky Way Galaxy, eds. H.van Woerden, R.J.Allen and W.B.Burton, p.335.

Blaauw, A., and Tolbert, C.R. 1966, B.A.N., **18**, 405.

Blades, J.C., Sahu, M.S., He. L., Crawford, I.A., Barlow, M.J., Diego, F. 1997, Ap. J., 478, 648.

Boulares, A., Cox, D.P. 1990, Ap.J., 365, 544.

Brand, J., Blitz, L. 1993, Astr. Astrophys., **275**, 67.

Burton, W.B. 1985, Astr. Astrophys. Supp., 62, 365.

Burton, W.B. 1987, in Galactic and Extragalactic Radio Astrono my, ed. K.I Kellerman and G.L Verschuur. (New York:Springer-Verlag)

Buscombe, W., Kennedy, P.M. 1962, Mon. Not. R. Astr. Soc., **125**, 195.

Chevalier, R. 1974, Ap. J., **188**, 501.

Christiansen, W.N., Hindman, I.V. 1952, Australian J. Sci. Res.(A), 5, 437.

Clark, B.G. 1965, Ap.J. **142**, 1398.

Condon, J.J., Cotton, W.D., Greisen, W.E., Yin, Q.F., Perley, R.A., Taylor, G.B., Broderick, J.J 1996, in preparation.

Cowie, L.L., McKee, C.F. 1977, Ap. J., **211**, 146.

Cowie, L.L., McKee, C.F., Ostriker, J.P. 1981, Ap. J., 247, 908.

Cowie, L.L, York, D.G. 1978, Ap. J., **223**, 876.

Cox, D.P., Smith, B.W. 1974, Ap.J.(Letters), **189**, L105.

Cox, D.P., Reynolds, R.J. 1987, Ann. Rev. Astr. Astrophys., 25, 303.

Crovisier. J. 1981, Astr. Astrophys., **94**, 162.

Danly, L., Lockman, F., Meade, M.R., Savage, B.D. 1992, Ap. J. Suppl., 81, 125.

Dickey, J.M., Salpeter, E.E., Terzian, Y. 1978, Ap. J. Suppl., **36**, 77.

Dickey, J.M., Salpeter, E.E., Terzian, Y. 1979, Ap. J., **228**, 465.

Eddington, A.S. 1926, Proc. R. Soc. London, A, **111**, 424.

Ewen, H.J., Purcell, E.M. 1951, Nature, 168, 356.

Field, G.B., Goldsmith, D.W., Habing, H.J. 1969, Ap. J.(Letters), 155, L149.
Goldstein, S.J., MacDonald, D.D. 1969, Ap. J., 157, 1101.
Goniadzki. D. 1972, Astr. and Astrophys., 17, 378.
Habing, H.J. 1968, B.A.N., 20. 120.
Habing, H.J. 1969, B.A.N., 20. 171.
Heathcote. S.R., Brand, P.W.J.L. 1983, Mon. Not. R. astr. Soc., 203, 67.
Heiles, C. 1974, Ap. J.(Letters), 193, L31.
Hester, J.J., Cox, D.P. 1986, Ap. J., 300, 675.
Hobbs, L.M. 1969, Ap. J., 157, 135.
Hobbs, L.M. 1984, Ap. J. Suppl., 56, 315.
Howard III, W.E., Wentzel, D.G., McGee, R.X. 1963, Ap. J., 138, 988.
.Jenkins. E.B., Silk, J., Wallerstein, G. 1976, Ap. J.(Letters), 200, L87.
Koo, B.-C., Yun, M.-S., Ho, P.T.P, Lee, Y. 1993, Ap. J., 417. 196.
Kulkarni, S.R., Clifton, T.C., Backer, D.C., Foster, R.S., Fruchter, A.S. 1988, Nature, 331, 50.
Kulkarni. S.R., and Fich, M. 1985, Ap.J., 289, 792.
Kulkarni, S.R., and Heiles, C. 1987, in Galactic and Extragalactic Radio Astrono my, ed. K.I Kellerman and G.L Verschuur. (New York:Springer-Verlag), pp. 95-153.
Lockman. F.J., Gehman, C.S. 1991, Ap.J., 382, 182.
Lozinskaya, T.A. 1984, Sov. Sci. Rev. E. Astrophys. Space Phys., 3, 35.
Martin, E.R, York, D.G. 1982, Ap. J., 257, 135.
Marschall, L.A., Hobbs, L.M. 1972, Ap. J., 173, 43.
McKee, C.F. 1988, in IAU Coll. No. 101 on Supernova remnants and the Interstellar Medium, eds. R.S Roger and T.L.Landecker, Cambridge Univ. Press.
McKee, C.F., Cowie, L.L. 1975. Ap. J., 195, 715.
McKee, C.F., Cowie, L.L. 1977. Ap. J., 215, 213.
McKee, C,F., Cowie, L.L., Ostriker, J.P. 1978, Ap. J.(Letters), 219, L23.
McKee, C.F., Ostriker, J.P. 1977, 218, 148.
Mebold, U. 1972, Astr. Astrophys., 19, 13.
Merrill, P.W., Sanford, R.F., Wilson, O.C., Burwell, C.G. 1937, Ap. J., 86, 274.
Merrill, P.W., Wilson, O.C. 1947, Pub. A. S. P., 59, 132.
Milne, D.K. 1987, Aus. J. Phys. 40, 771.
Milne, D.K., Haynes, R.F. 1994, Mon. Not. R. astr. Soc., 270, 106.
Muller, C.A., Oort, J.H. 1951, Nature, 168, 357.
Münch, G. 1957, Ap. J., 125, 42.

Münch, G. 1968, in Nebulae and Interstellar Matter, vol.7, eds. B.M. Midlehurst and L.H. Aller, University of Chicago Press, pp 365-301.
Munch, G., and Zirrin, H. 1961, Ap.J., 133, 11.
Nittman, J., Falle, S., Gaskell, P. 1982, Mon. Not. R. astr. Soc., 201, 833.
Oort, J.H., Spitzer, L. 1955, Ap. J., 121, 6.
Plaskett, J.S., Pearce, J.A. 1933, Pub. Dom. Ap. Obs. Victoria, 5, 167.
Pottasch, S.R. 1972, Astr. and Ap., 20, 245.
Radhakrishnan, V., Goss, W.M. 1972, Ap. J. Suppl., 24, 161.
Radhakrishnan, V., Goss, W.M., Murray, J.D., Brooks, J.W. 1972a, Ap. J. Suppl., 24, 49.
Radhakrishnan, V., Murray, J.D., Lockhart. P., Whittle, R.P.J. 1972b, Ap. J. Suppl., 24, 15.
Radhakrishnan, V., and Sarma, N.V.G. 1980, Astr. Astrophys., 85, 249.
Radhakrishnan, V. and Srinivasan, G. 1980, J. Astrophys. Astr., **1**, 47.
Reynolds, R.J., Scherb, F., Roesler, F.L. 1973, Ap. J.(Letters), 181, L79.
Routly, P.M., and Spitzer, L.Jr. 1952, Ap.J., 115, 227.
Savage, B.D et *al.*1993, Ap. J., 413, 116.
Schwarz, U.J., Ekers, R.D., and Goss, W.M. 1982, Astr.Ap., 110, 100.
Schluter A., Schmidt, H., and Stumpf, P. 1953, Z. Ap., 33, 194.
Searle, L. 1952, Ap. J., 116, 650.
Sedov, L.I. 1959, Similarity and Dimensional Methods in Mechanics, New York, Academic.
Sembach, K.R., Danks, A.C. 1994. Astr. Astrophys., 289, 539.
Sgro, A.G. 1975, Ap. J., 197, 621.
Shaver, P.A., Radhakrishnan, V., Anantharamiah, K.R., Retallack, D.S., Wamsteker, W., Danks, A.C. 1982, Astr. Astrophys. 106, 105.
Siluk, R.S., and Silk, J. 1974, Ap.J., 192, 51.
Slavin, J.D. Cox, D.P. 1993, Ap.J., 417, 187.
Spitzer, L.Jr. 1956, Ap. J., 124, 20.
Spitzer, L.Jr. 1968, in Nebulae and Interstellar Matter, vol.7, eds. B.M Middlehurst and L.H. Aller (Chicago:University of Chicago Press), pp. 1-64.
Spitzer, L.Jr. 1978, Physical Processes in the Interstellar Medium (New York:Wiley-Interscience).
Spitzer, L.Jr. 1990, Ann. Rev. Astr. Astrophys.. 28, 71.
Spitzer, L.Jr.. Fitzpatrick, E.L. 1993, Ap. J.. 409, 299.
Takakubo, K. 1967, **R.A.N., 19**, 125.

Taylor, G.I. 1950, Proc. R. Soc. London Ser. A., 201, 175.
Taylor, J.H., Cordes, J.M. 1993, Ap. J., 411, 674.
Vallerga, J.V., Vedder, P.W., Craig, N., Welsh, B.Y., 1993, Ap. J., 411, 729.
van der Hulst, J.M., Terlouw, J.P., Begeman, K., Zwitzer, W., Roelfsema, P.R., in GIPSY in Astronomical Data Analysis Softaware and Systems I, eds. D.M.Worall, C.Biemesderfer, J.Barnes, ASP Conf. Series no. 25, p.131, 1992.
Weaver H.F., and Williams D.R.W. 1973, Astr. Astrophys. Suppl., **8,** 1.
Welty, D.E., Morton, D.C., Hobbs, L.M. 1996, Ap. J. Suppl., 106, 533.
Welty, D.E., Hobbs, L.M., Kulkarni, V.P. 1994, Ap. J., 436, 152.
Wilson, O.C., Merrill, P.W., 1937, Ap. J., **79,** 280.
Woltjer, J. 1972, Ann. Rev. Astr. Astrophys., 10, 129.
Woodward, P.R. 1976, Ap. J., 207, 484.

Appendix

In this Appendix, we present the HI absorption spectra (optical depths) obtained towards each field. The fields are arranged in order of increasing HD number. For each field, a plot of the imaged region is shown first, labelled by the HD number of the field. The plot indicates the position of the star by a "star" symbol. The radio sources towards which absorption is measured are labelled by numbers. The synthesized beam size for each field is indicated in the bottom left corner. The spectra towards each of the radio sources in the particular field follow the field plot. The spectra are labelled by the HD number of the star (top right, outside the figure) and the number of the radio source as in the field plot (top right, inside the figure). The velocities of the optical absorption features seen towards the star are indicated by arrows on the velocity axis. Those fields with no measured HI absorption are not included in the Appendix. Note:

1. Field 14143 contains two stars, HD 14143 and HD 14134, close together. These are indicated in the field plot by the letters A and B. The field plot and spectra are labelled HD 14143.

2. In fields 141637, 212978 and 214680, the star positions are outside the region shown in the field plot and so are riot marked in the plot.

3. Sources 1 and 2 in field 37742 have identical spectra. The spectrum towards 1 is shown here.

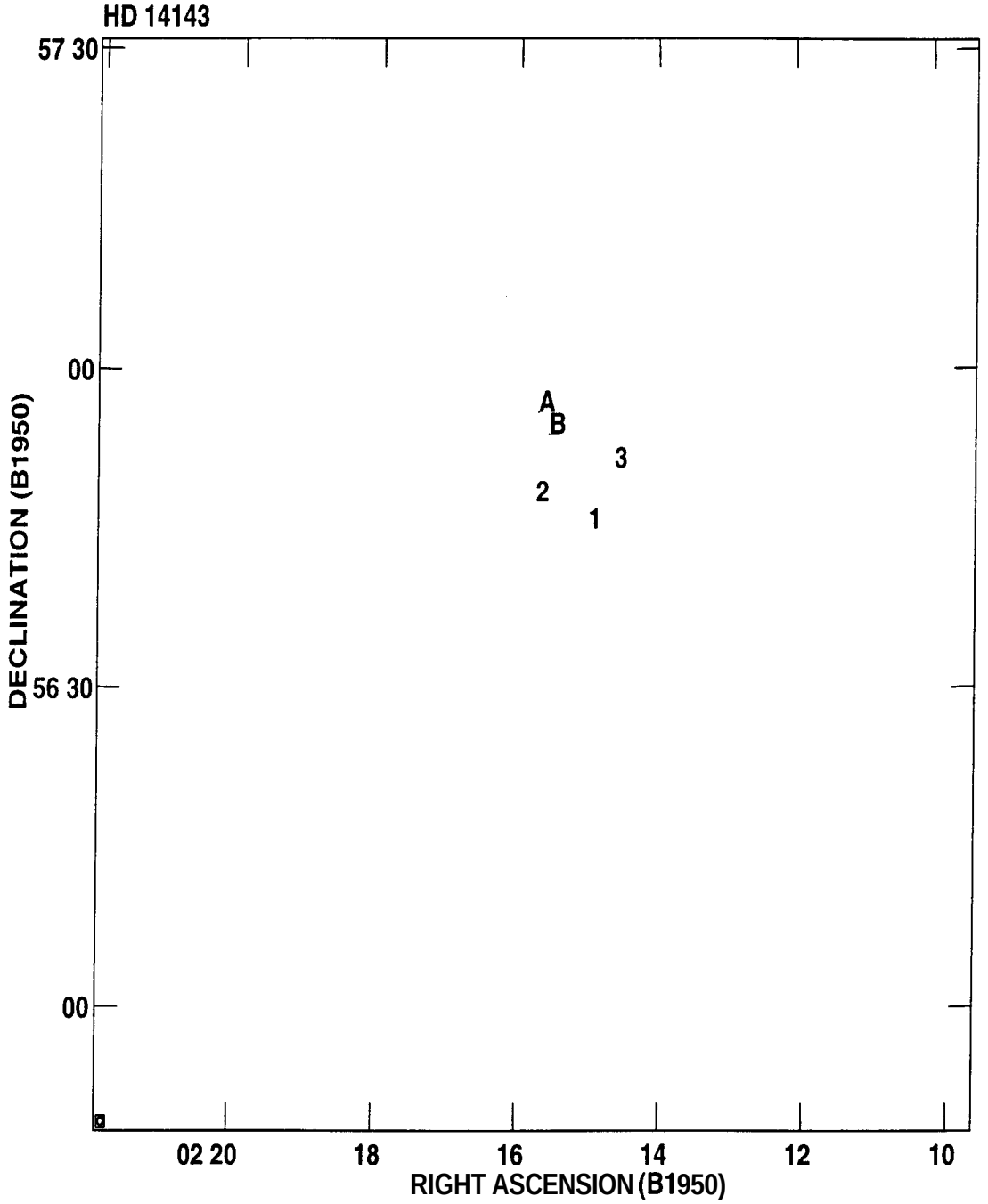
HD 14143
57 30
00
56 30
00
DECLINATION (B1950)
A
B
3
2
1
02 20
18
16
14
12
10
RIGHT ASCENSION (B1950)

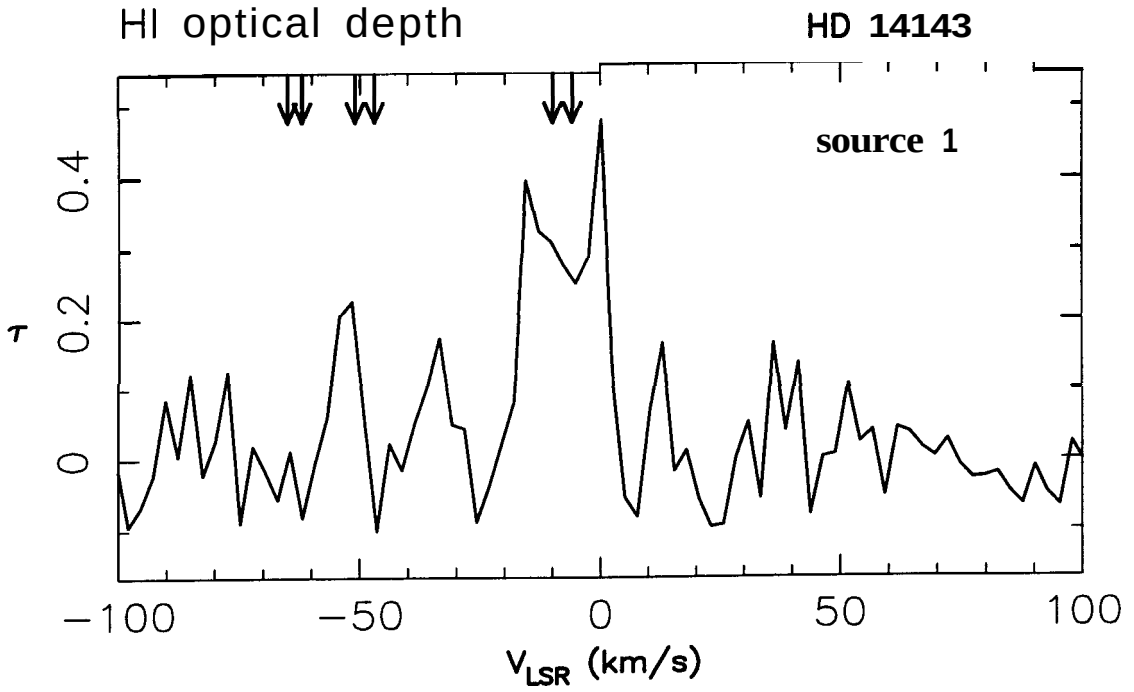
HI optical depth
HD 14143
source 1
τ
0
0.2
0.4
−100
−50
0
50
100
V_LSR (km/s)

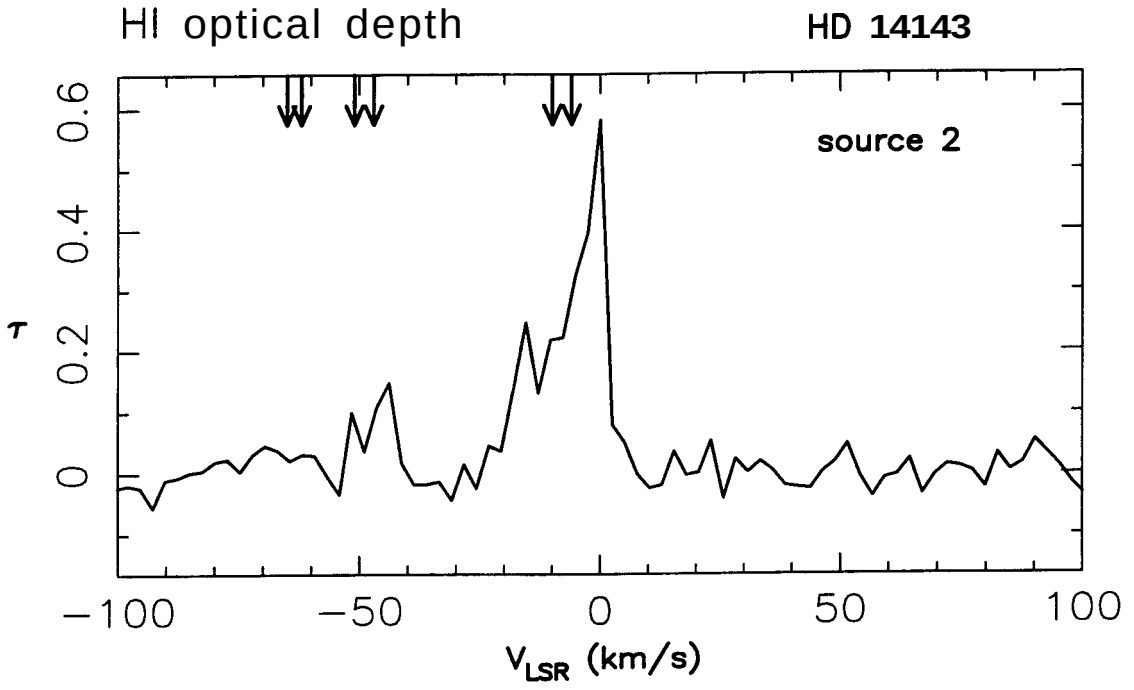
HI optical depth
HD 14143
source 2
τ
0
0.2
0.4
0.6
−100
−50
0
50
100
V_LSR (km/s)

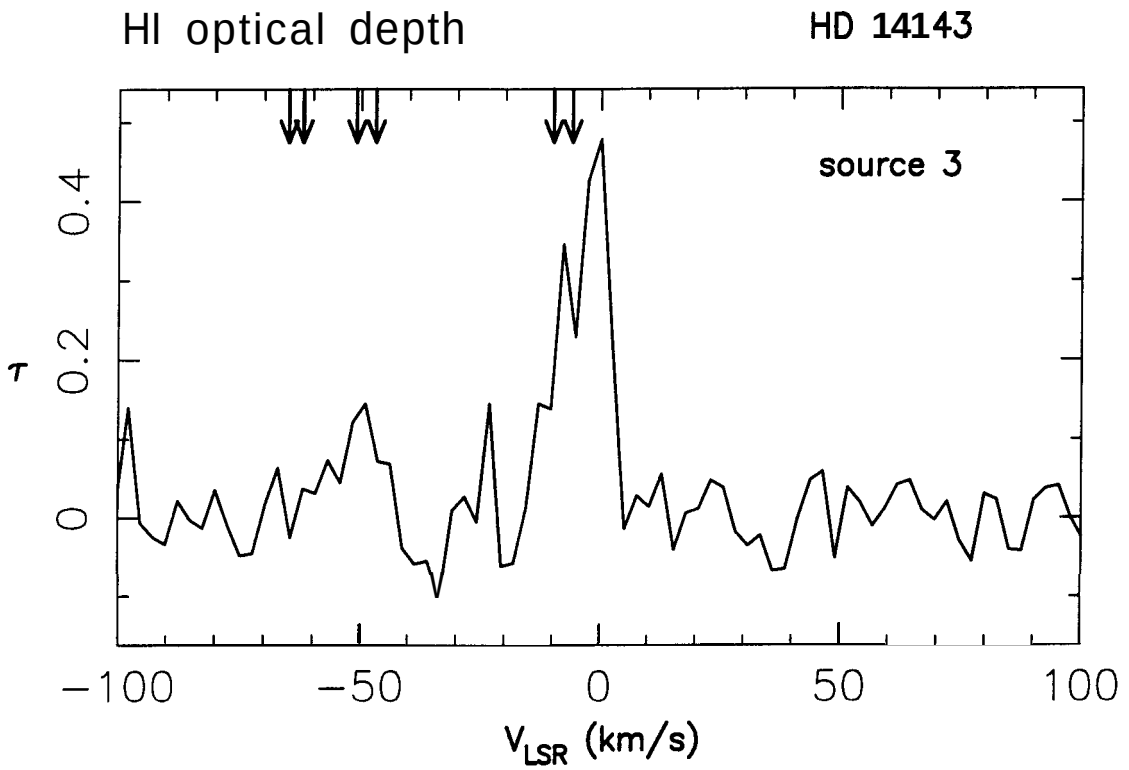
HI optical depth
HD 14143
source 3
τ
0
0.2
0.4
−100
−50
0
50
100
V_LSR (km/s)

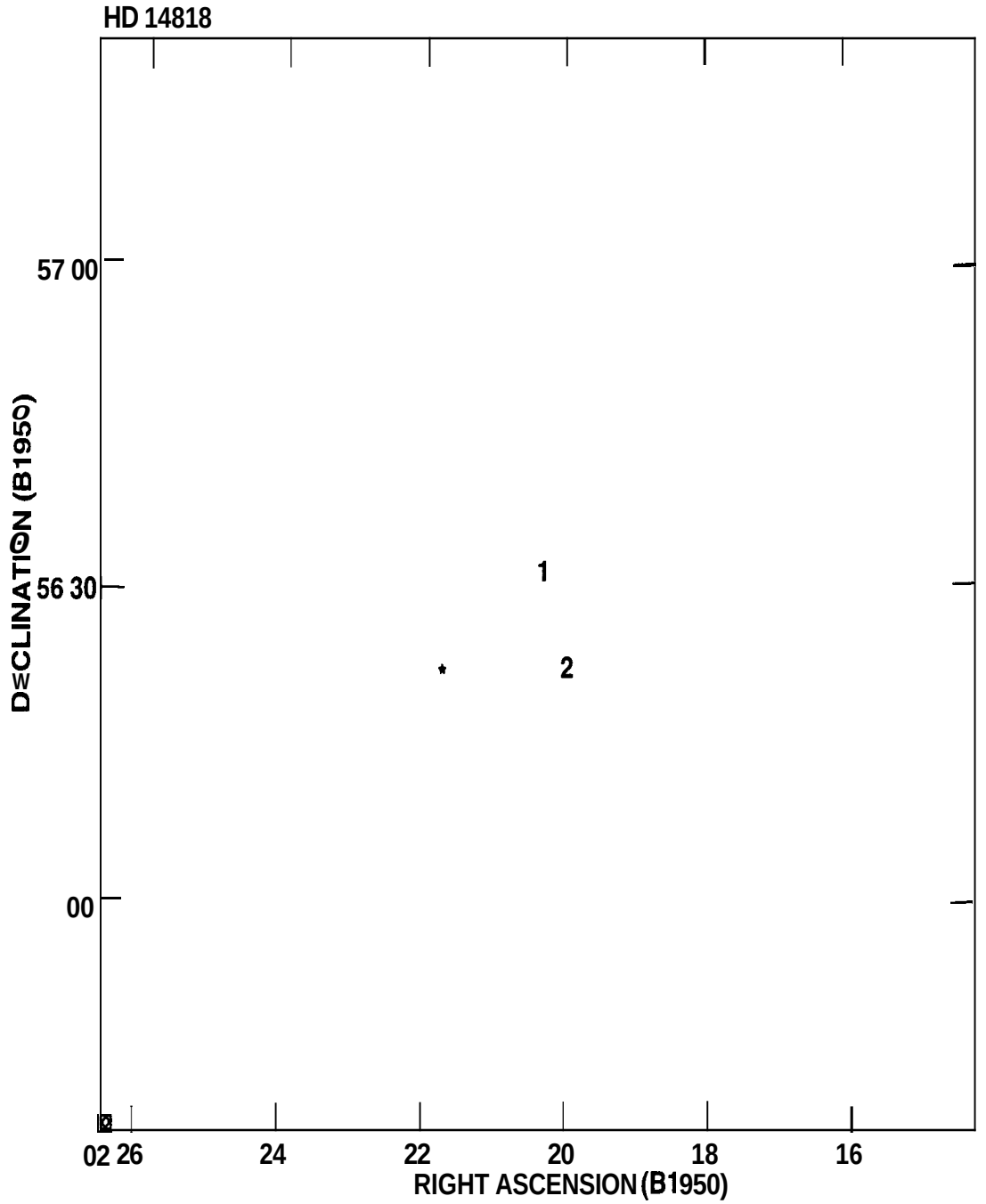
HD 14818
57 00
56 30
00
DECLINATION (B1950)
1
2
02 26
24
22
20
18
16
RIGHT ASCENSION (B1950)

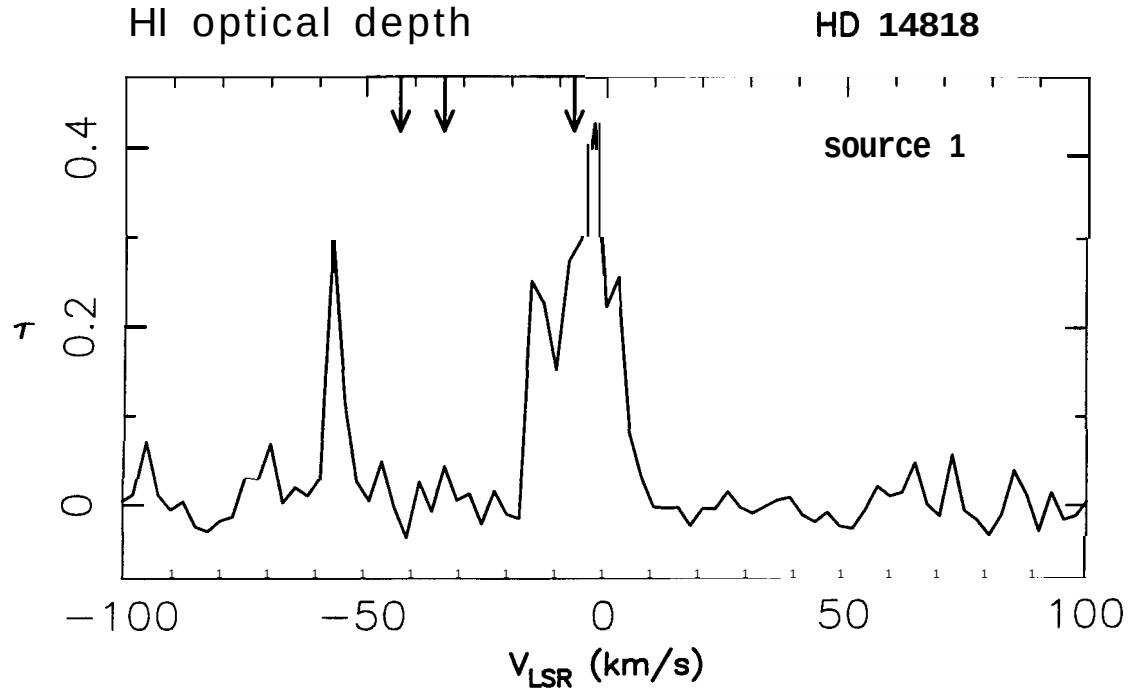
HI optical depth
HD 14818
source 1
τ
0.4
0.2
0
−100
−50
0
50
100
V_{LSR} (km/s)

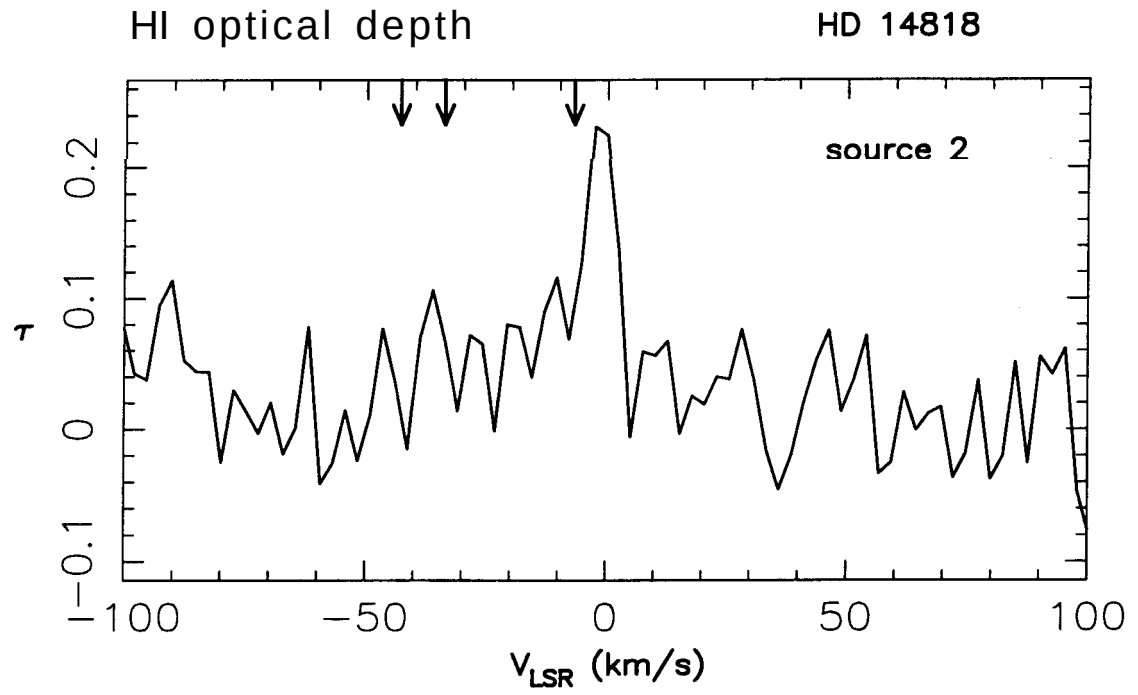
HI optical depth
HD 14818
source 2
τ
0.2
0.1
0
−0.1
−100
−50
0
50
100
V_{LSR} (km/s)

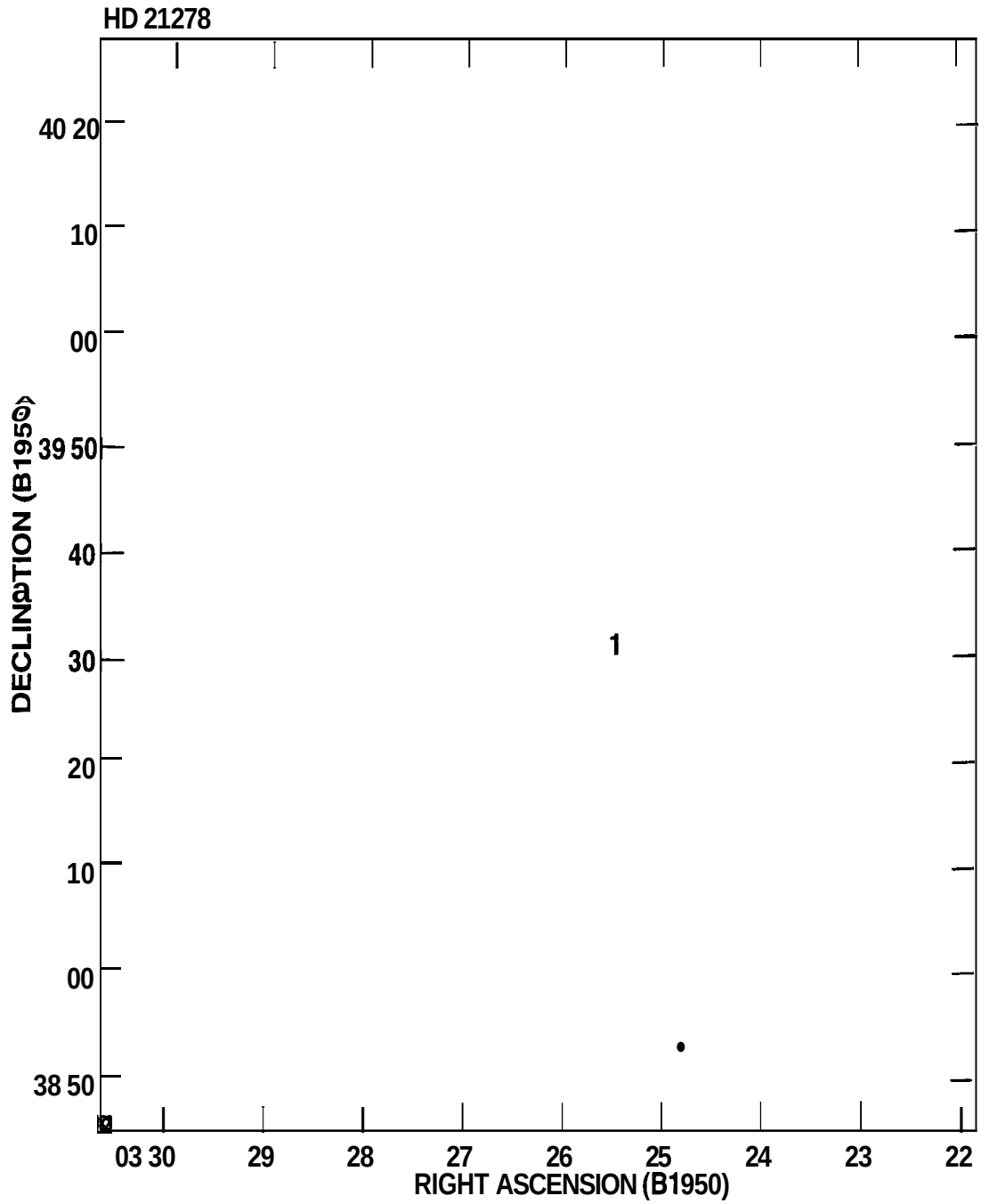
HD 21278
40 20
10
00
39 50
40
30
20
10
00
38 50
DECLINATION (B1950)
1
03 30
29
28
27
26
25
24
23
22
RIGHT ASCENSION (B1950)

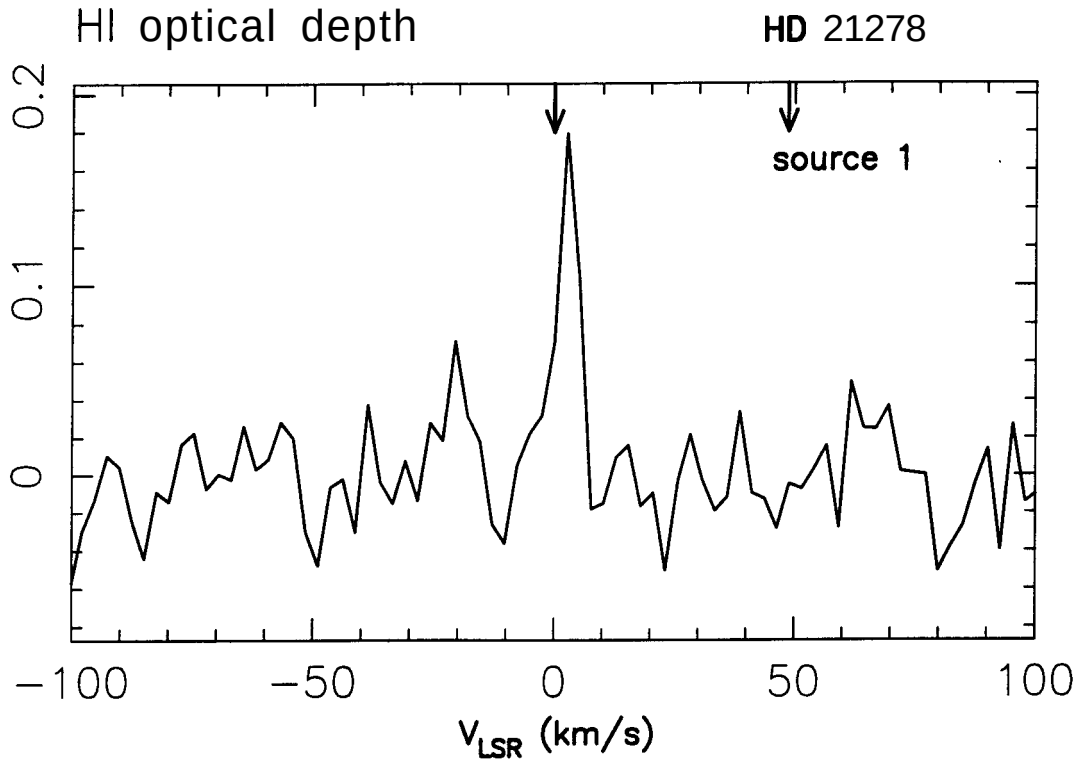
HI optical depth
HD 21278
source 1
0.2
0.1
0
−100
−50
0
50
100
V_{LSR} (km/s)

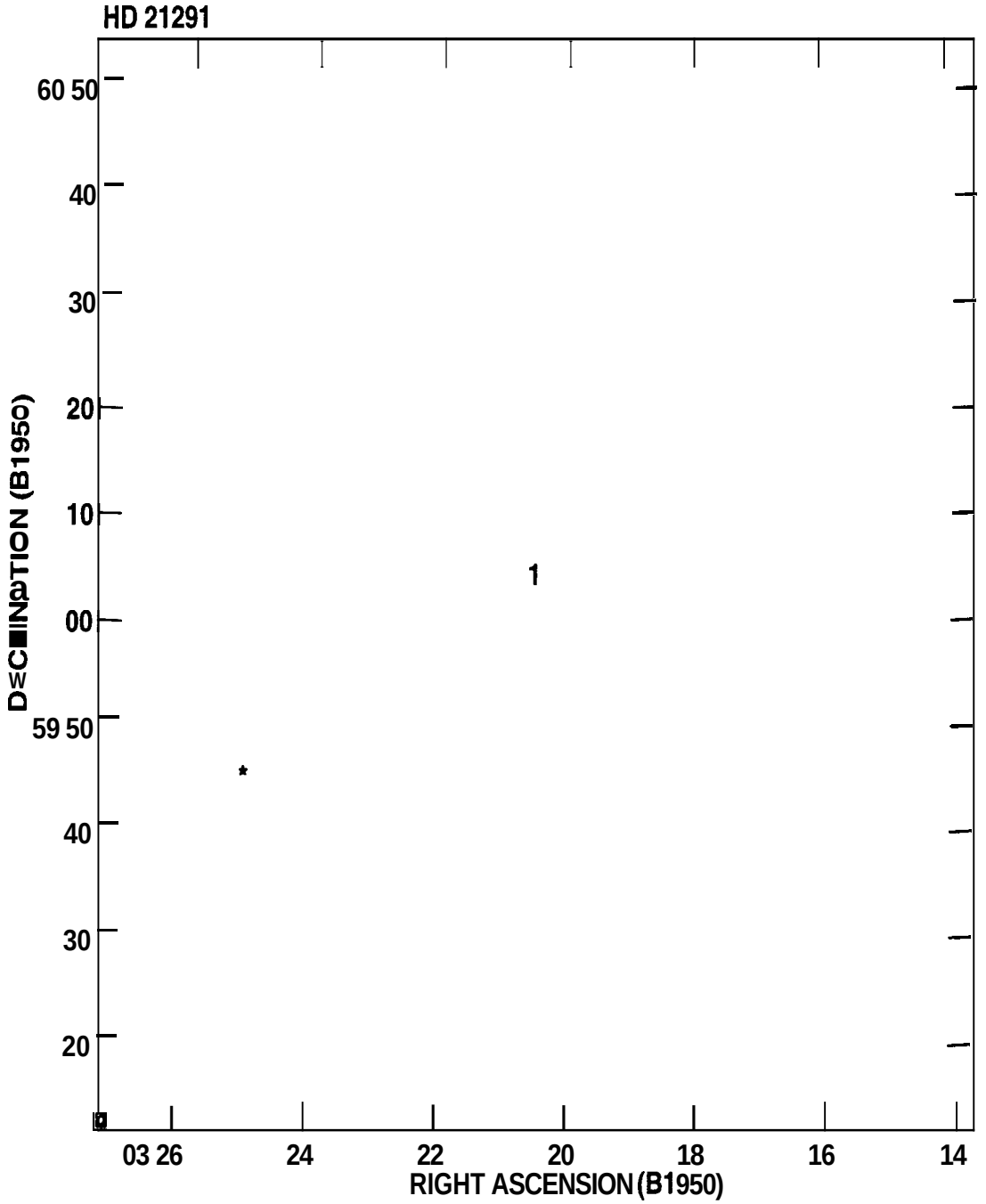
HD 21291
60 50
40
30
20
10
00
59 50
40
30
20
1
03 26
24
22
20
18
16
14
RIGHT ASCENSION (B1950)

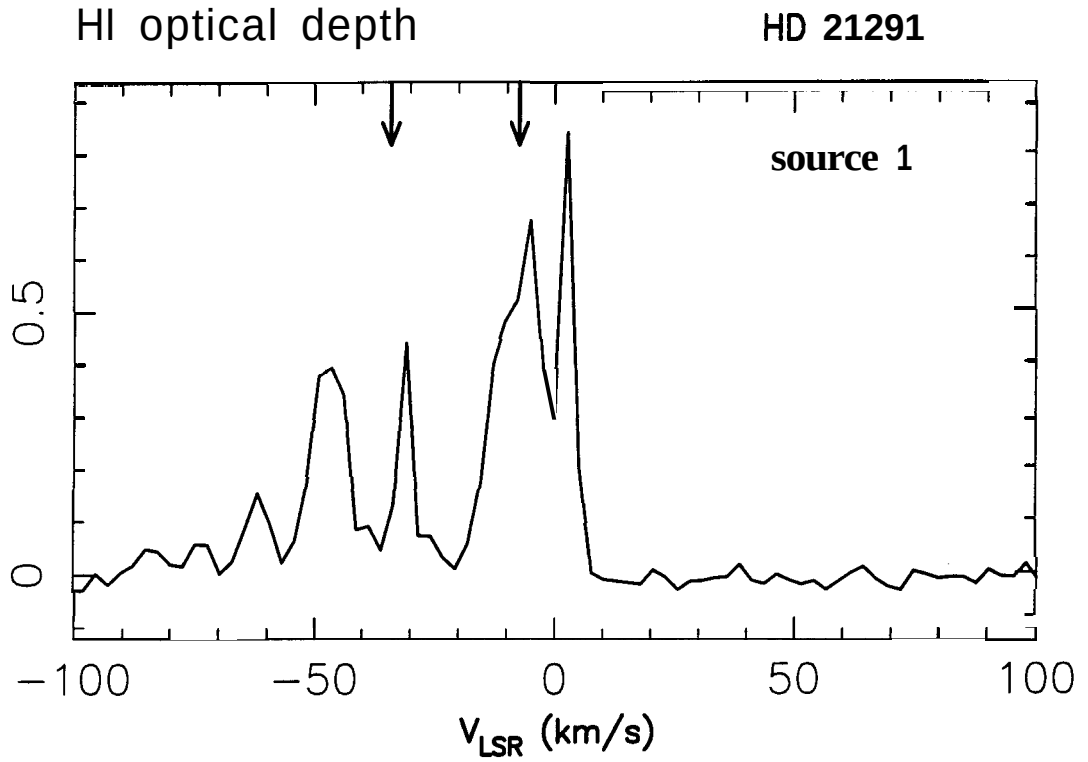
HI optical depth
HD 21291
source 1
0.5
0
−100
−50
0
50
100
V_{LSR} (km/s)

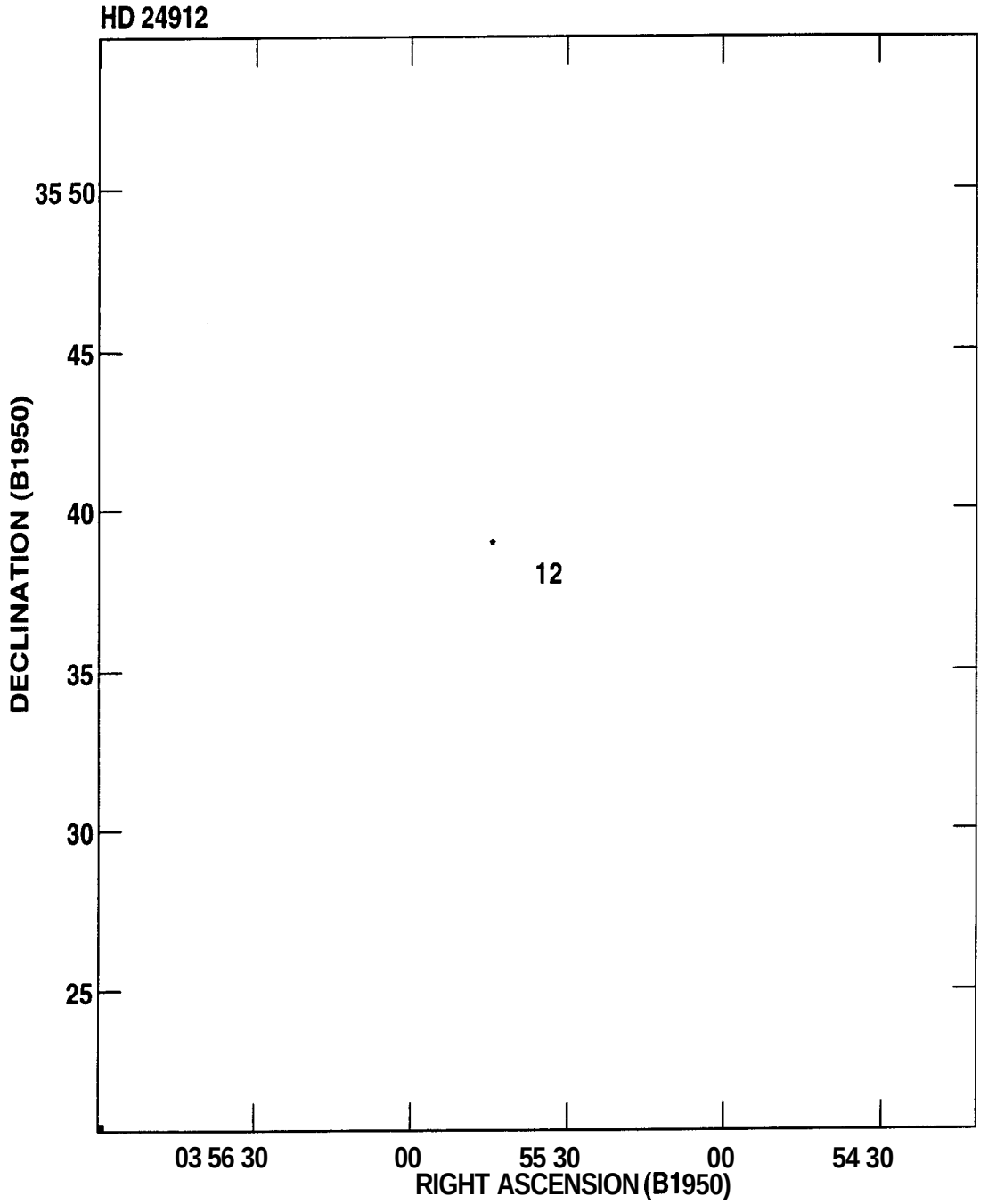
HD 24912
35 50
45
40
35
30
25
DECLINATION (B1950)
12
03 56 30
00
55 30
00
54 30
RIGHT ASCENSION (B1950)

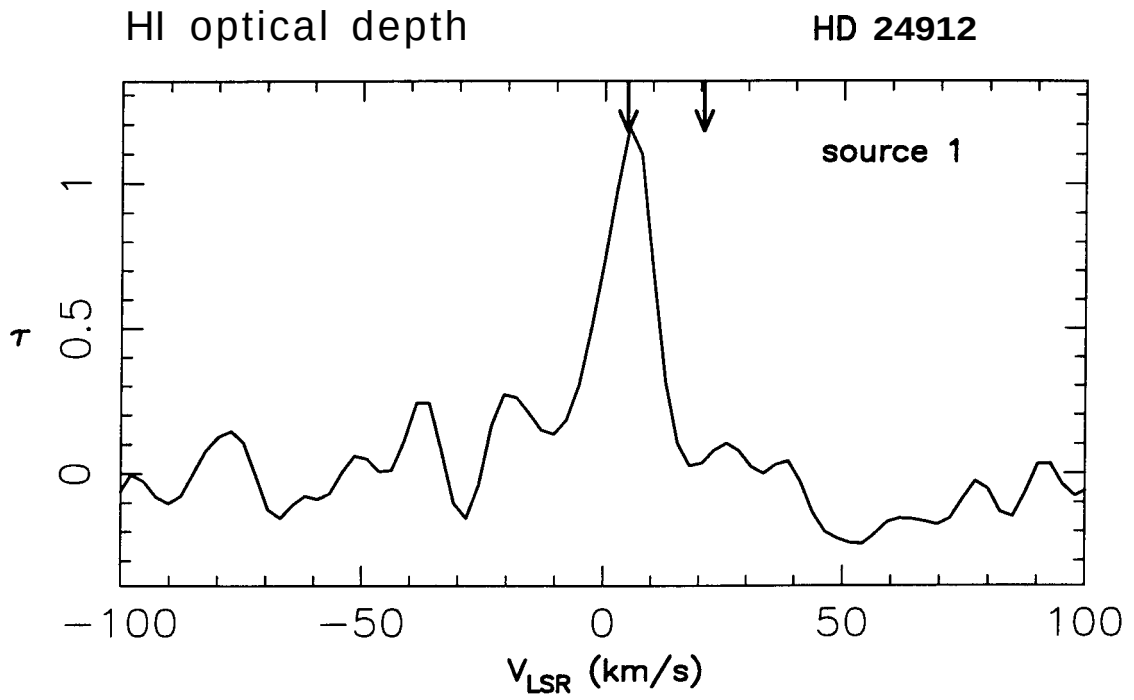
HI optical depth
HD 24912
source 1
τ
0
0.5
1
−100
−50
0
50
100
V_LSR (km/s)

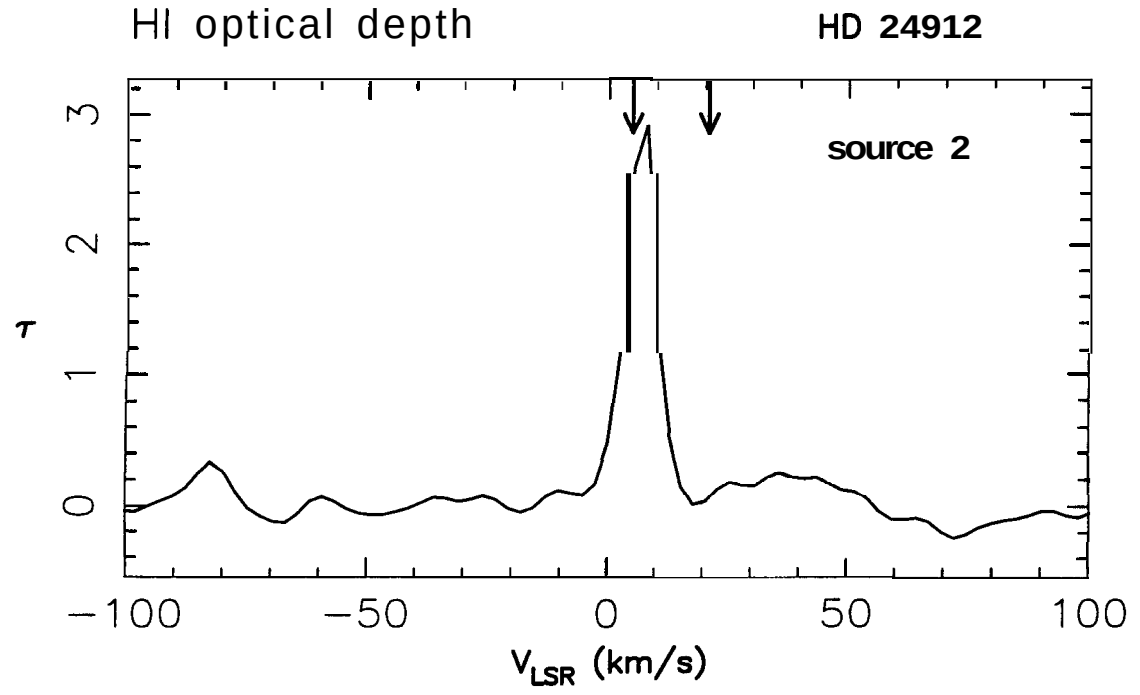
HI optical depth
HD 24912
source 2
τ
0
1
2
3
−100
−50
0
50
100
V_LSR (km/s)

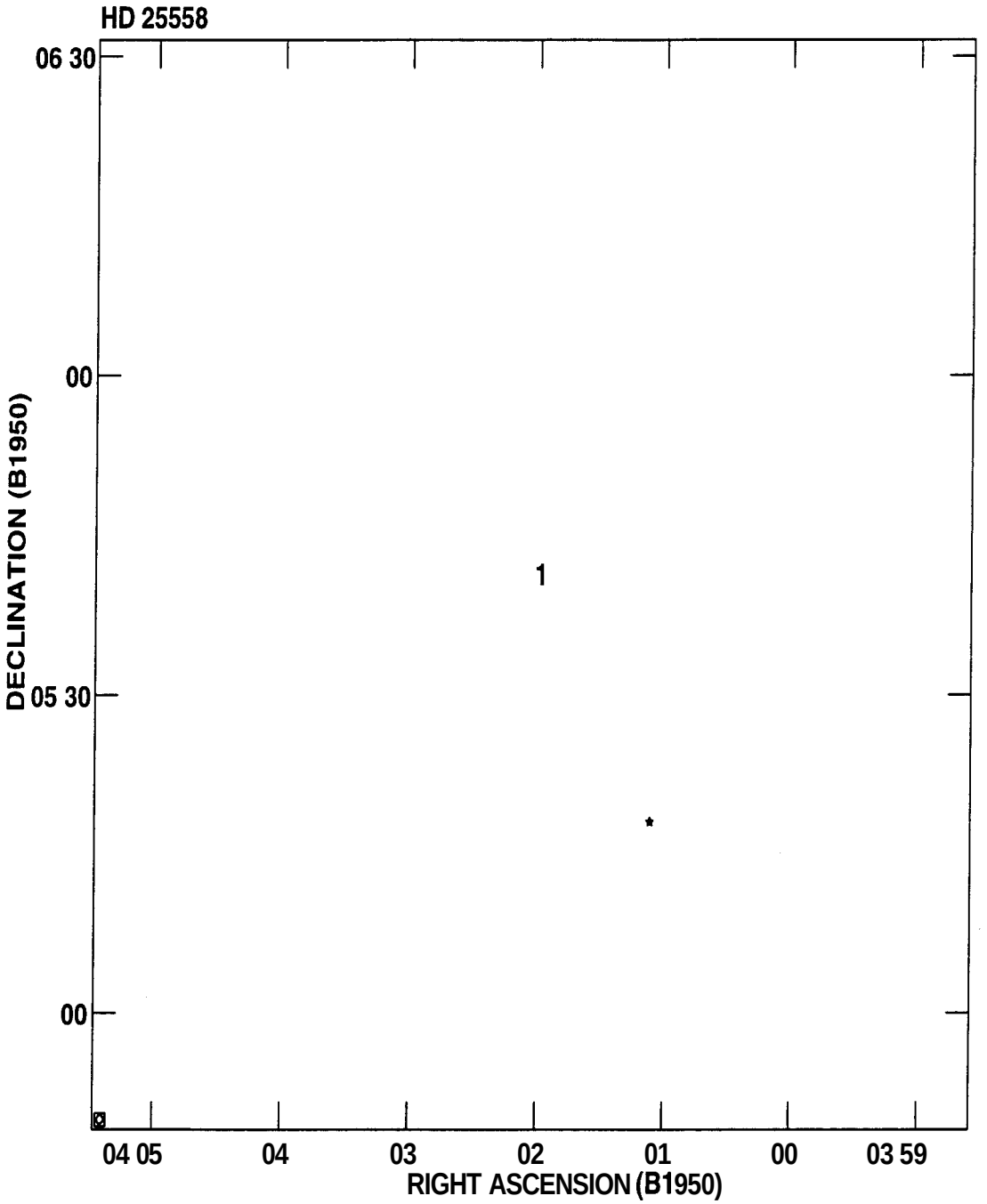
HD 25558
06 30
00
05 30
00
DECLINATION (B1950)
1
04 05
04
03
02
01
00
03 59
RIGHT ASCENSION (B1950)

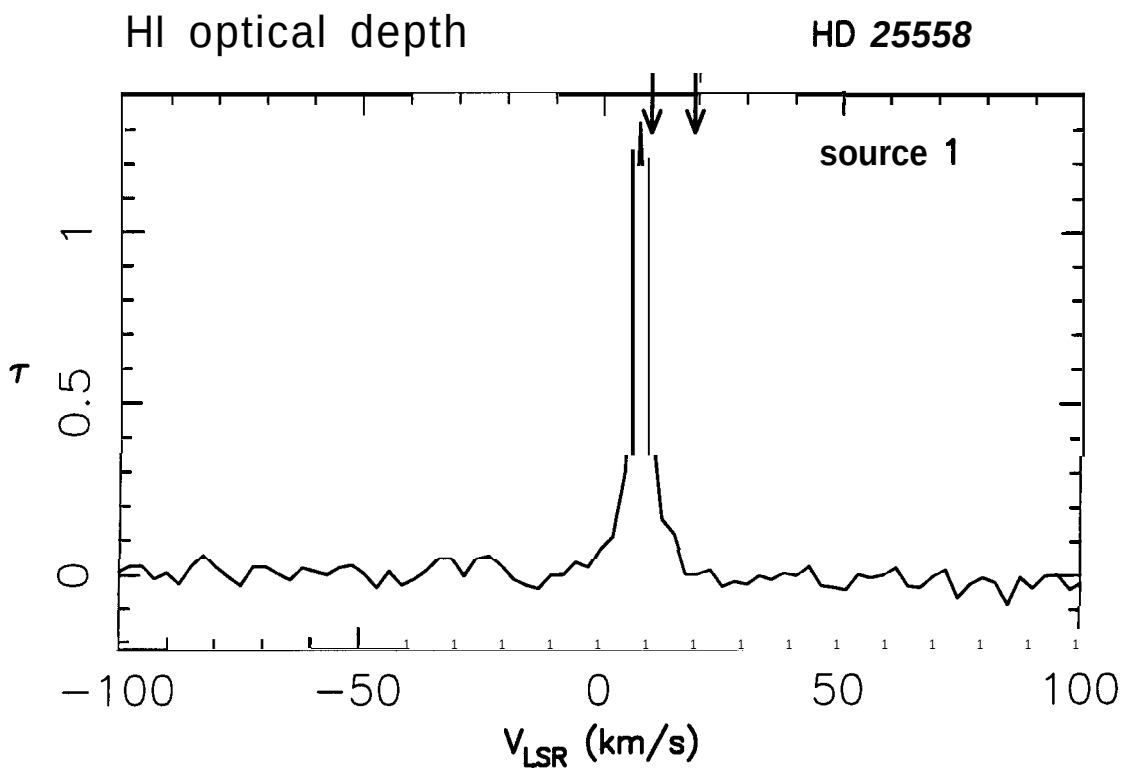
HI optical depth
HD 25558
source 1
τ
0
0.5
1
−100
−50
0
50
100
V_LSR (km/s)

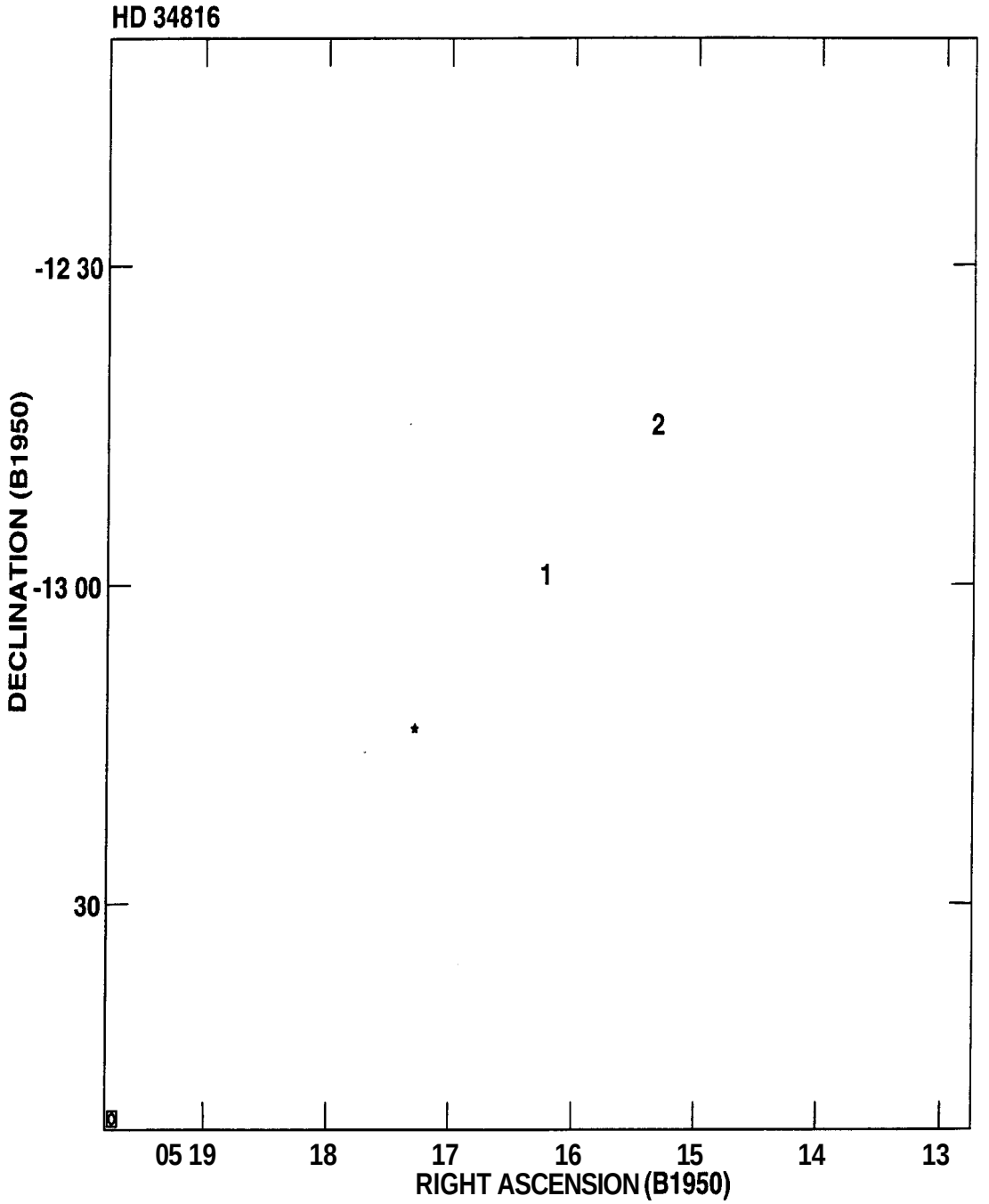
HD 34816
-12 30
-13 00
30
DECLINATION (B1950)
2
1
05 19
18
17
16
15
14
13
RIGHT ASCENSION (B1950)

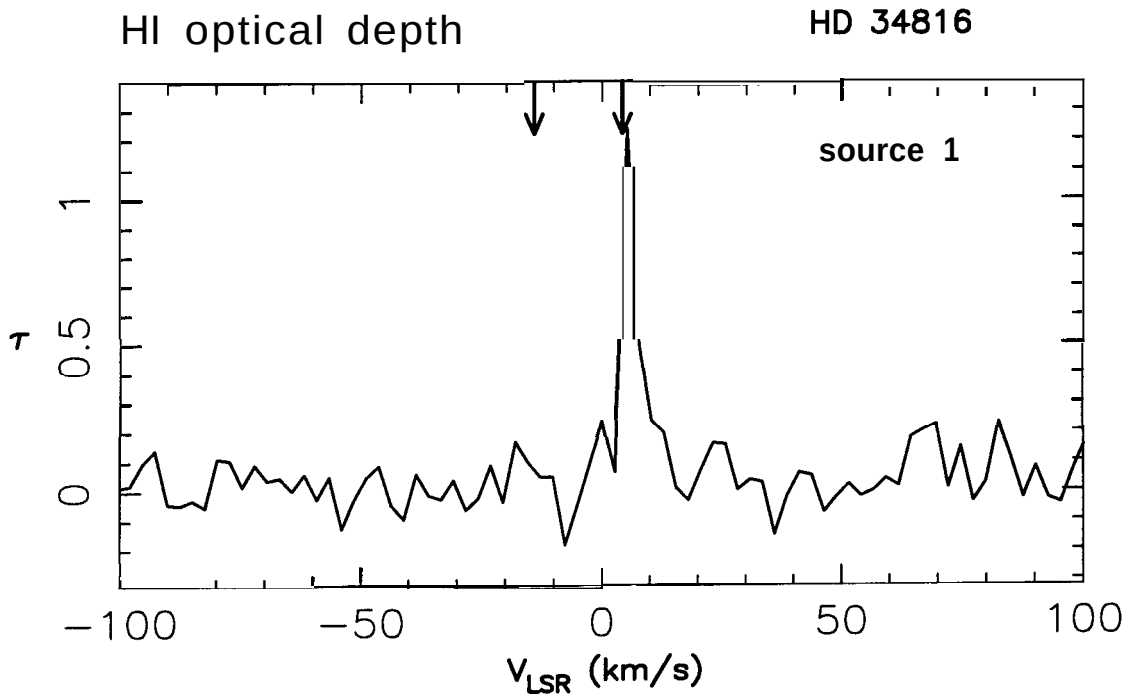
HI optical depth
HD 34816
source 1
τ
0
0.5
1
−100
−50
0
50
100
V_LSR (km/s)

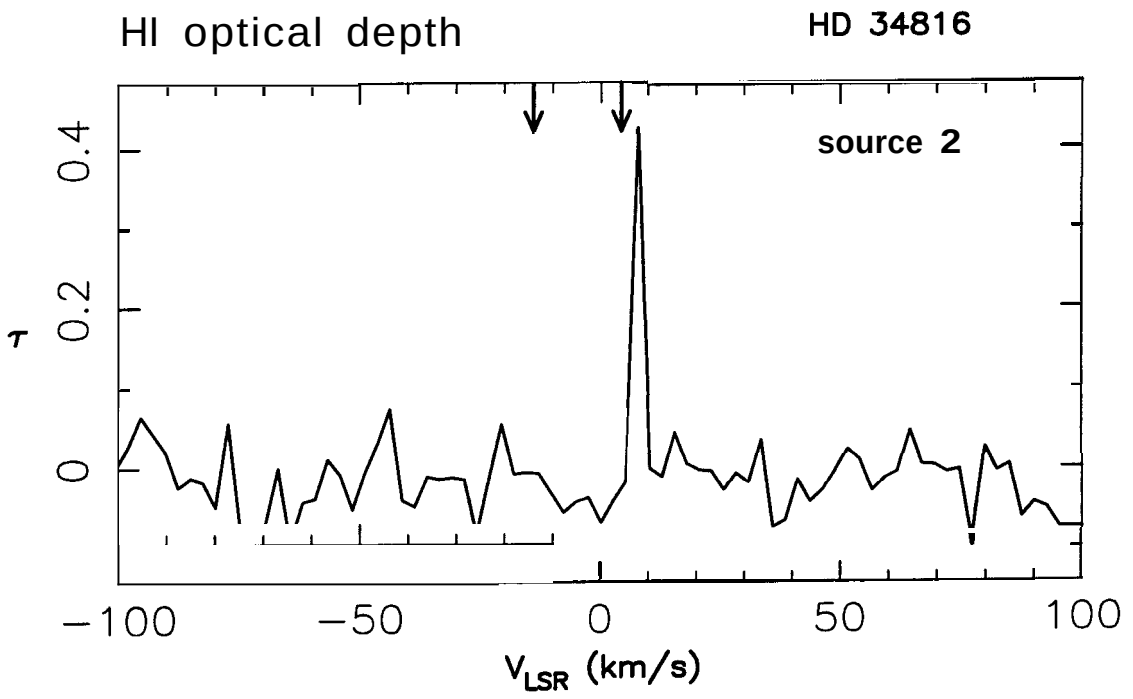
HI optical depth
HD 34816
source 2
τ
0
0.2
0.4
−100
−50
0
50
100
V_LSR (km/s)

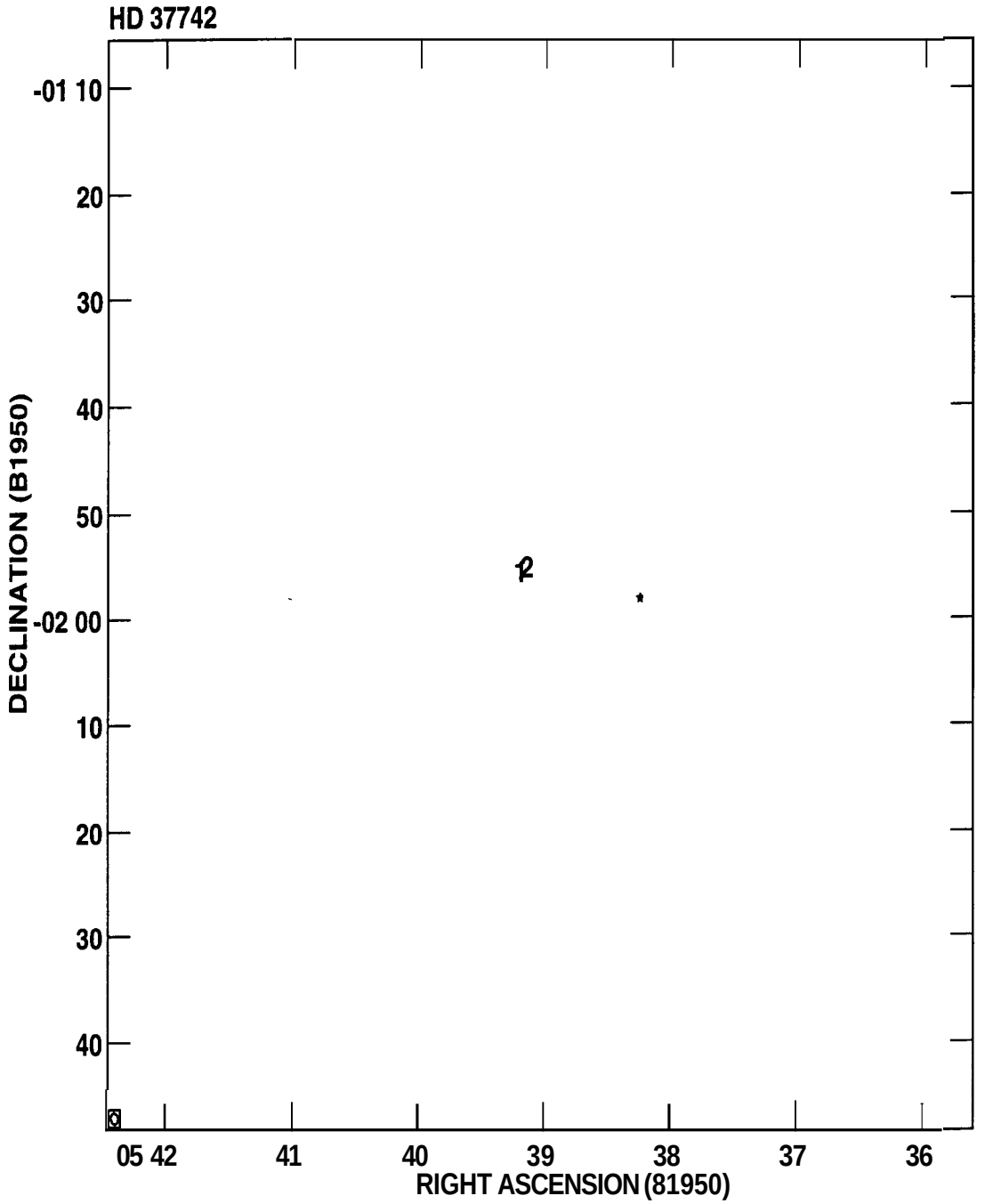
HD 37742
-01 10
20
30
40
50
-02 00
10
20
30
40
DECLINATION (B1950)
05 42
41
40
39
38
37
36
RIGHT ASCENSION (81950)

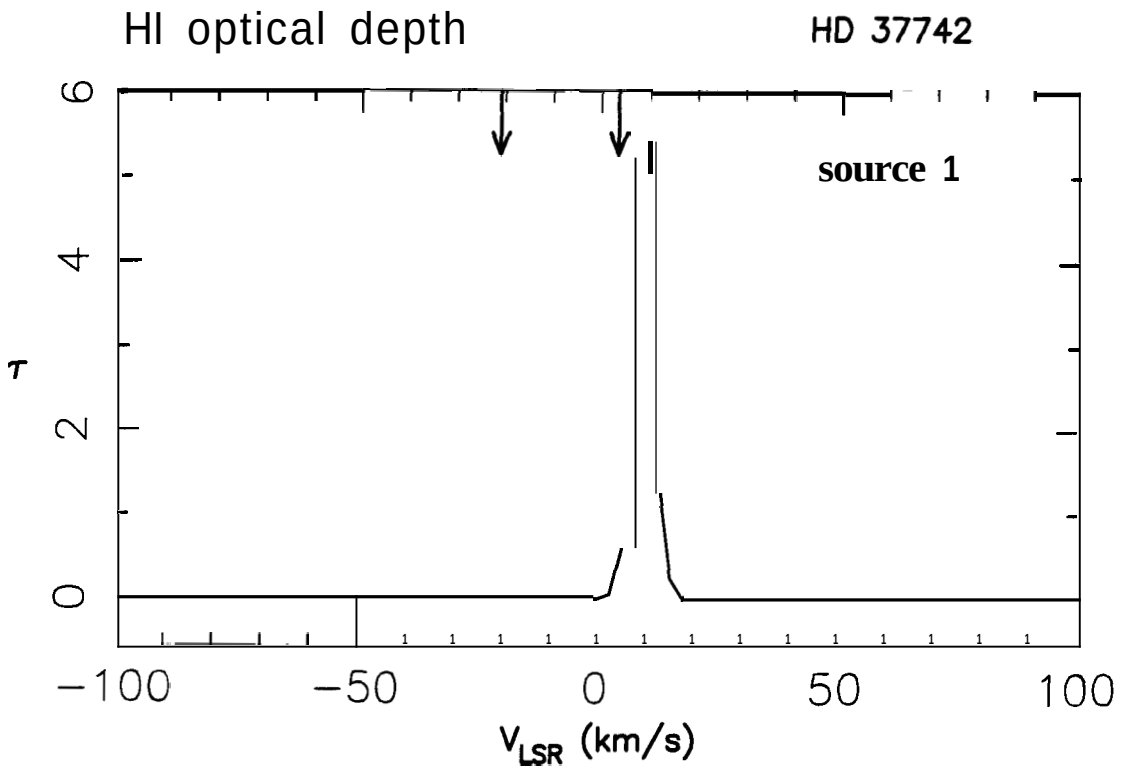
HI optical depth
HD 37742
source 1
τ
0
2
4
6
−100
−50
0
50
100
V_LSR (km/s)

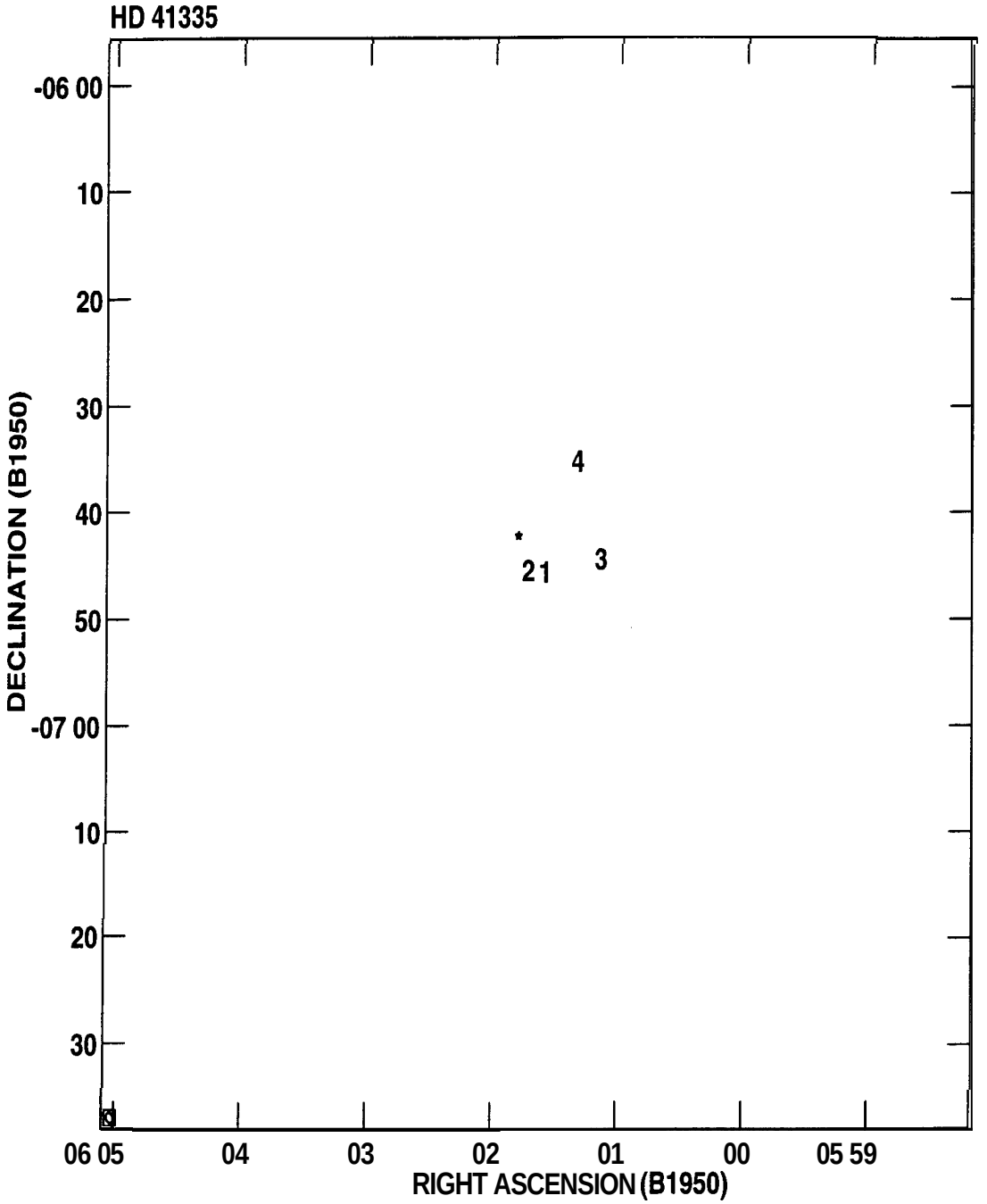
HD 41335
-06 00
10
20
30
40
50
-07 00
10
20
30
DECLINATION (B1950)
4
3
2 1
06 05
04
03
02
01
00
05 59
RIGHT ASCENSION (B1950)

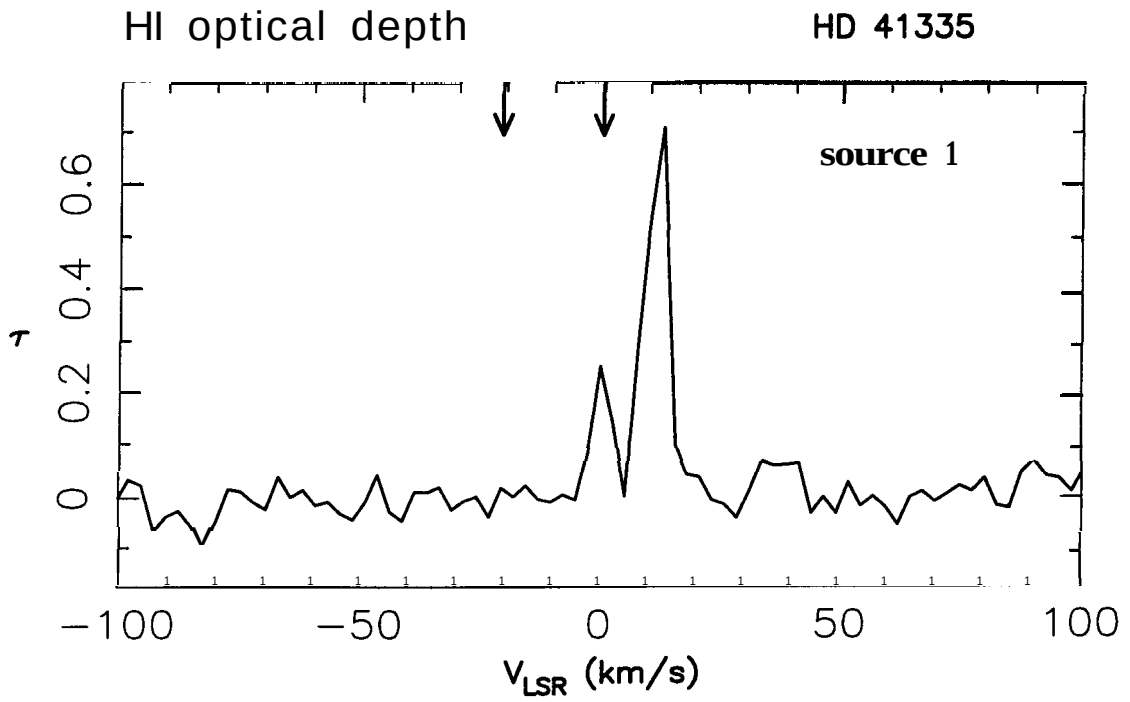
HI optical depth
HD 41335
source 1
τ
0
0.2
0.4
0.6
−100
−50
0
50
100
V_LSR (km/s)

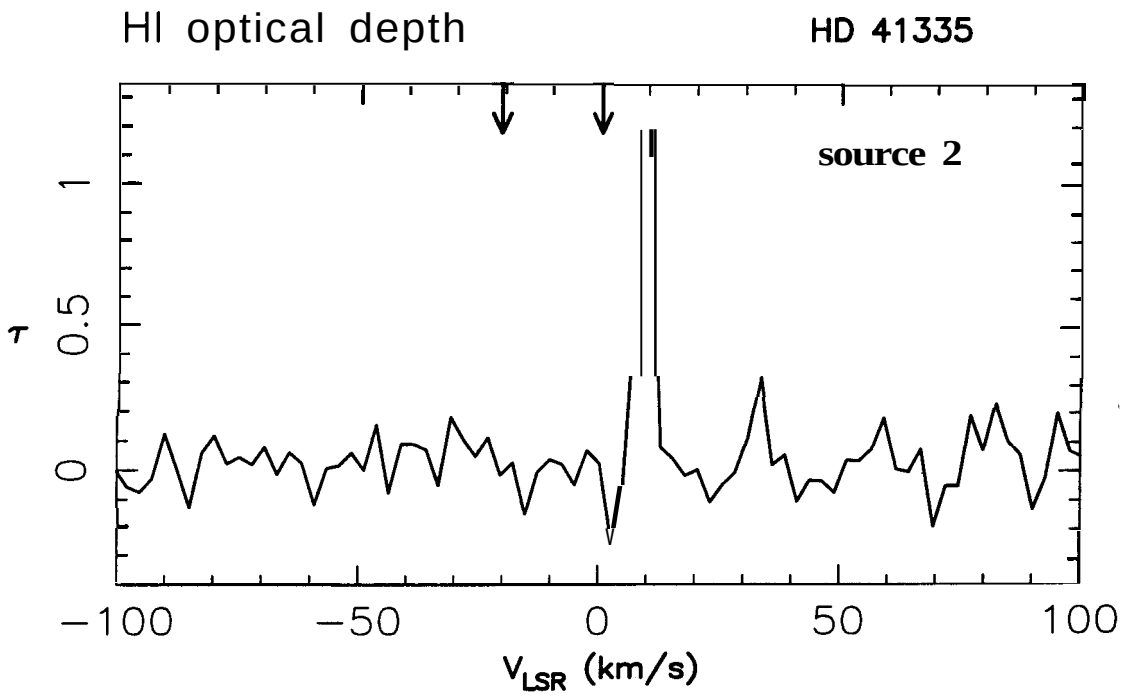
HI optical depth
HD 41335
source 2
τ
0
0.5
1
−100
−50
0
50
100
V_LSR (km/s)

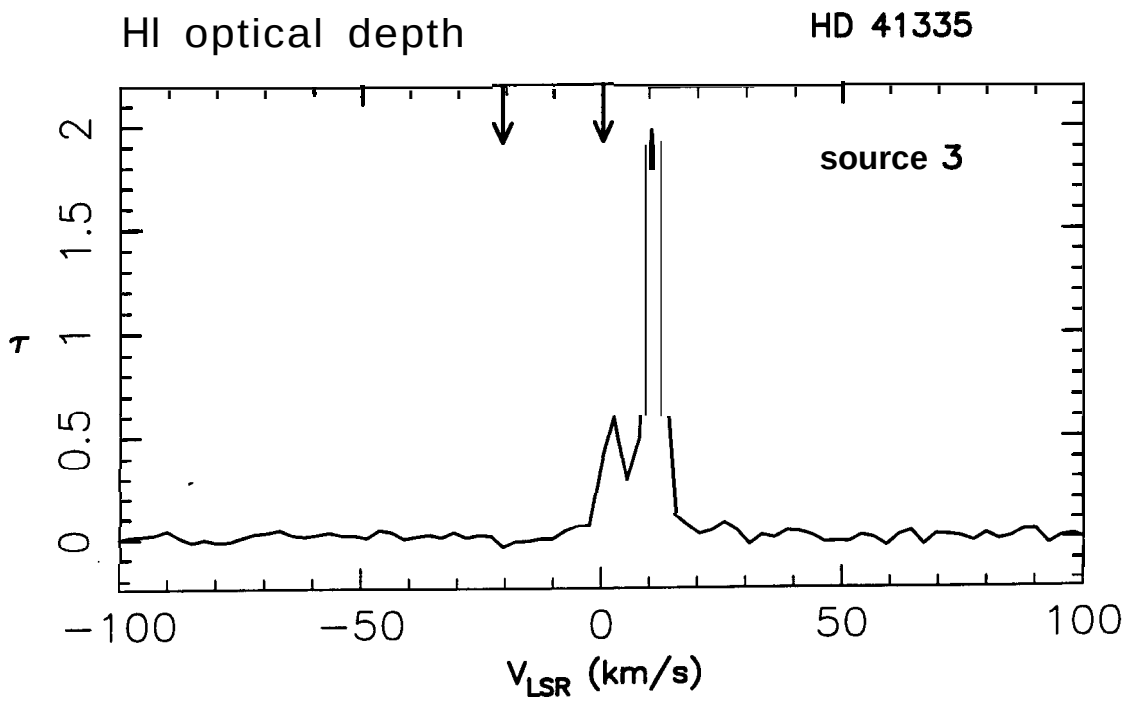
HI optical depth
HD 41335
source 3
τ
0
0.5
1
1.5
2
−100
−50
0
50
100
V_LSR (km/s)

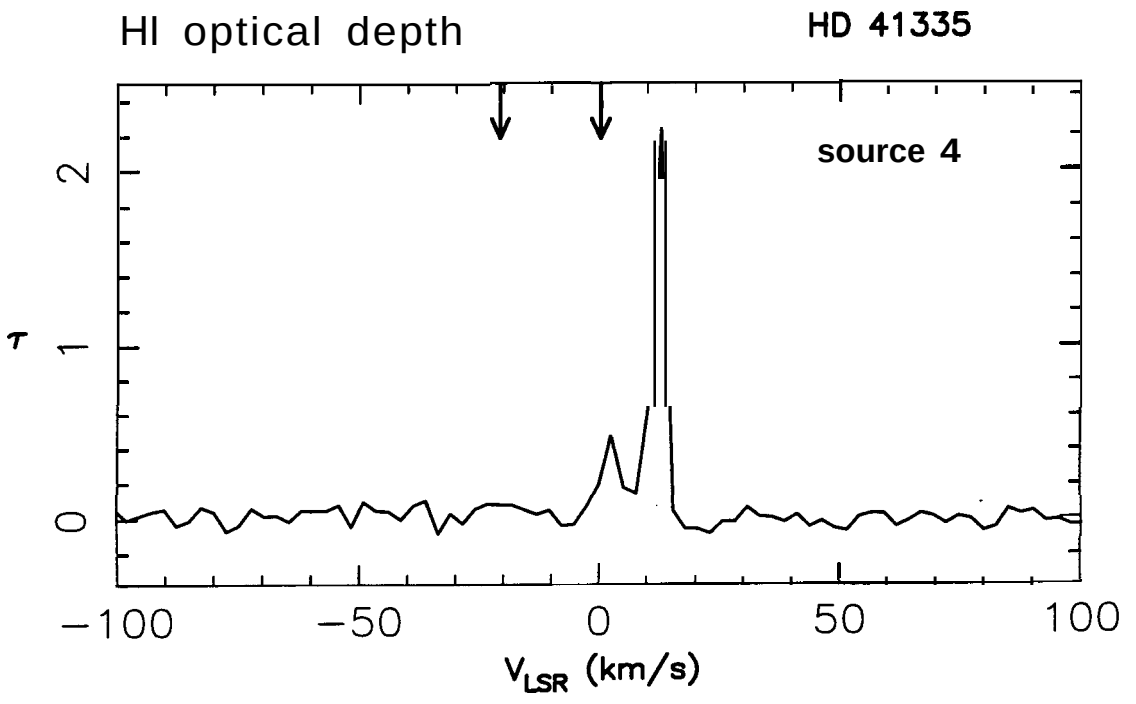
HI optical depth
HD 41335
source 4
τ
0
1
2
−100
−50
0
50
100
V_LSR (km/s)

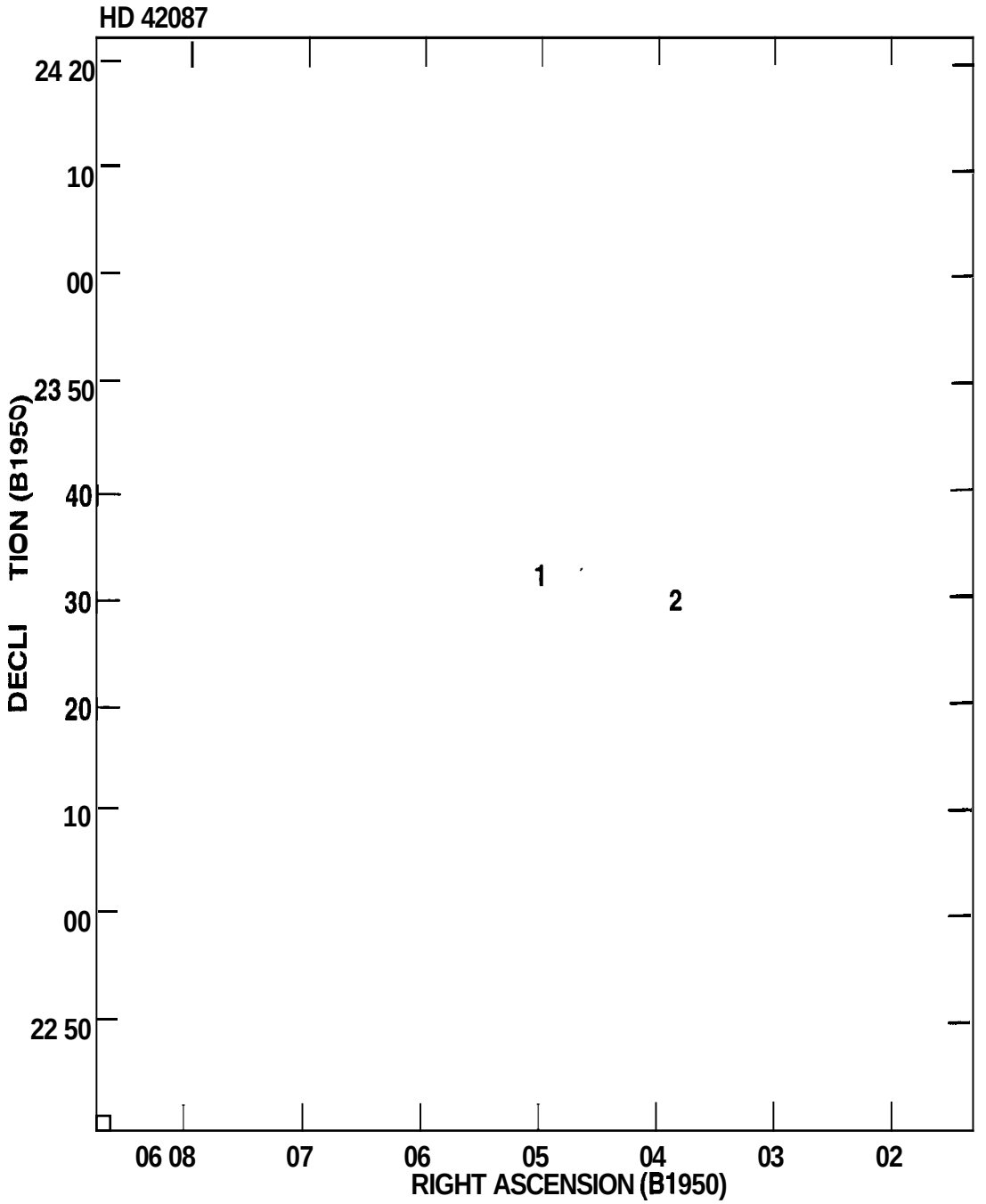
HD 42087
24 20
10
00
23 50
40
30
20
10
00
22 50
DECLI TION (B1950)
1
2
06 08
07
06
05
04
03
02
RIGHT ASCENSION (B1950)

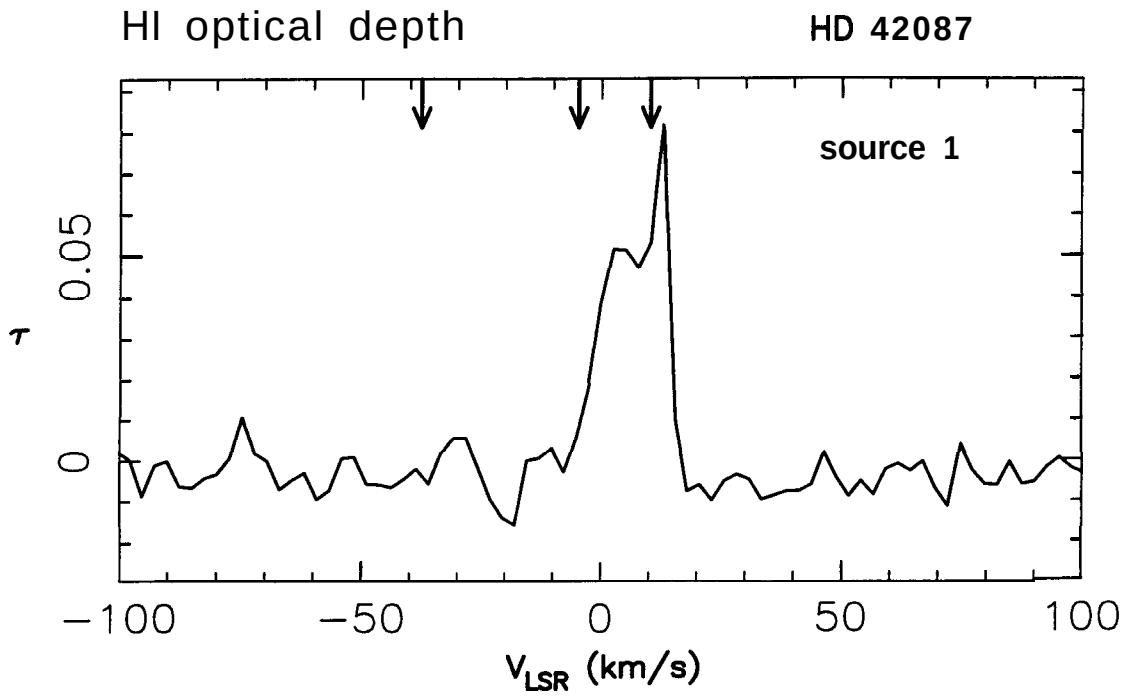
HI optical depth
HD 42087
source 1
τ
0.05
0
−100
−50
0
50
100
V_LSR (km/s)

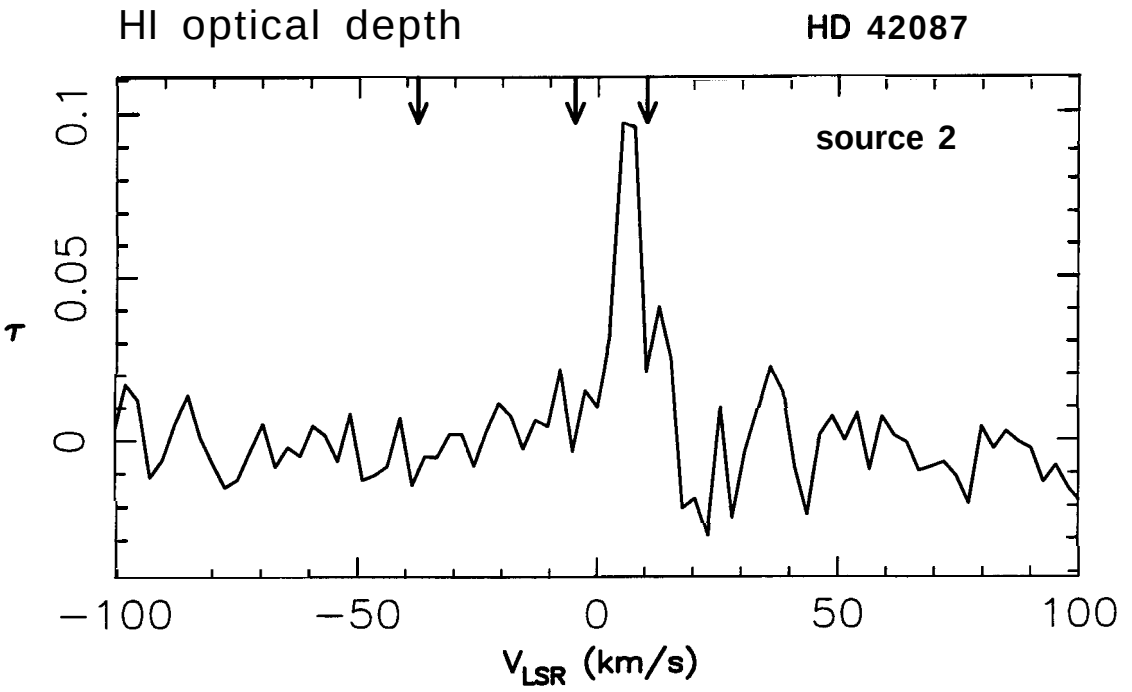
HI optical depth
HD 42087
source 2
τ
0.1
0.05
0
−100
−50
0
50
100
V_LSR (km/s)

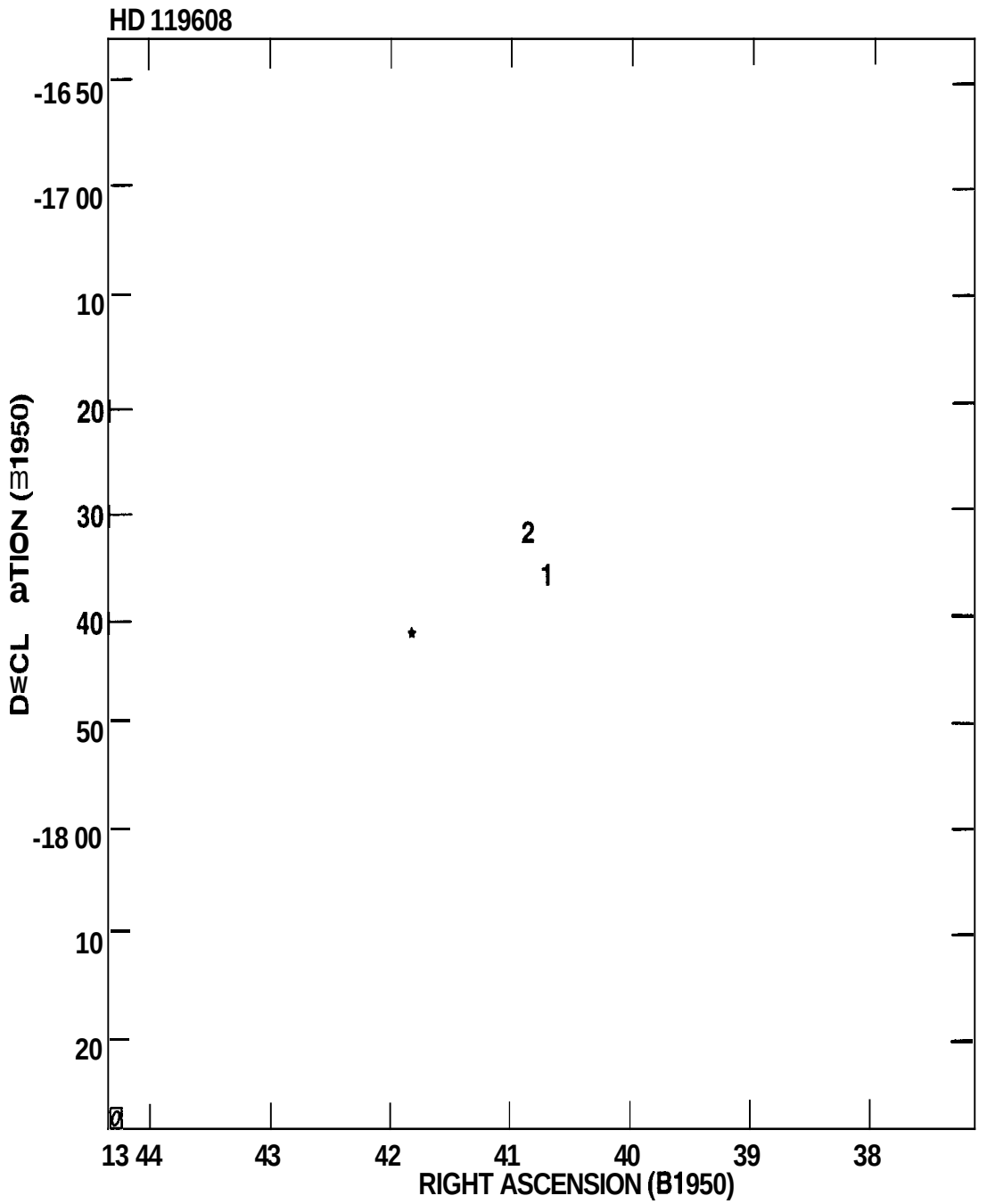
HD 119608
-16 50
-17 00
10
20
30
40
50
-18 00
10
20
2
1
13 44
43
42
41
40
39
38
RIGHT ASCENSION (B1950)

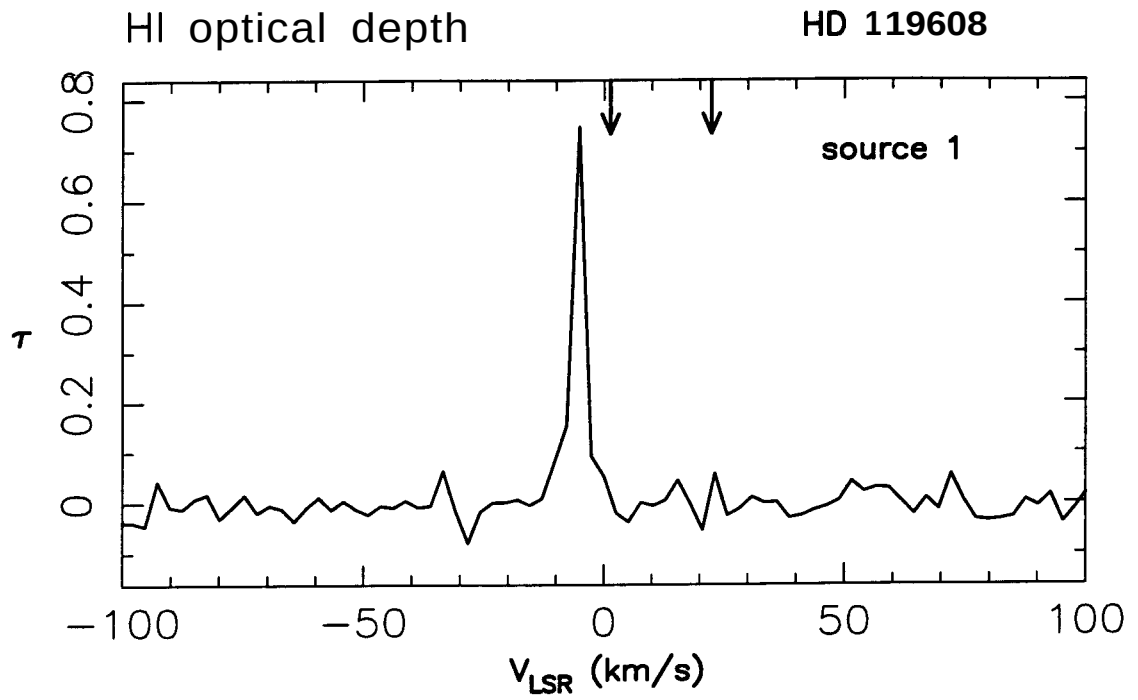
HI optical depth
HD 119608
source 1
τ
0
0.2
0.4
0.6
0.8
−100
−50
0
50
100
V_LSR (km/s)

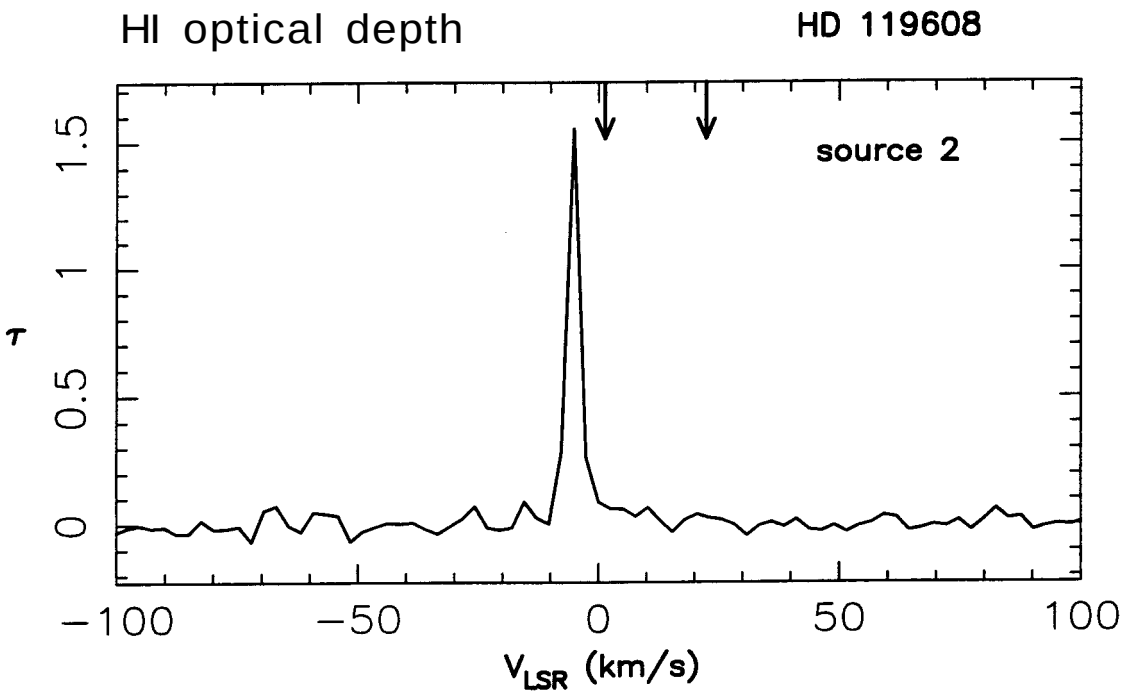
HI optical depth
HD 119608
source 2
τ
0
0.5
1
1.5
−100
−50
0
50
100
V_LSR (km/s)

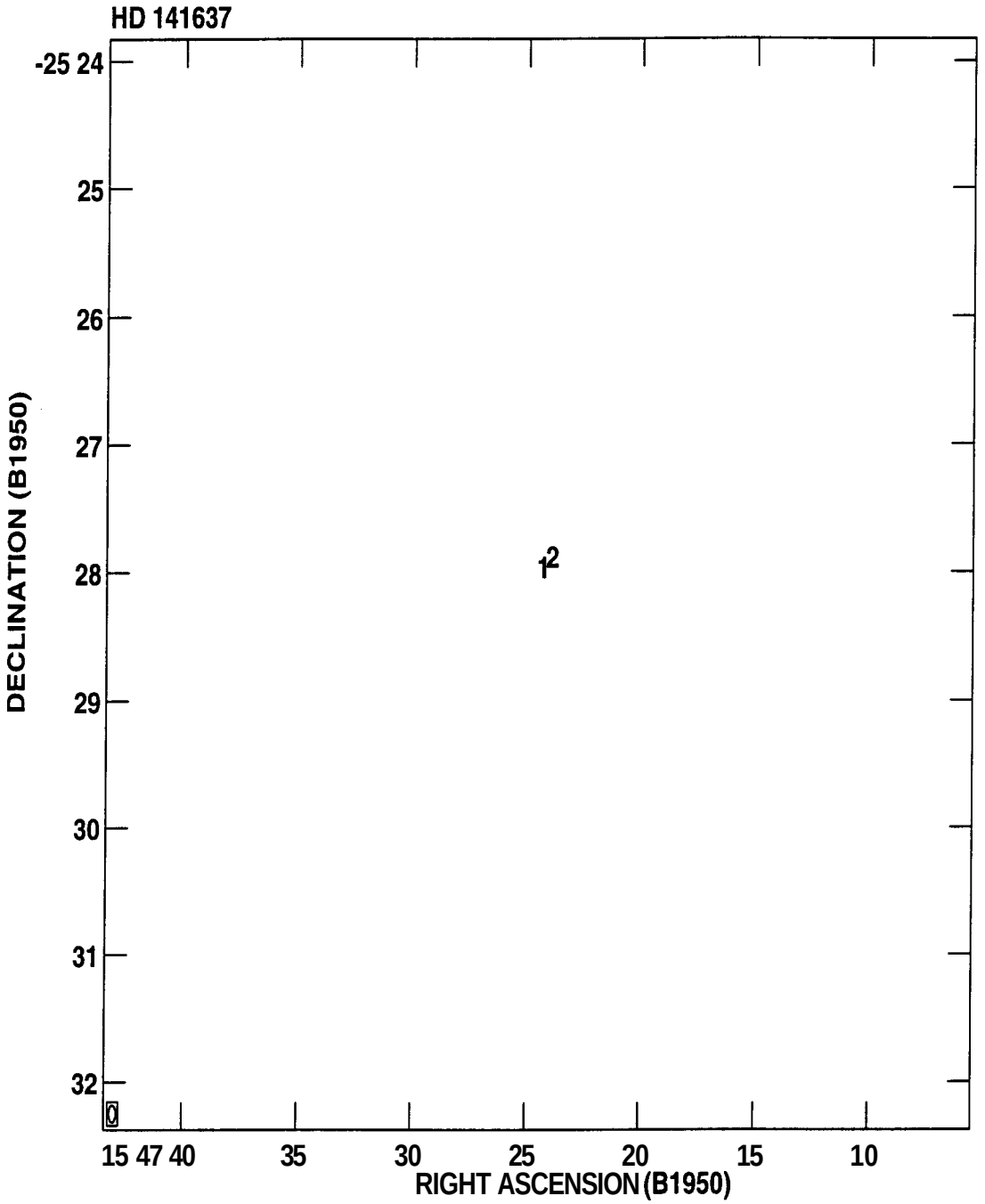
HD 141637
-25 24
25
26
27
28
29
30
31
32
DECLINATION (B1950)
15 47 40
35
30
25
20
15
10
RIGHT ASCENSION (B1950)

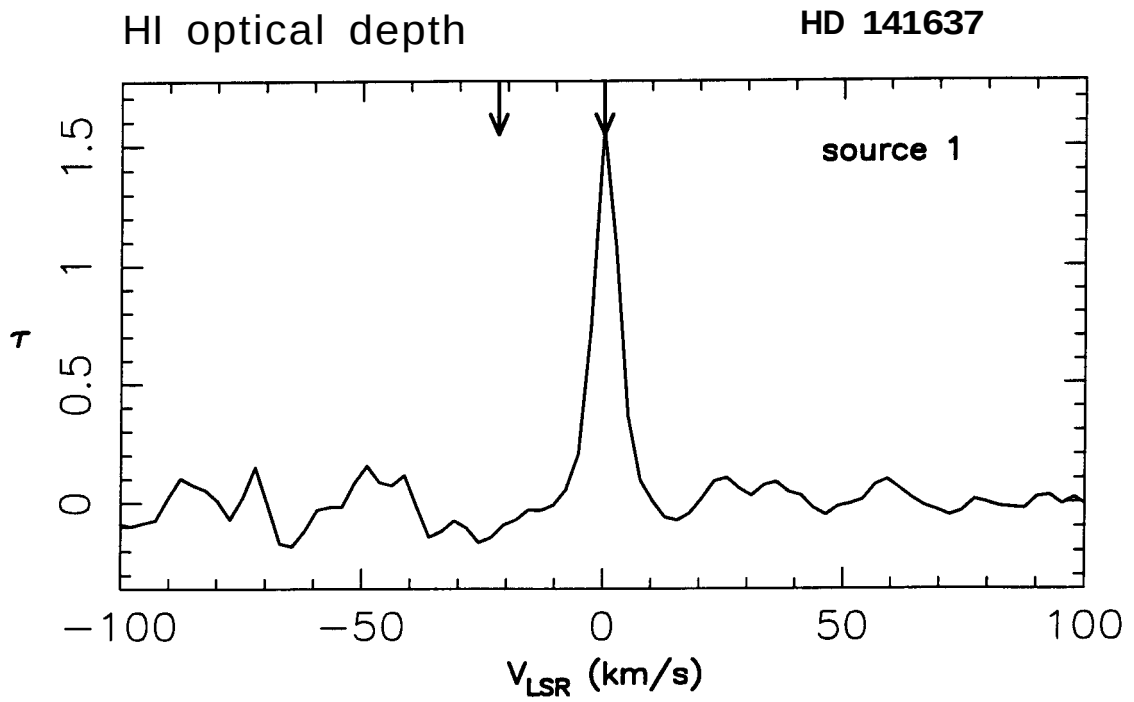
HI optical depth
HD 141637
source 1
τ
0
0.5
1
1.5
−100
−50
0
50
100
V_{LSR} (km/s)

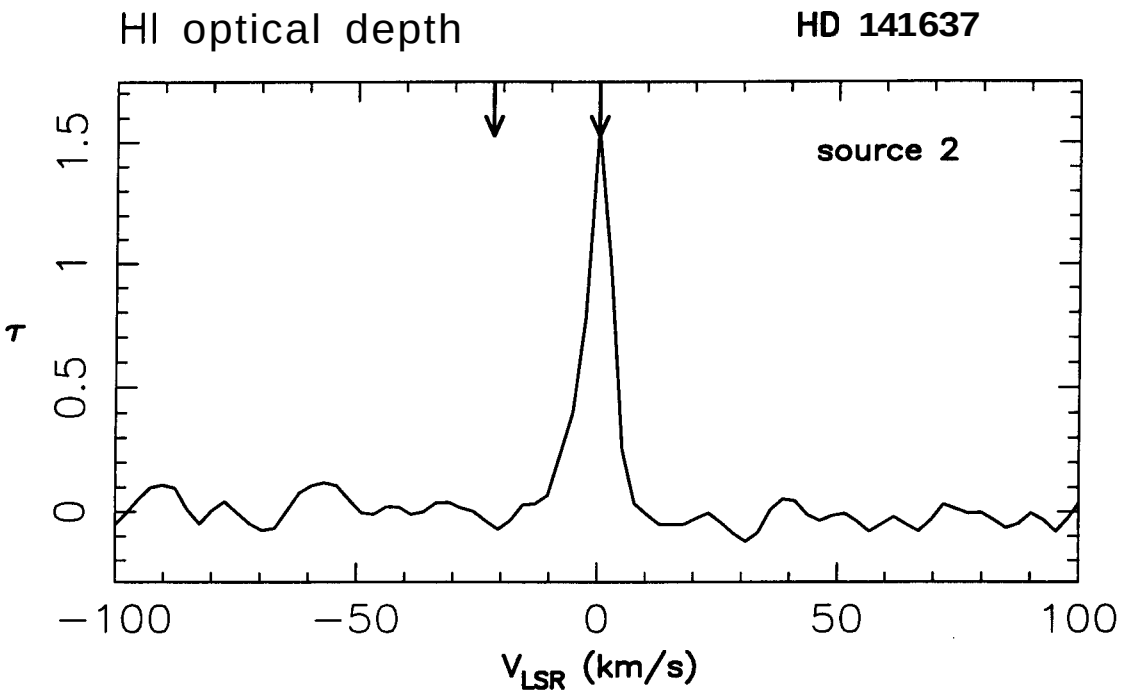
HI optical depth
HD 141637
source 2
τ
0
0.5
1
1.5
−100
−50
0
50
100
V_{LSR} (km/s)

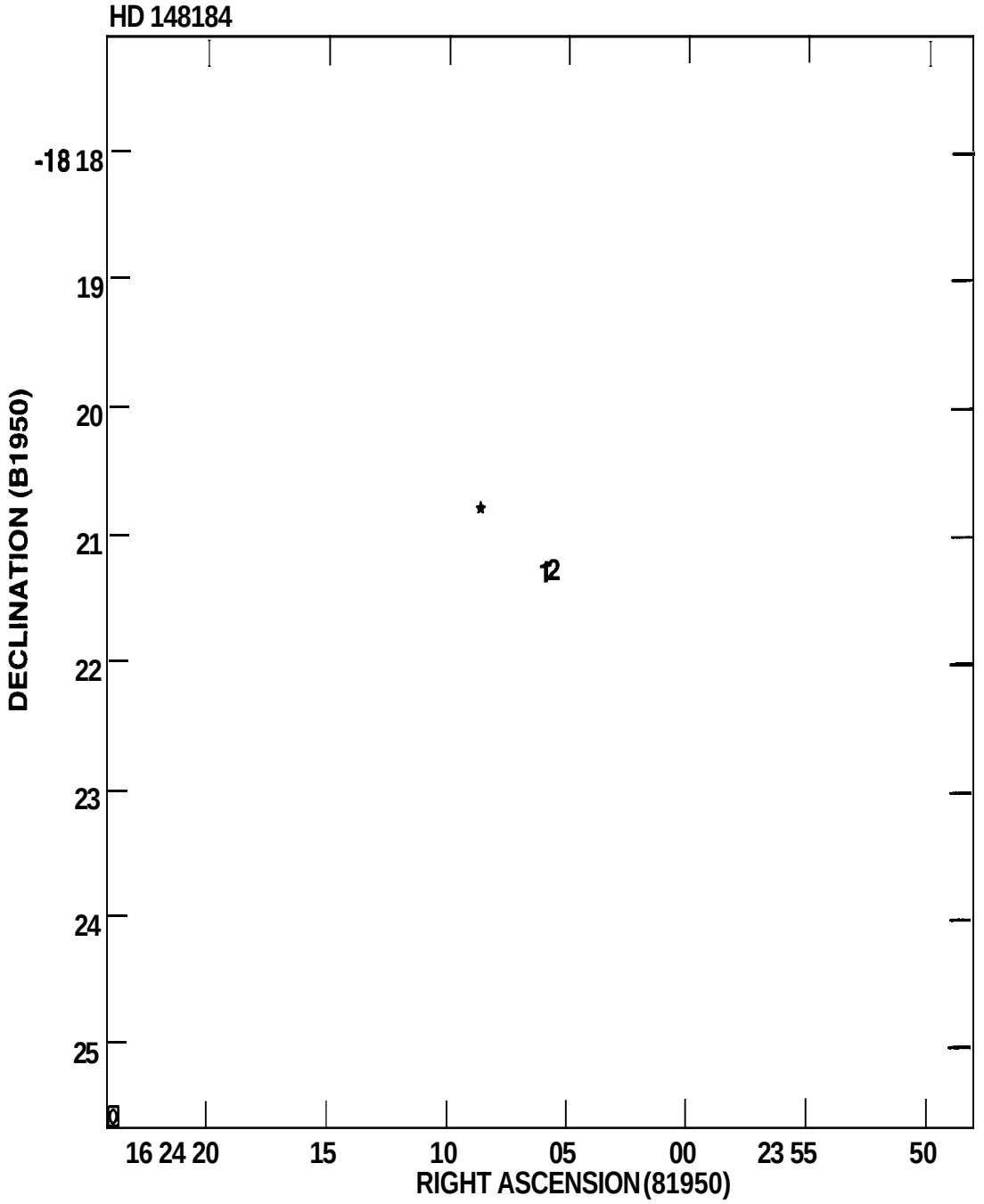
HD 148184
-18 18
19
20
21
22
23
24
25
DECLINATION (B1950)
16 24 20
15
10
05
00
23 55
50
RIGHT ASCENSION (81950)

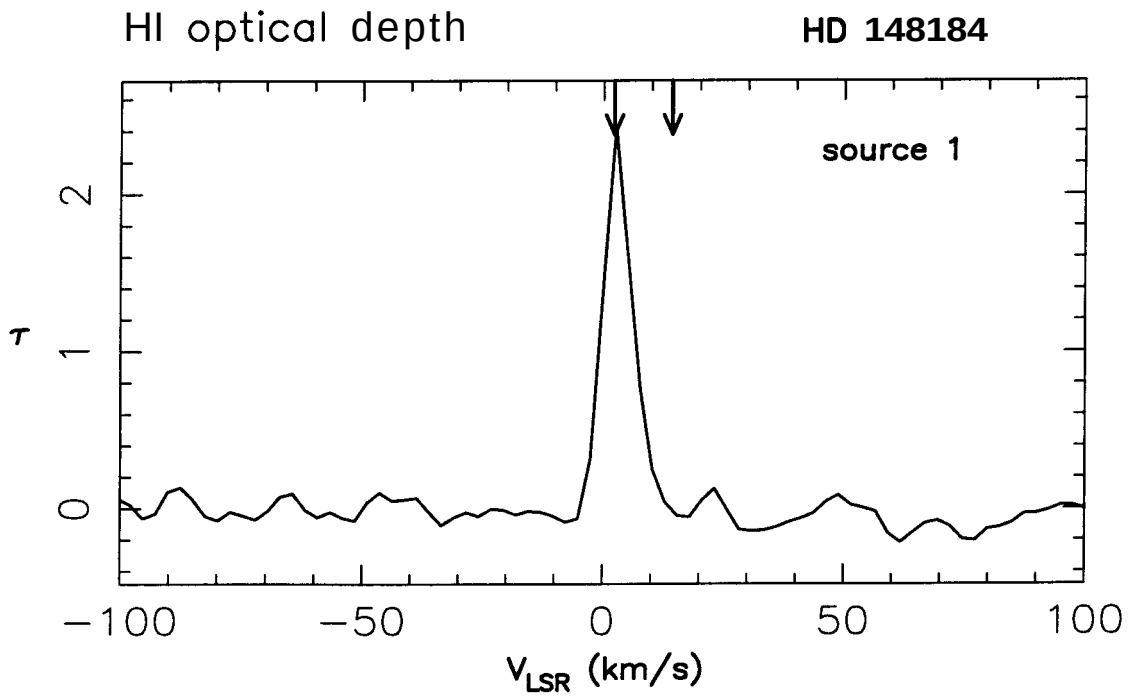
HI optical depth
HD 148184
source 1
τ
0
1
2
−100
−50
0
50
100
V_LSR (km/s)

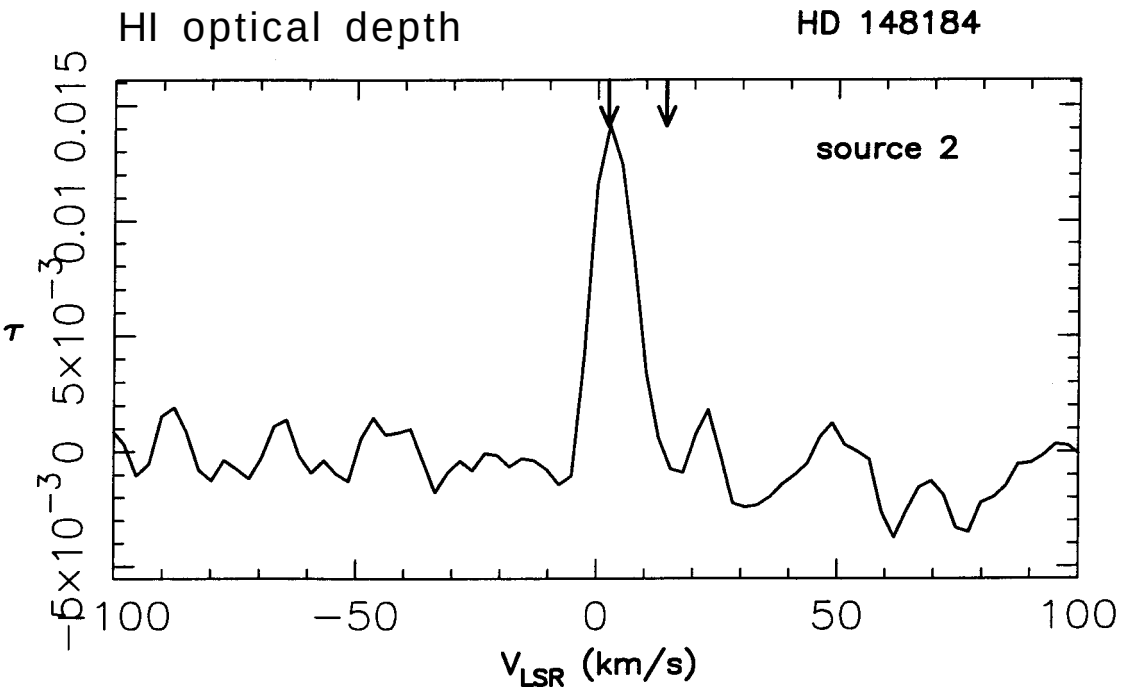
HI optical depth
HD 148184
source 2
τ
−5×10^−3
0
5×10^−3
0.01
0.015
−100
−50
0
50
100
V_LSR (km/s)

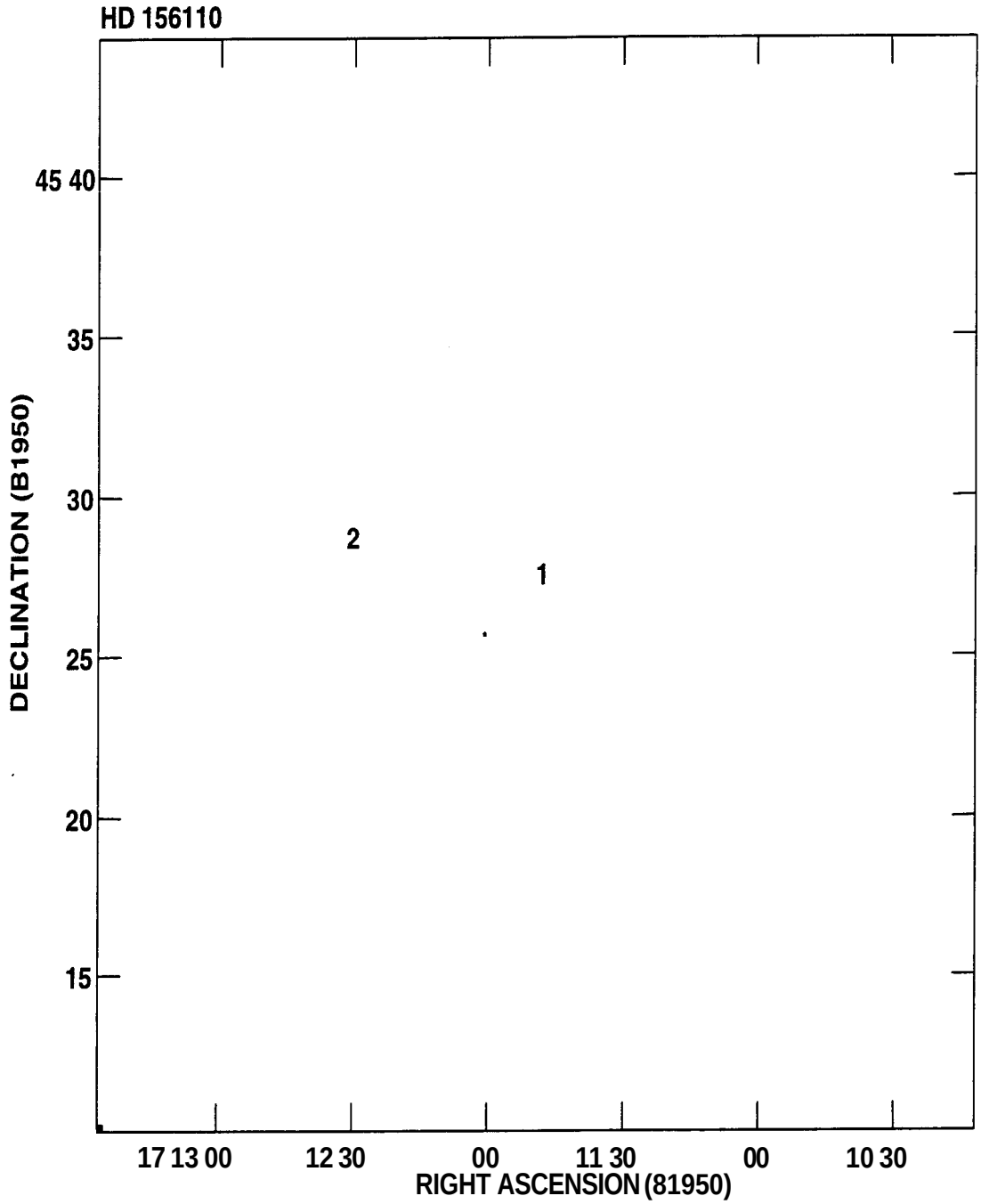
HD 156110
45 40
35
30
25
20
15
DECLINATION (B1950)
2
1
17 13 00
12 30
00
11 30
00
10 30
RIGHT ASCENSION (81950)

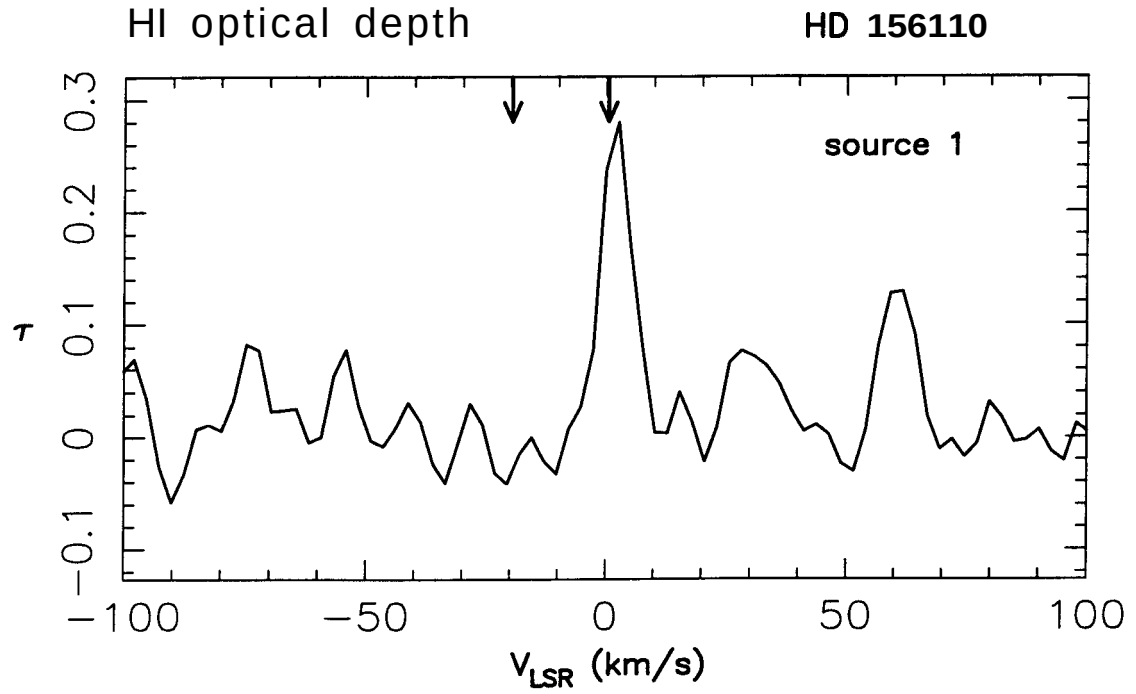
HI optical depth
HD 156110
source 1
τ
0.3
0.2
0.1
0
−0.1
−100
−50
0
50
100
V_LSR (km/s)

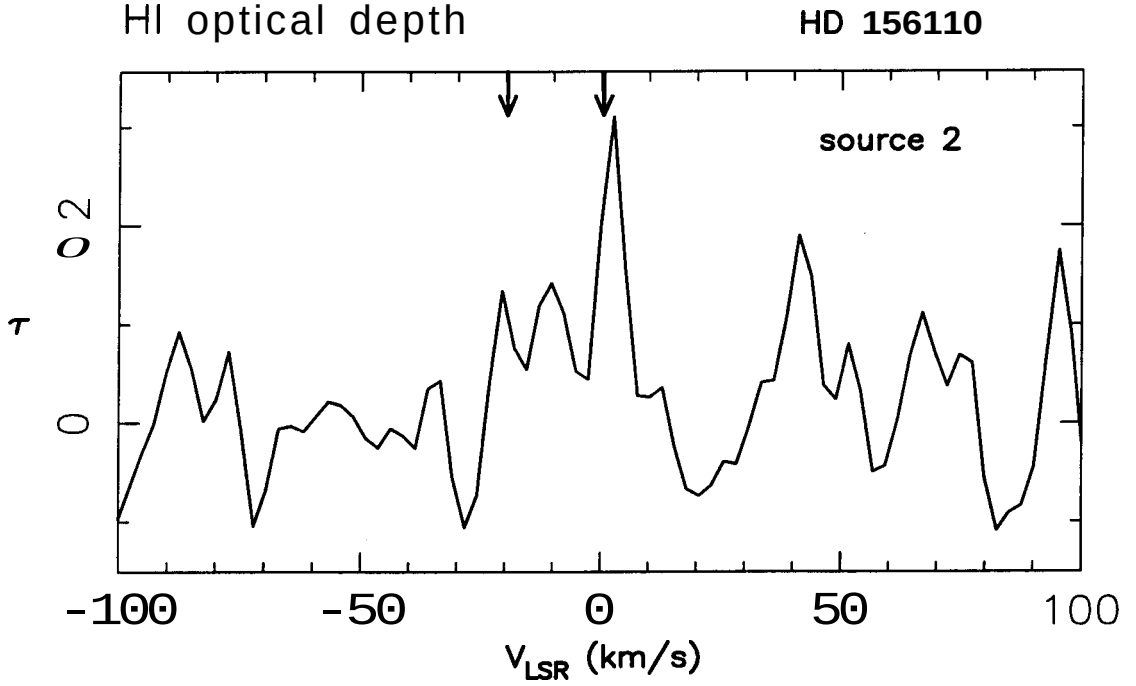
HI optical depth
HD 156110
source 2
τ
0.2
0
-100
-50
0
50
100
V_LSR (km/s)

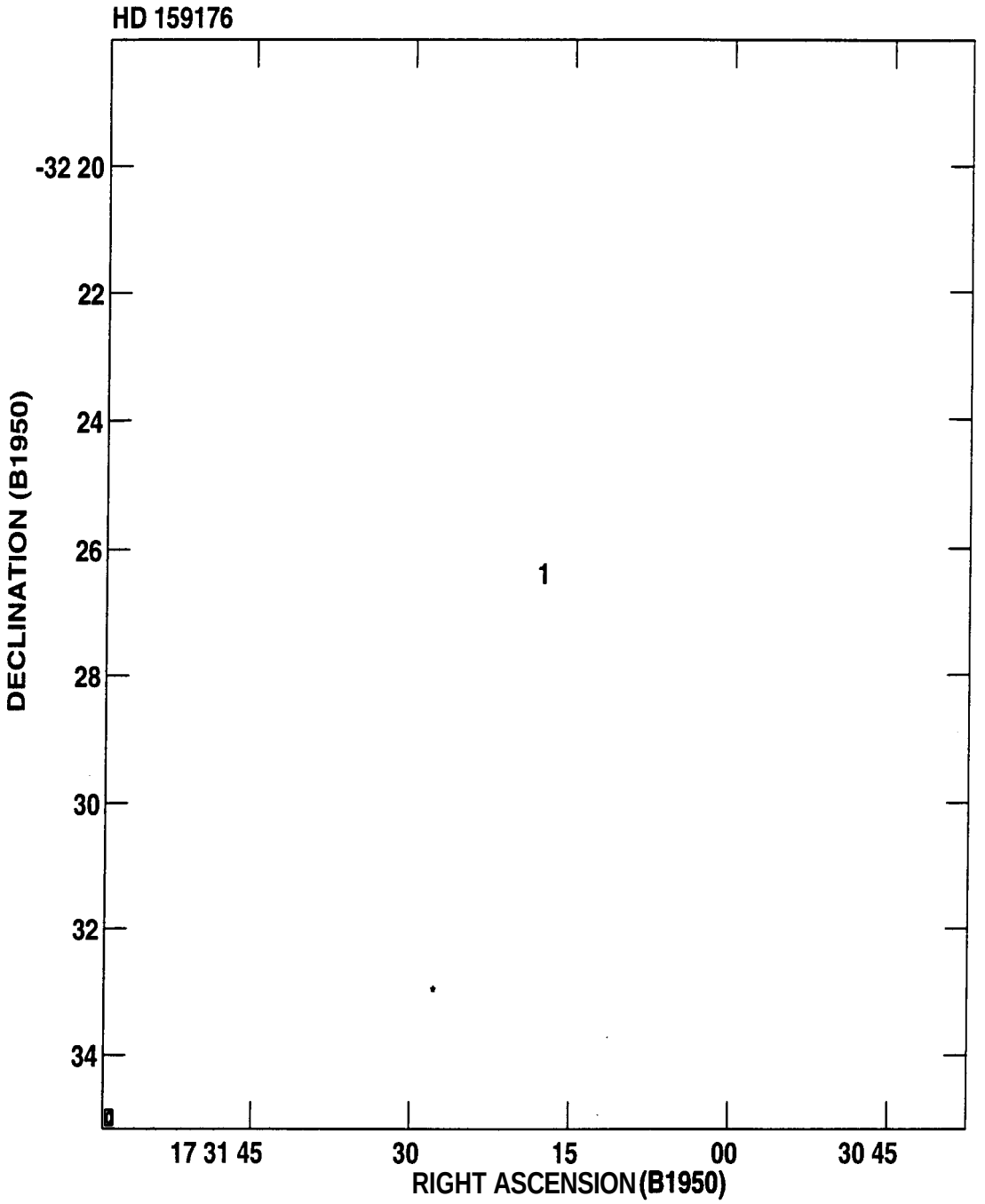
HD 159176
-32 20
22
24
26
28
30
32
34
DECLINATION (B1950)
1
17 31 45
30
15
00
30 45
RIGHT ASCENSION (B1950)

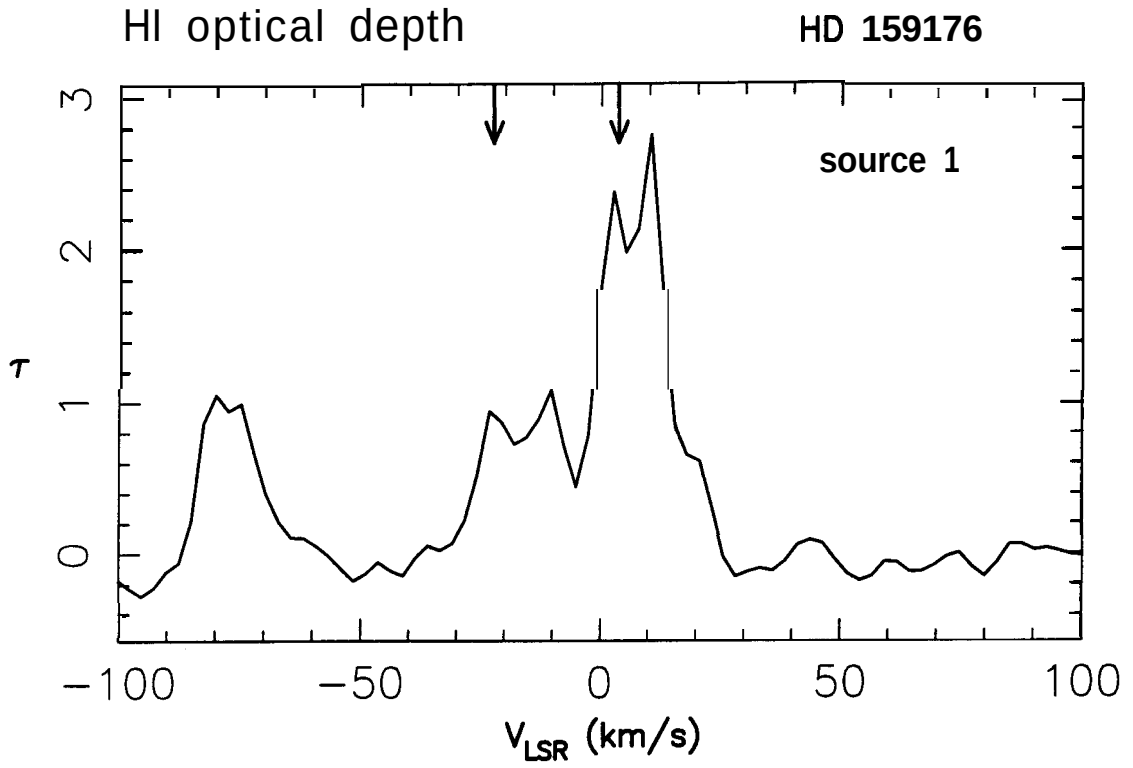
HI optical depth
HD 159176
source 1
τ
0
1
2
3
−100
−50
0
50
100
V_LSR (km/s)

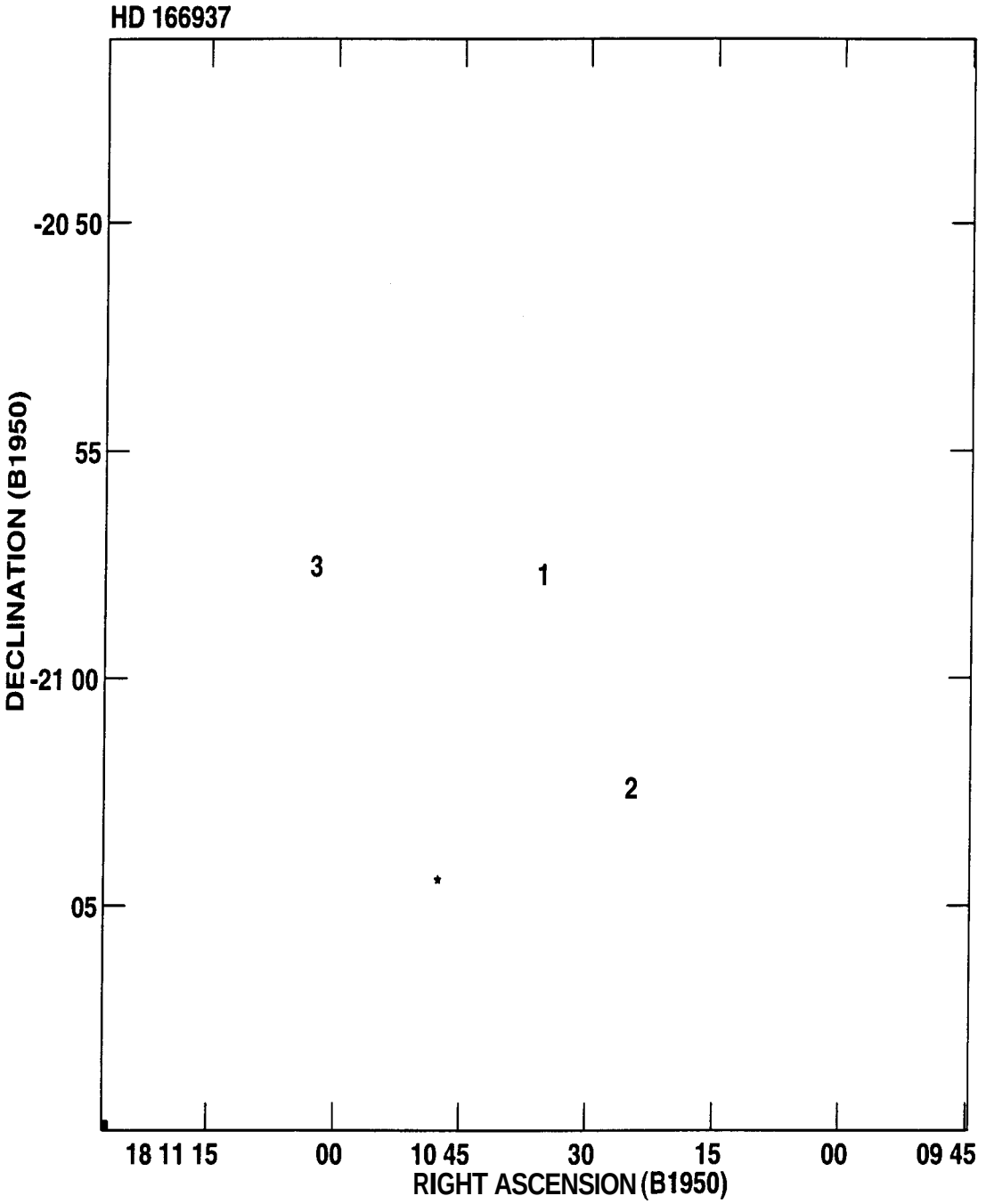
HD 166937
-20 50
55
-21 00
05
DECLINATION (B1950)
3
1
2
18 11 15
00
10 45
30
15
00
09 45
RIGHT ASCENSION (B1950)

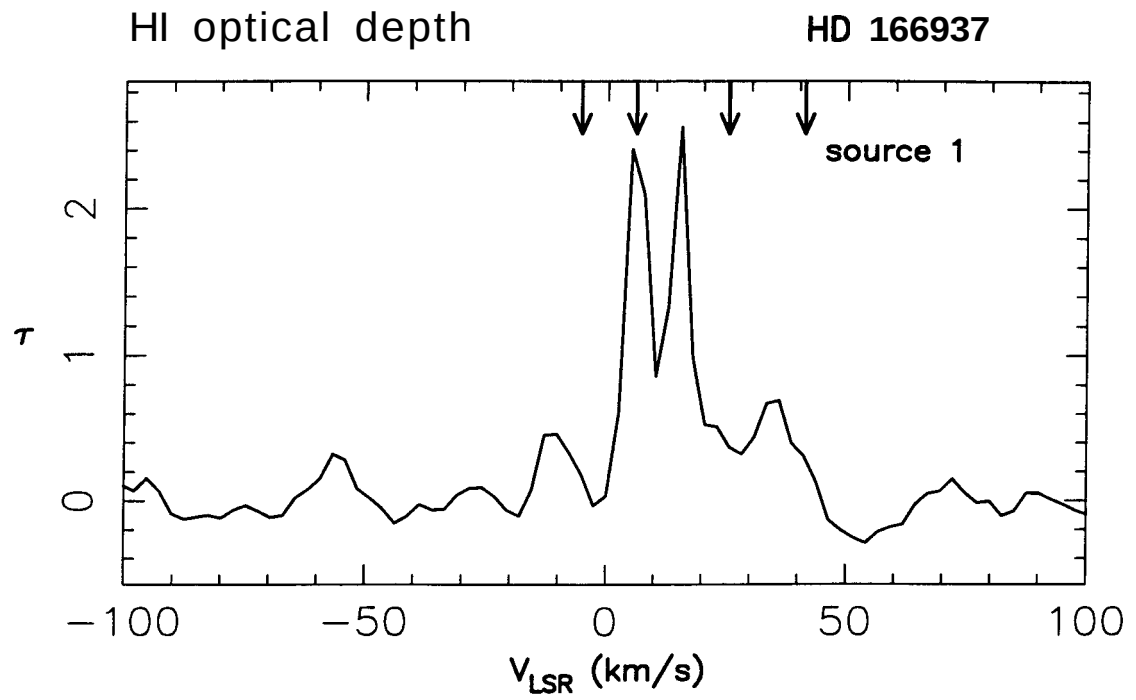
HI optical depth
HD 166937
source 1
τ
2
1
0
−100
−50
0
50
100
V_LSR (km/s)

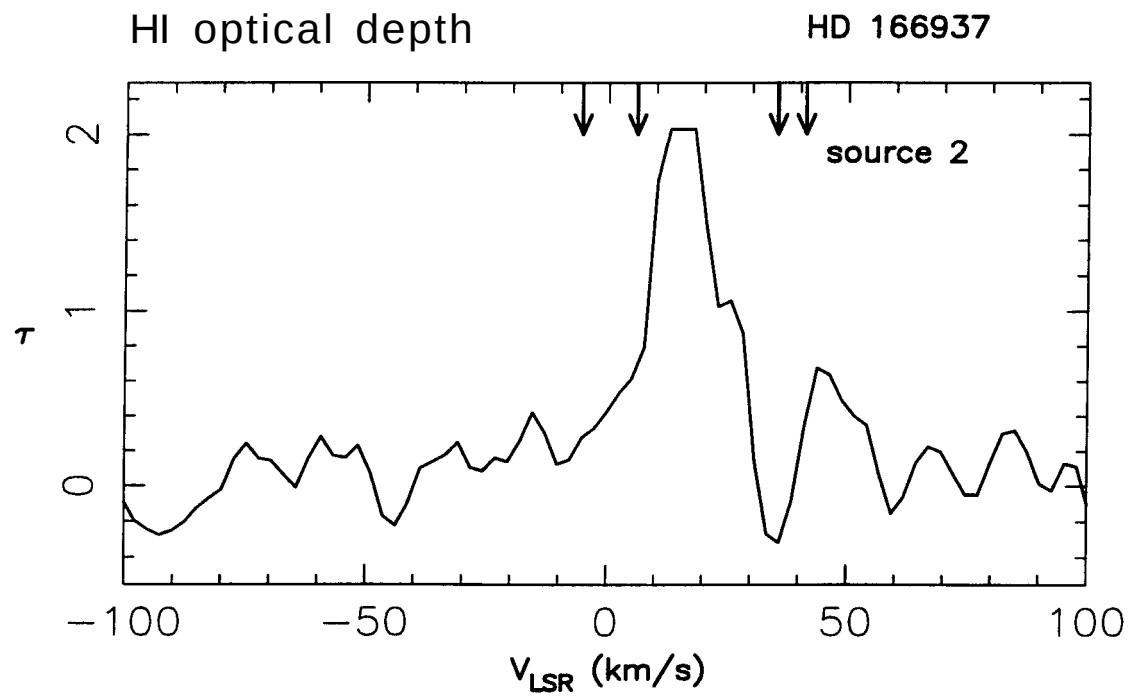
HI optical depth
HD 166937
source 2
τ
2
1
0
−100
−50
0
50
100
V_LSR (km/s)

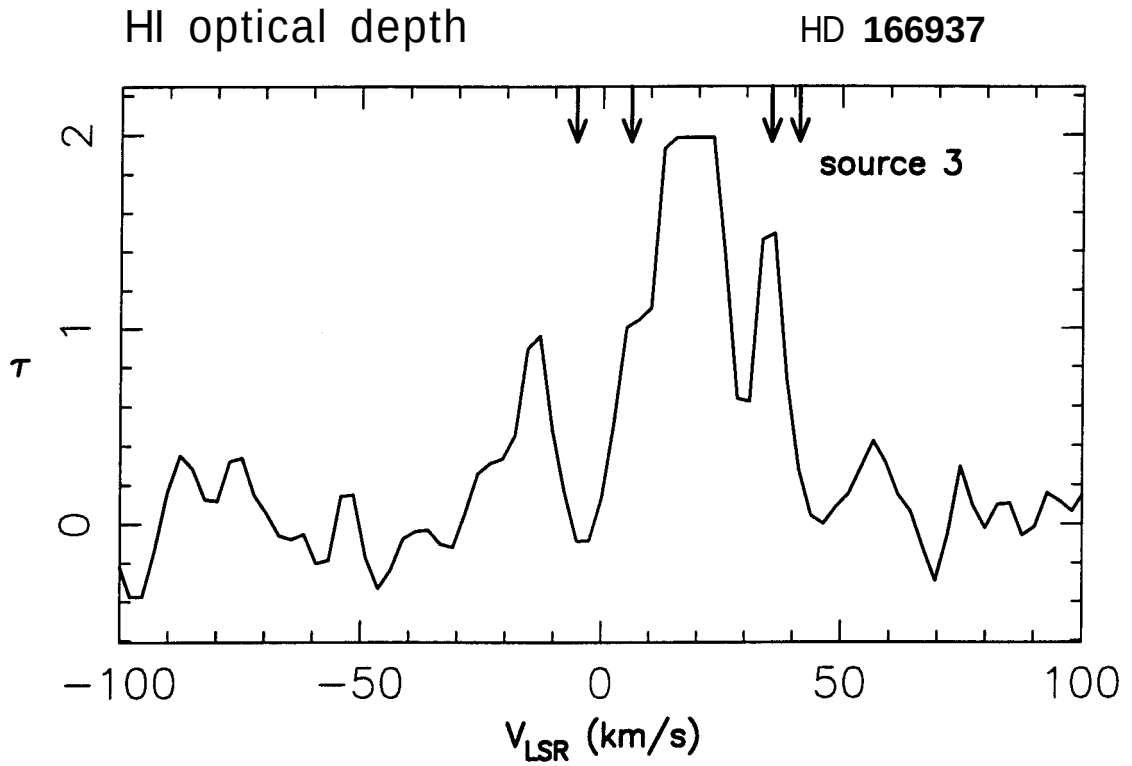
HI optical depth
HD 166937
source 3
τ
2
1
0
−100
−50
0
50
100
V_LSR (km/s)

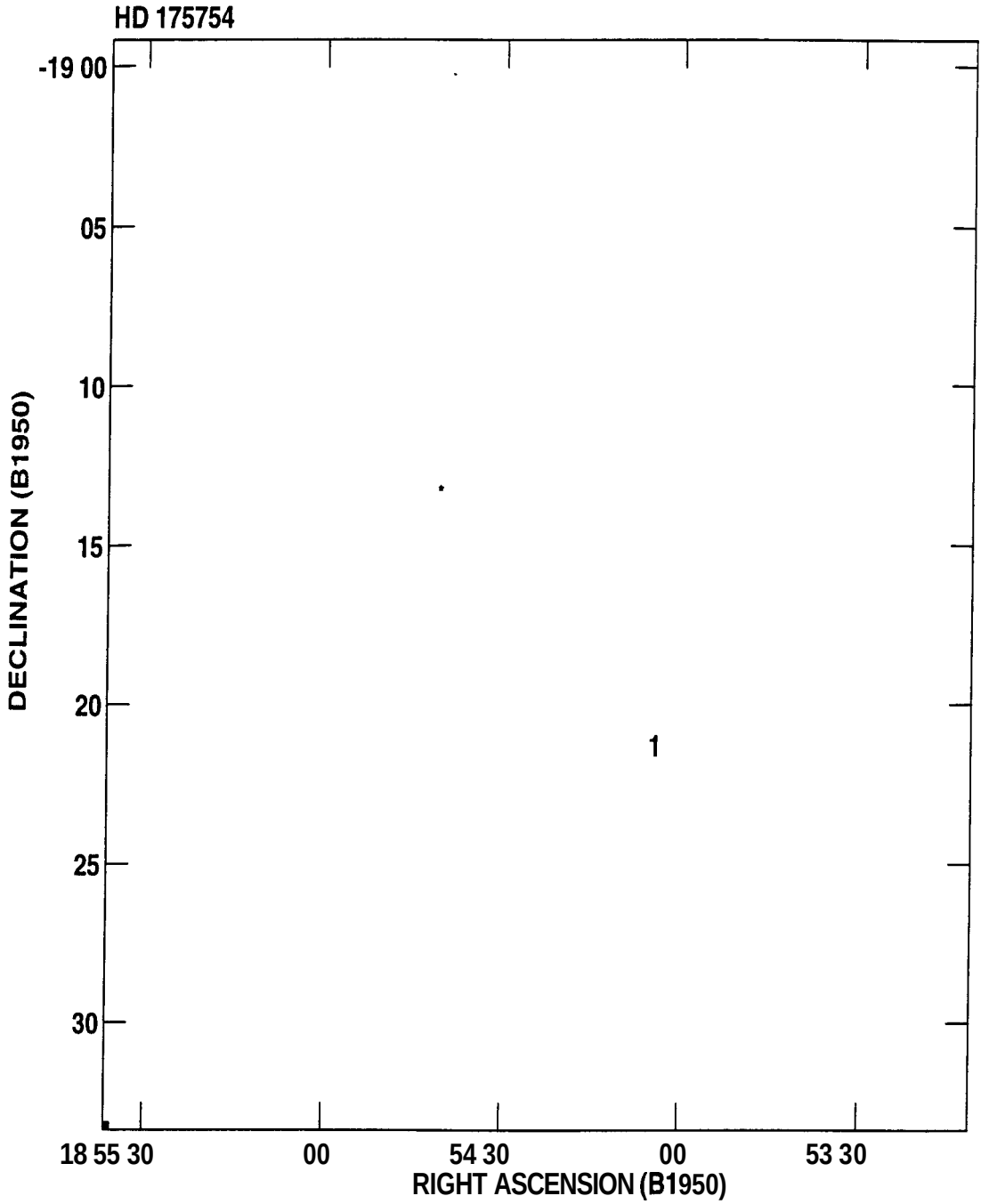
HD 175754
-19 00
05
10
15
20
25
30
DECLINATION (B1950)
1
18 55 30
00
54 30
00
53 30
RIGHT ASCENSION (B1950)

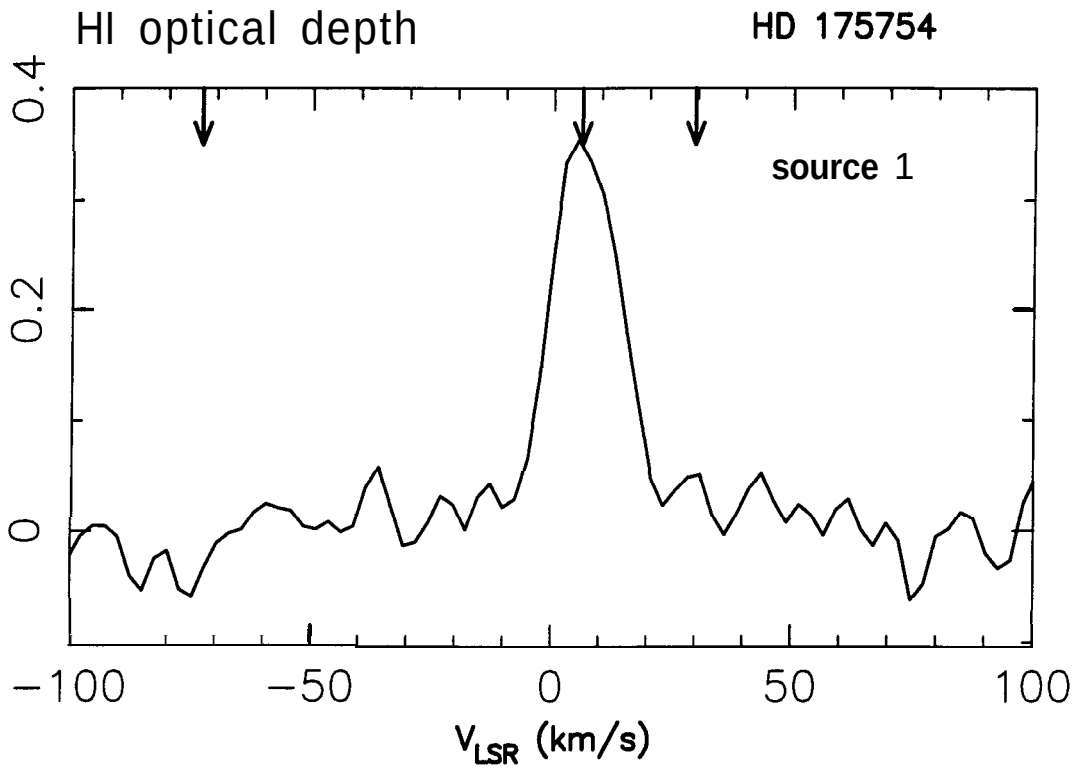
HI optical depth
HD 175754
source 1
0.4
0.2
0
−100
−50
0
50
100
V_{LSR} (km/s)

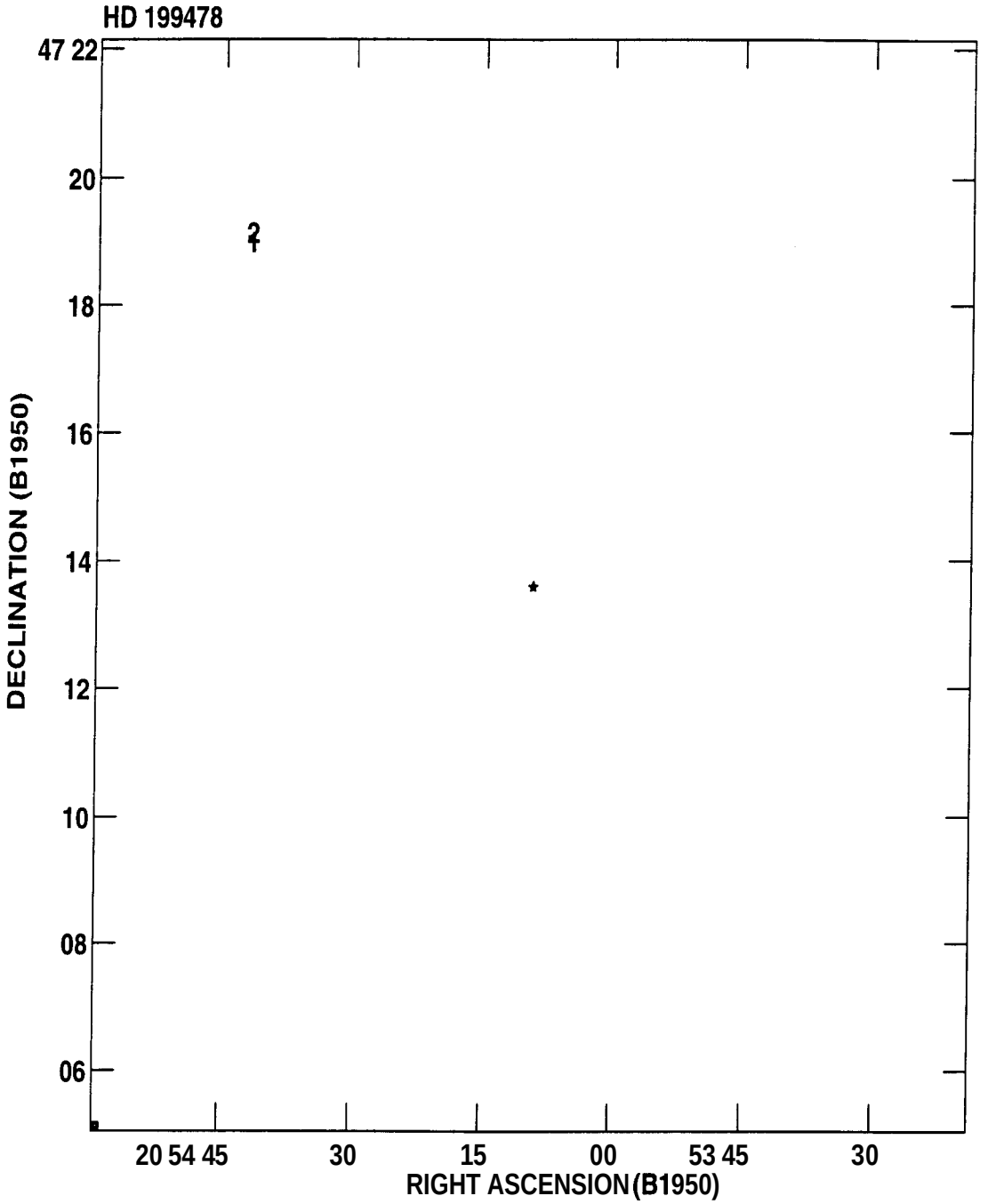
HD 199478
47 22
20
18
16
14
12
10
08
06
DECLINATION (B1950)
20 54 45
30
15
00
53 45
30
RIGHT ASCENSION (B1950)

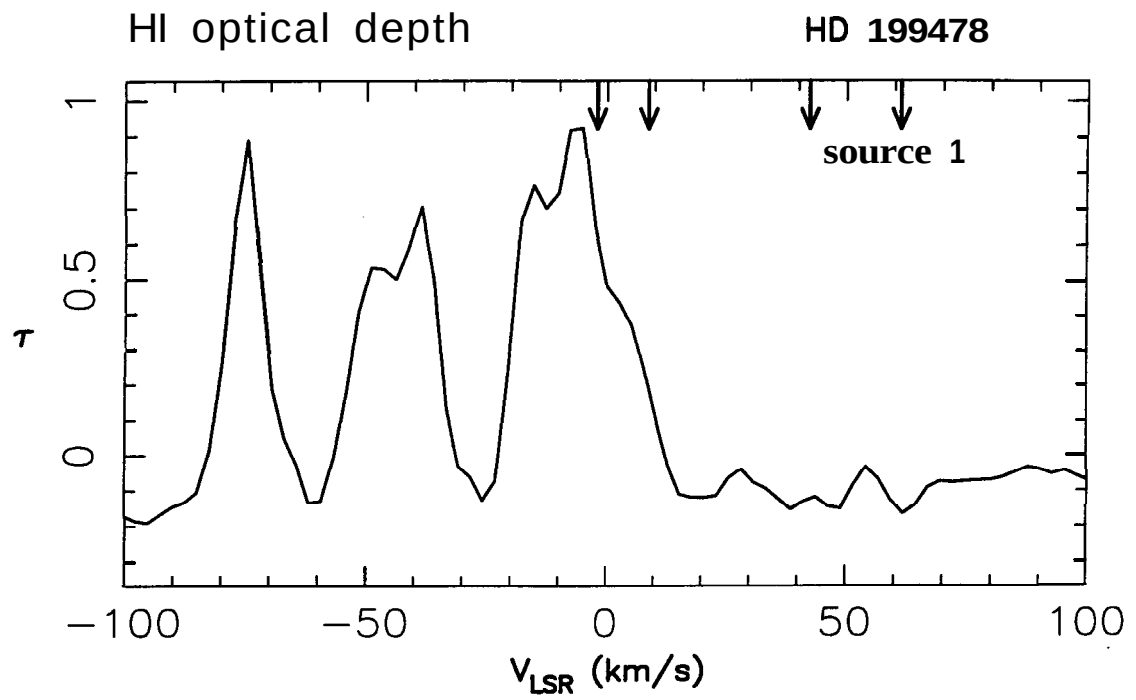
HI optical depth
HD 199478
source 1
τ
1
0.5
0
−100
−50
0
50
100
V_LSR (km/s)

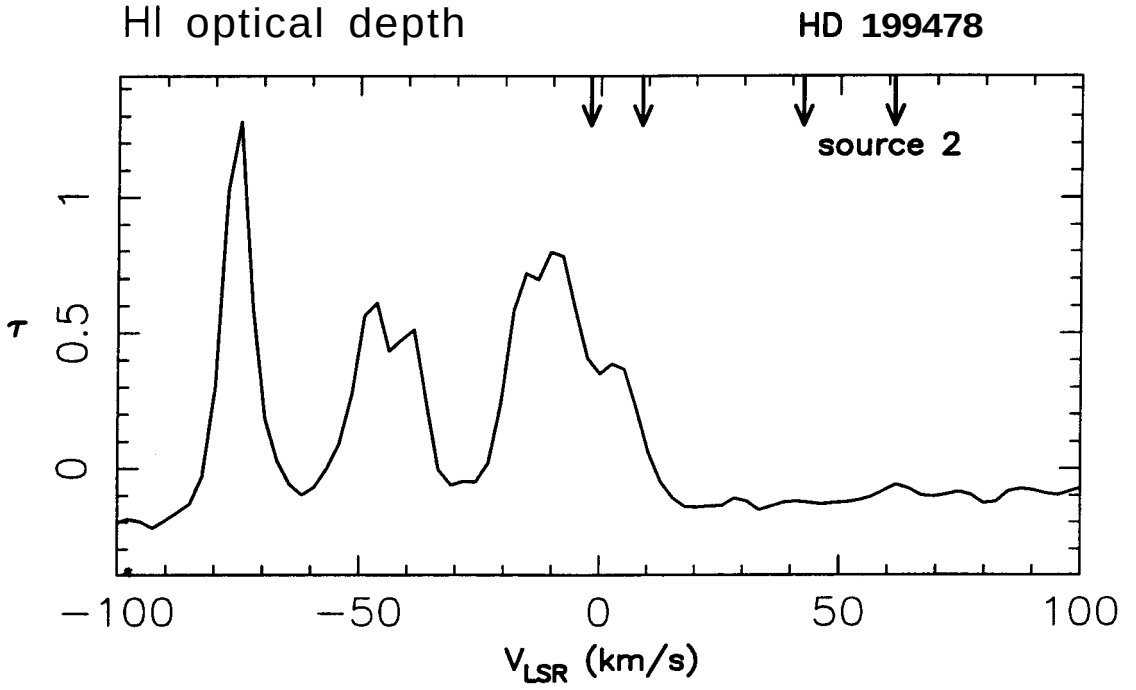
HI optical depth
HD 199478
source 2
τ
1
0.5
0
−100
−50
0
50
100
V_LSR (km/s)

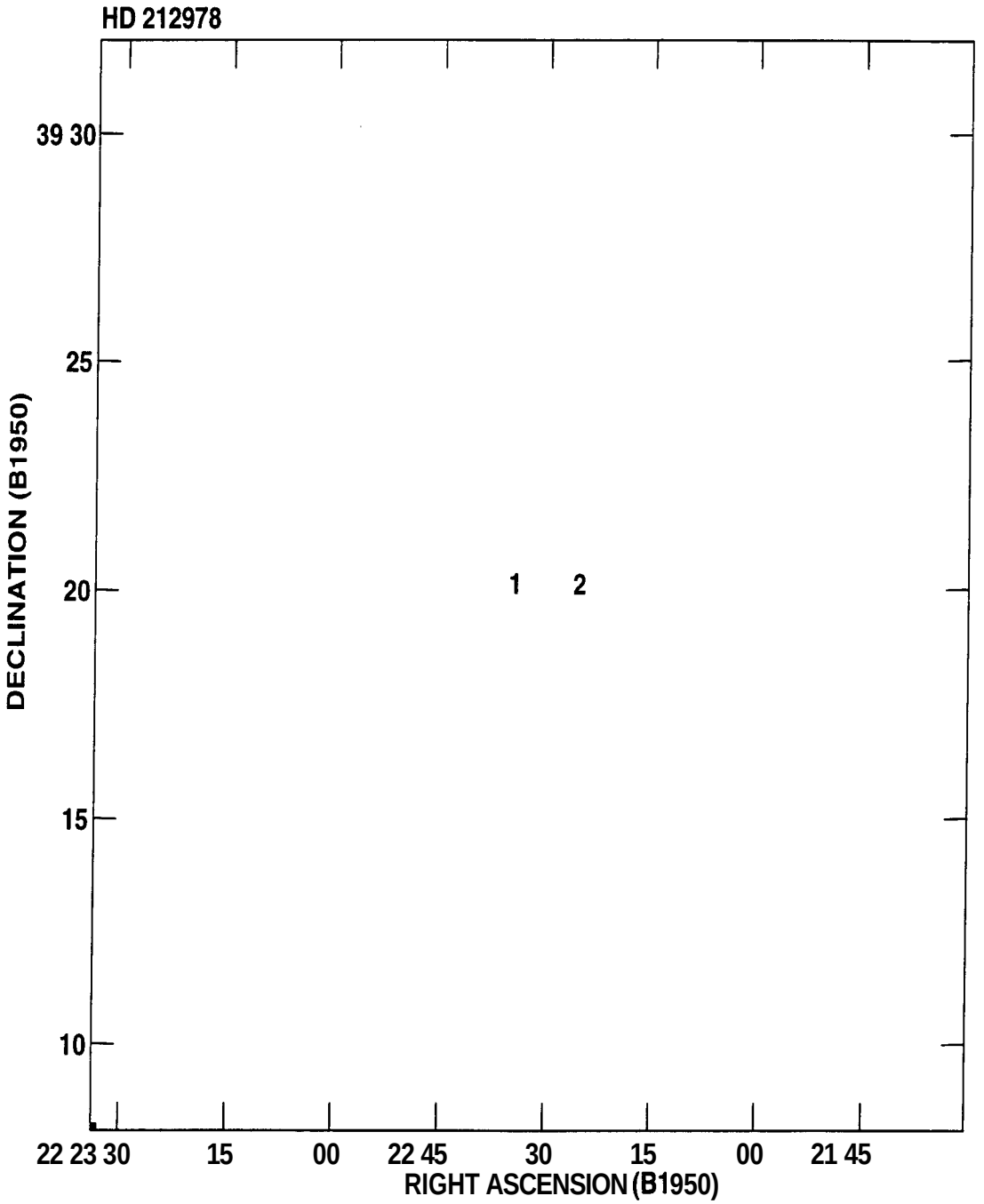
HD 212978
39 30
25
20
15
10
DECLINATION (B1950)
1
2
22 23 30
15
00
22 45
30
15
00
21 45
RIGHT ASCENSION (B1950)

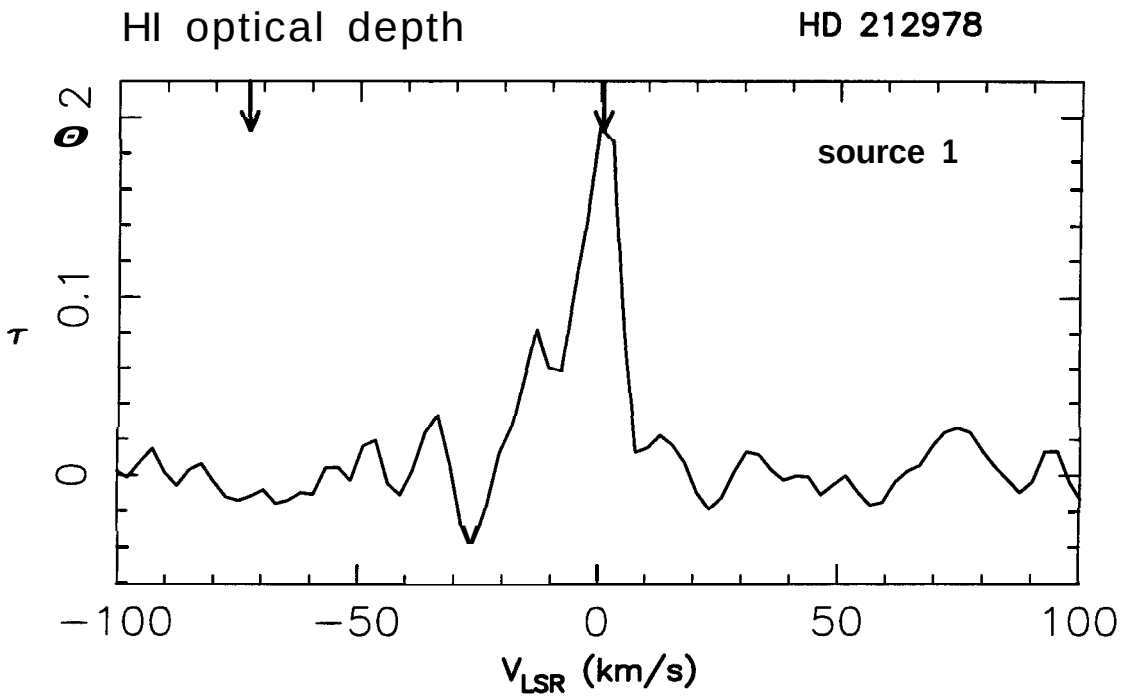
HI optical depth
HD 212978
source 1
τ
0.2
0.1
0
−100
−50
0
50
100
V_{LSR} (km/s)

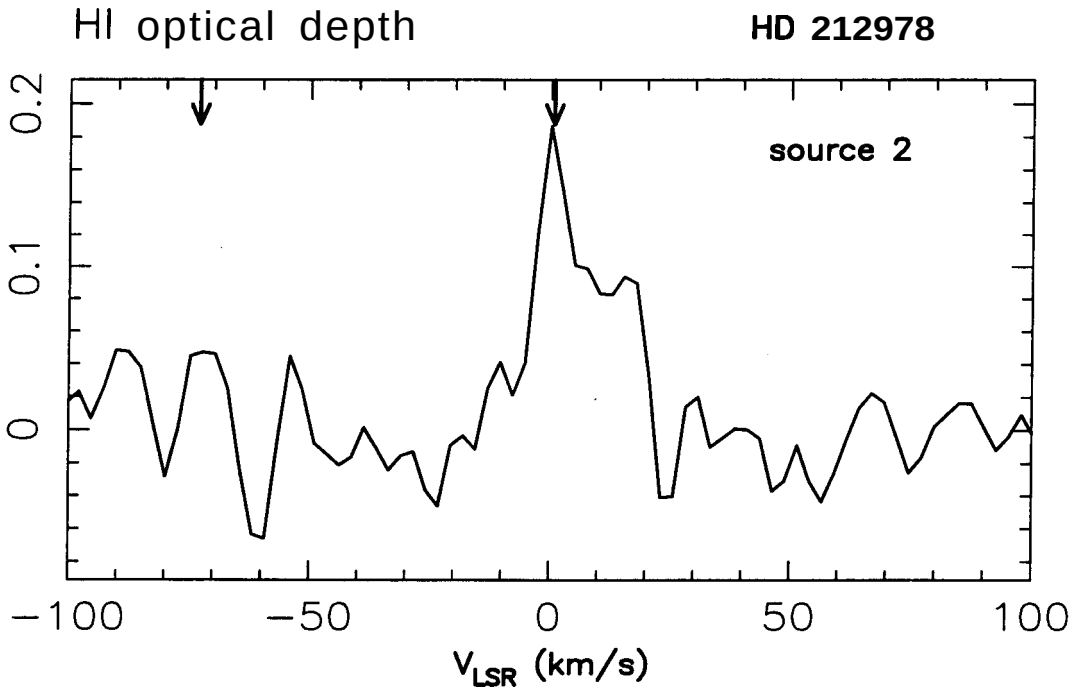
HI optical depth
HD 212978
source 2
0.2
0.1
0
−100
−50
0
50
100
V_{LSR} (km/s)

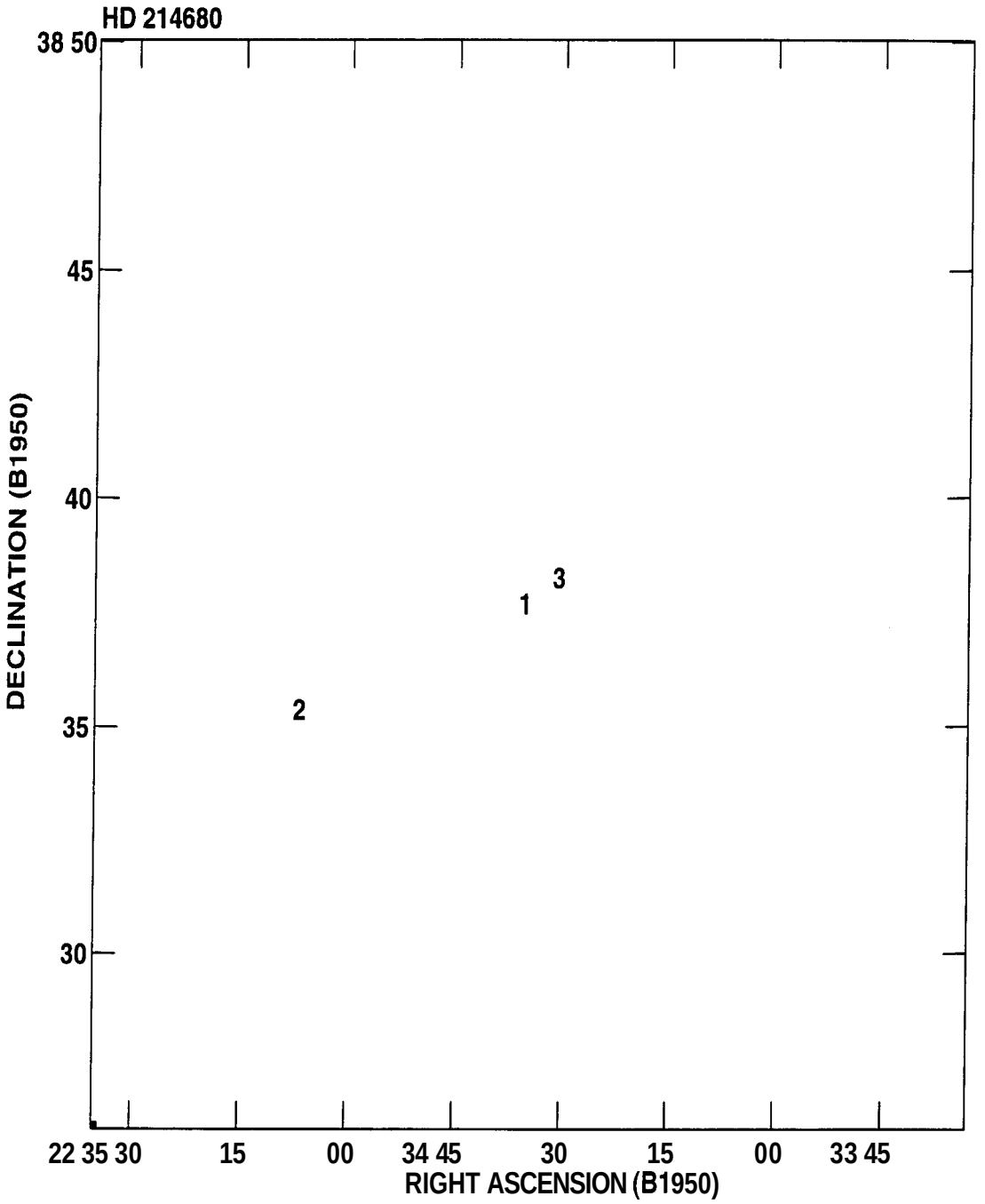
HD 214680
38 50
45
40
35
30
DECLINATION (B1950)
1
2
3
22 35 30
15
00
34 45
30
15
00
33 45
RIGHT ASCENSION (B1950)

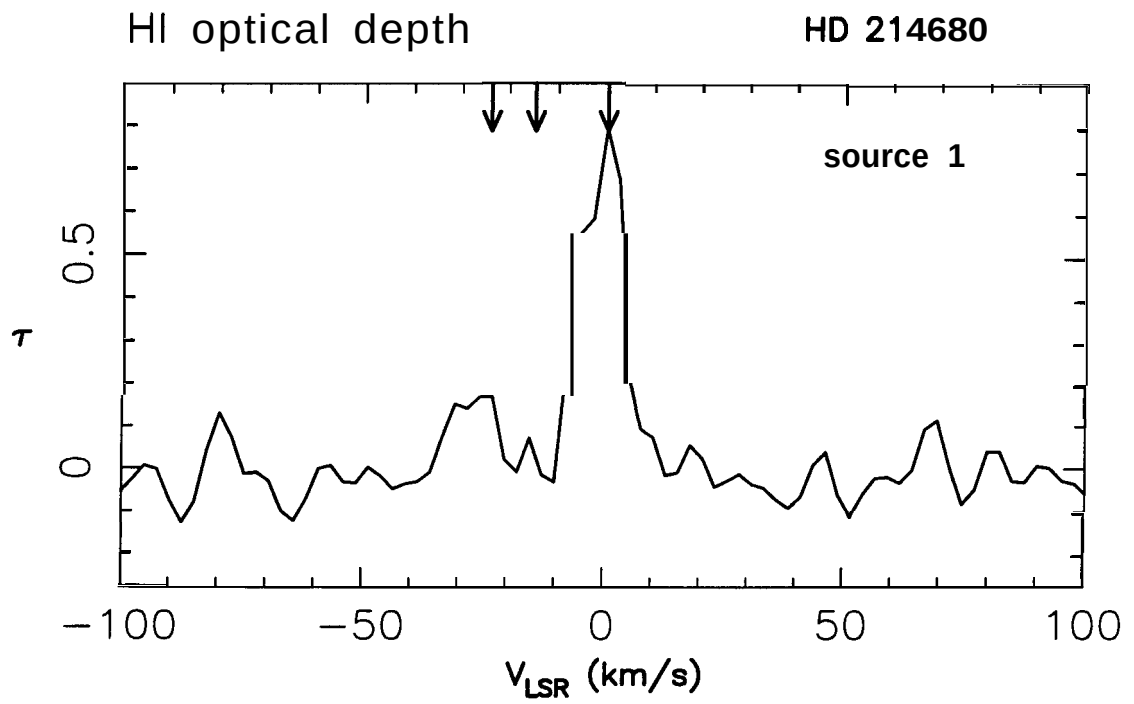
HI optical depth
HD 214680
source 1
τ
0.5
0
−100
−50
0
50
100
V_{LSR} (km/s)

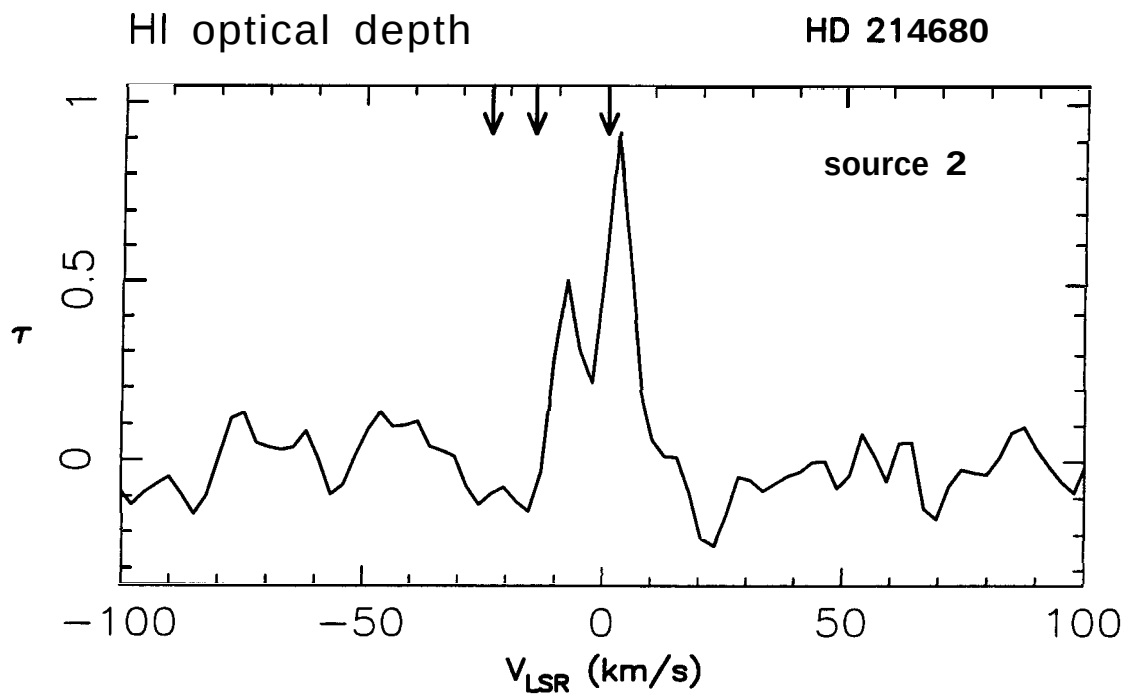
HI optical depth
HD 214680
source 2
τ
1
0.5
0
−100
−50
0
50
100
V_{LSR} (km/s)

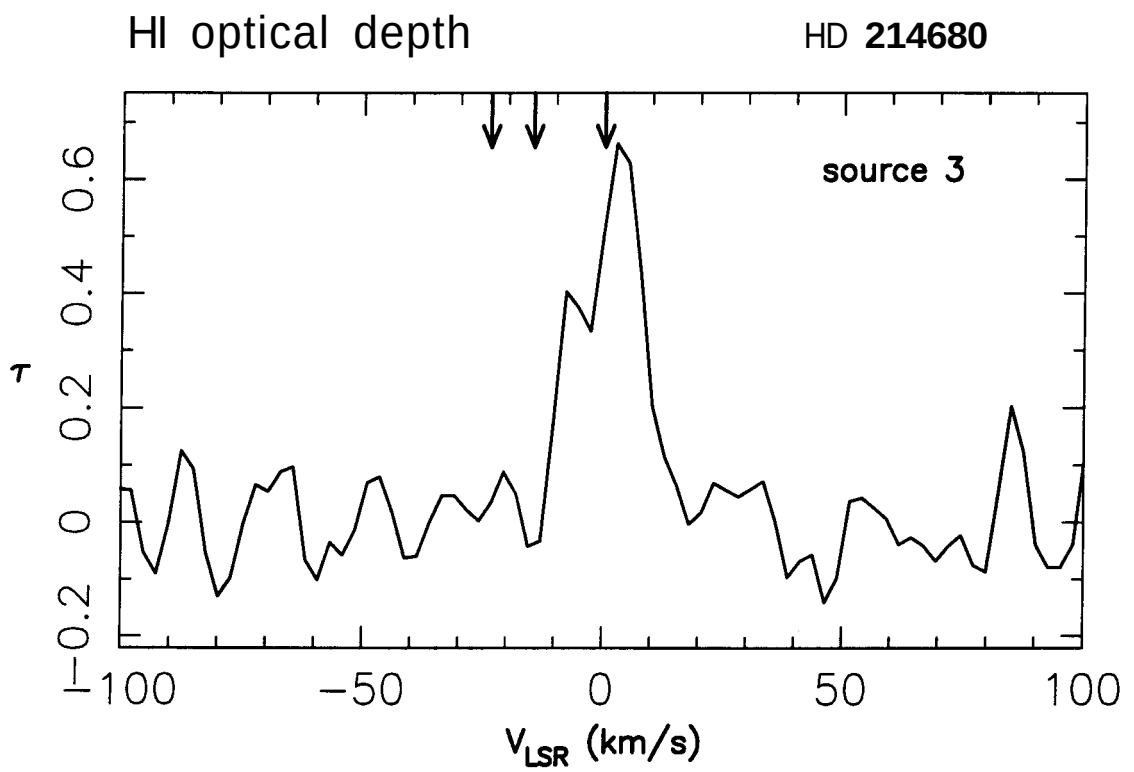
HI optical depth
HD 214680
source 3
τ
0.6
0.4
0.2
0
−0.2
−100
−50
0
50
100
V_LSR (km/s)